



Universitetet
i Stavanger

FACULTY OF SCIENCE AND TECHNOLOGY

MASTER'S THESIS

Study programme/specialization: Natural Gas	Spring semester, 2019 Open
Author: Julie Tanum (signatur forfatter)
Faculty Supervisor: Rune Wiggo Time Hermonja A. Rabenjafimanantsoa	External Supervisors: Gunnar Solheim Åsmund Singstad
Title of master's thesis: Heat Transport in Geothermal Wells – A Comparison of Laboratory-Scale and Full-Scale Construction at Bryne VGS	
Credits: 30	
Keywords: Renewable Energy, Geothermal Heat, Wells, Heat Pump, Optimalization, Geology, Convection, Conduction, Thermal Fluid Science, Inertial Flow, Pasco, Flow Measurements, Flow Visualization.	Number of pages: 90 + 36 Stavanger, 05.06.2019

**Title page for Master's Thesis
Faculty of Science and Technology**

Acknowledgements

This thesis is a result of collaboration and contributions of many people. I would like to start by thanking students and employees at Bryne Videregående Skole for the friendly accommodation and help. I particularly want to thank the students from 1TIPA for building the laboratory setup, and their teacher Geir Bjelland for guiding them and cooperating with us. Thanks to Gunnar Solheim and Åsmund Singstad for working with me trying to understand their geothermal system and technical guidance along the way.

At the University of Stavanger, the setup of the system similarly included help from numerous, but a special thanks to Hermonja A. Rabenjafimanantsoa for help and follow-up at the laboratory. Thanks to Rune Wiggo Time for outlining this fascinating proposal which allowed me to deepen in the world of heat transfer and unfold at the laboratory. Thank you for helping me with experimental inputs, literature studies and discussions along the way.

My last thanks go to all my friends and classmates for the support and brightening of the long days, you've made the years at the University of Stavanger an unforgettable and joyful experience.

Abstract

Utilization of geothermal wells in combination with a heat pump has become gradually more popular, and great effort is made to optimization of heat pumps. The occurrences in the subsurface however, seems to be less investigated. By exploring an operating geothermal system in Bryne and carry out experiments in a laboratory setup of a geothermal well, heat transport information about both the internal flow and external environment was obtained. By investigating the system in Bryne, a simplified model of the geothermal energy structure was created. Visualized in the laboratory, the internal flow causes the external flow in the close vicinity to transfer heat to the copper tube. The fluid cooled down will resultingly sink towards the bottom in a mix of laminar and turbulent flow regime as the density is increased. Due to the heat transfer and sinking of cold water, the water cylinder will obtain a temperature profile where the bottom temperature is severely lower than the top temperature. An increase of the flowrate reduces the temperature difference from the inlet to the outlet of the well. The energy output of the subsurface loop depends on the mass rate and temperature difference, which are opposite proportional to the flowrate. The coherence of the temperature and mass rate to the flowrate allows for calculation of an optimal flowrate. For the laboratory system the optimal flowrate was calculated to be $1.53\text{E-}05 \text{ m}^3/\text{s}$ by use of enthalpy. A test of the exact flowrate proved to be difficult to achieve. However, a flowrate close to the optimal was reached, and the flowrate $1.575\text{E-}05 \text{ m}^3/\text{s}$ provides the energy 105.2 J/s or W . The energy obtained by the geothermal wells in Bryne is 6.01 kW per well, and a total of 204.29 kW combined.

Table of Contents

ACKNOWLEDGEMENTS	I
ABSTRACT	II
NOMENCLATURE	V
LIST OF FIGURES	VI
LIST OF TABLES	VII
LIST OF EQUATIONS	VIII
1 INTRODUCTION	1
2 THEORY	2
2.1 THERMAL FLUID SCIENCE.....	2
2.1.1 Heat transfer.....	2
2.1.2 Fluid Mechanics.....	8
2.1.3 Other types of flow.....	13
2.1.4 Density Dependence of Temperature.....	14
2.1.5 Flow Visualization.....	16
2.1.6 Thermodynamics.....	18
2.2 GEOTHERMAL HEAT.....	23
2.2.1 Geothermal Rock Differences.....	23
2.2.2 Utilization of Geothermal Heat.....	24
2.3 GEOTHERMAL SYSTEMS.....	26
2.3.1 Deep or Shallow.....	26
2.3.2 Open or Closed.....	26
2.3.3 Drilling and sizing.....	27
3 THE GEOTHERMAL SYSTEM AT BRYNE VGS	28
3.1 OPERATION PLANNING.....	28
3.2 BRINGING THE SYSTEM TO LIFE.....	31
3.2.1 Heating Cycle.....	34
3.2.2 Refrigeration and Combination.....	37
3.3 APPLICATION OF THE GEOTHERMAL SYSTEM.....	39
3.3.1 Display of Heat Production.....	39
3.4 EXTERNAL AND INTERNAL EFFECTS OF GEOTHERMAL USAGE.....	40
4 EXPERIMENTAL METHOD	41
4.1 EXPERIMENTAL SETUP.....	42
4.2 EQUIPMENT.....	44
4.2.1 Pasco.....	45
4.2.2 Software.....	45
4.2.3 Julabo.....	45
4.2.4 Gardena Water Smart Flow Meter.....	46
4.2.5 Electromagnetic flow meter.....	46
4.2.6 Experimental Preparation.....	48
4.3 INTERNAL FLUID FLOW.....	49
4.3.1 Equipment.....	49
4.3.2 Experimental Setup.....	49
4.4 EXTERNAL FLUID.....	50
4.4.1 Free Convection in the Cylinder.....	50
4.4.2 Temperature distribution over time.....	52
4.5 EXPLORATION OF AN OPTIMAL RATE.....	53
5 EXPERIMENTAL RESULTS	54

5.1	INTERNAL FLUID FLOW	56
5.1.1	<i>Fast Rate</i>	56
5.1.2	<i>Intermediate flowrates</i>	57
5.1.3	<i>Low flowrates</i>	57
5.2	EXTERNAL FLUID	58
5.2.1	<i>Free Convection in the Cylinder (Thymol Blue)</i>	58
5.2.2	<i>Temperature distribution over time</i>	60
5.3	CALCULATIONS OF OBTAINED HEAT.....	64
5.3.1	<i>Laboratory</i>	64
5.3.2	<i>Bryne VGS</i>	65
5.4	EXPLORATION OF AN OPTIMAL RATE	66
5.5	COMPARISON OF DIMENSIONLESS NUMBERS AND PROPERTIES IN BRYNE AND AT THE LABORATORY... 68	
6	DISCUSSION AND OBSERVATIONS	70
6.1	PROPERTIES.....	70
6.2	INTERNAL FLOW.....	70
6.3	EXTERNAL FLOW	73
6.3.1	<i>Ground-Water Flow</i>	74
6.3.2	<i>Temperature in the ground</i>	75
6.4	INTERNAL FLOW, ENERGY OUTPUT	76
7	CONCLUSION.....	78
	FURTHER RESEARCH.....	80
	REFERENCES.....	81
	APPENDIX 1,2,3,4,5.....	83

Nomenclature

$[H^+]$ = concentration of hydrogen	T = temperature [°C]
A_0 = Cross section of the surface area [m ²]	T_∞ = Temperature sufficiently far from any surface [°C]
A_{lm} = Logarithmic mean surface area [m ²]	T_n (n=1,2,...) = Temperature at a given place [°C]
A_n (n=1,2,...) = Areal at a given place [m ²]	$T_{s,w}$ = Temperature at a surface [°C]
A_s = Surface area [m ²]	u = Internal energy [J]
c_p = Specific heat / heat capacity [J/K]	U = Overall heat transfer coefficient [W/m ² K]
D = pipe Diameter [m]	v = Velocity [m/s]
coefficient [W/m ² K]	V = Volume [m ³]
h = Enthalpy [kJ/kg]	W = Work [w]
h' = Convective heat transfer coefficient [W/m ² K]	z = Compressibility factor
K = Boltzmann constant [J/K]	Δr = Wall thickness [m]
k = Thermal conductivity [W/mK] substance [W/mK]	ΔT = Temperature difference [°C] [K]
\dot{m} = mass rate [kg/s]	Δx = wall thickness of a substance heat is transferred through [m]
N = Number of microstates of the system	α = Thermal diffusivity [W/mK]
P = Pressure [atm]	β = Coefficient of volume expansion [1/K]
Q = Heat flow rate [W]	μ = Viscosity [Pa s]
Q_{cond} = Heat flow by conduction [W] = [J/s]	ρ = Density [kg/m ³]
Q_{conv} = Heat flow by convection [W]	
Q_H = Supplied heat [W]	
Q_L = Delivered heat [W]	
R = Universal gas constant [J/Kmol]	
S = Entropy [kJ/kgK]	

List of Figures

FIGURE 2.1.1 HEAT CONDUCTION THROUGH A WALL.....	3
FIGURE 2.1.2 CYLINDRICAL HEAT TRANSFER	6
FIGURE 2.1.3 LAMINAR AND TURBULENT FLOW REGIMES	10
FIGURE 2.1.4 A TYPICAL REVERSED CARNOT CYCLE.....	20
FIGURE 2.1.5 GRAPHS PROVIDING PRESSURE VS. VOLUME AND TEMPERATURE VS ENTROPY FOR A REVERSED CARNOT CYCLE	21
FIGURE 3.1.1 A MINIATURE MODEL OF THE SUBSURFACE IN BRYNE	29
FIGURE 3.1.2 TEMPERATURE VS. DEPTH, MEASURED IN THE TEST WELL	30
FIGURE 3.2.1 A MODEL OF THE GEOLOGY, U-TUBE AND CASING IN BRYNE.....	32
FIGURE 3.2.2 VISUALIZATION OF THE HEAT TRANSPORT FROM THE WELLS	34
FIGURE 3.2.3 HEAT PUMP 1 (13.03.19 10:00), SHOWING HEAT TRANSFER FROM THE WELL (BLUE) THROUGH THE HEAT PUMP (RED) TO THE HEATING MEDIUM SPREADING THE HEAT ENERGY (GREEN).....	35
FIGURE 3.2.4 TRANSPORTATION OF THE FLUID TO AND FROM THE HEAT PUMP	35
FIGURE 3.2.5 FLUID TRANSPORT TO AND FROM THE ACCUMULATOR	36
FIGURE 3.2.6 TRANSPORT OF FLUID TO THE GROUND	36
FIGURE 3.2.7 THE COMBINED HEATING AND COOLING CYCLE, FLOW FROM THE WELLS	37
FIGURE 3.2.8 THE COMBINED HEATING AND COOLING CYCLE, FLOW TO THE WELLS.....	38
FIGURE 3.2.9 TWO IMAGES PRESENTING THE WHOLE SCHEMATIC DESIGN	38
FIGURE 4.3.4.1 THE LABORATORY SETUP	41
FIGURE 4.1.1 PLACEMENT OF TEMPERATURE SENSORS	43
FIGURE 4.2.1 (ENDRESS + HAUSER) ELECTROMAGNETIC FLOW METER	47
FIGURE 4.5.1 TEMPERATURE VS. TIME.....	55
FIGURE 5.2.1 VISUALIZATION OF THE FLOW PATTERNS CLOSE TO THE U-TUBE	58
FIGURE 5.2.2 PRESENTING THE FREE CONVECTION OCCURRING IN THE CYLINDER OVER TIME	59
FIGURE 5.2.3 TEMPERATURE VS. TIME. FLOW RATE = $8.5E-05 \text{ M}^3/\text{S}$	60
FIGURE 5.2.4 TEMPERATURE VS. TIME, FLOW RATE = $16.67E-05 \text{ M}^3/\text{S}$	61
FIGURE 5.2.5 EXTERNAL TEMPERATURE VS. TIME FOR FLOW RATE = $1.006E-05 \text{ M}^3/\text{S}$	61
FIGURE 5.2.6 EXTERNAL TEMPERATURE VS. TIME, 44-HOUR RUN.....	62
FIGURE 5.2.7 TEMPERATURE IN THE CYLINDER CAPTURED BY A THERMOGRAPHIC CAMERA .	63
FIGURE 5.4.1 ENERGY OUTPUT VS. FLOWRATE.....	66
FIGURE 5.4.2 TEMPERATURE DIFFERENCE VS. FLOW RATE WITH LINEAR (LEFT) AND POLYNOMIAL (RIGHT) FIT.....	66

List of Tables

TABLE 2.1.1 LIST OF THERMAL CONDUCTIVITY FOR SOME MATERIALS	4
TABLE 2.1.2 WATER DENISTY VS. TEMPERATURE.....	15
TABLE 2.1.3 (WIKIPEDIA 2019)) THE COLOR RANGE OF PH INDICATORS	17
TABLE 3.3.1 CALCULATED HEAT OBTAINED FROM THE GEOTHERMAL WELLS	39
TABLE 4.5.1 TEMPETRUE VS. TIME.....	54
TABLE 5.1.1 TEMP DIFFERENCE VS. FLOWRATE, FAST RATES	56
TABLE 5.1.2 TEMPERATURE DIFFERENCE VS. FLOW RATE, INTERMEDIATE FLOW RATES.....	57
TABLE 5.1.3 TEMPERATURE DIFFERENCE VS. FLOWRATE, LOW FLOWRATES	57
TABLE 5.5.1 PROPERTIES OF THE GEOTHERMAL SYSTEM IN BRYNE AND AT THE LABORATORY SETUP.....	68
TABLE 5.5.2 DIMENSIONLESS NUMBERS	69

List of Equations

EQUATION (2.1)	2
EQUATION (2.2)	5
EQUATION (2.3)	6
EQUATION (2.4)	6
EQUATION (2.5)	6
EQUATION (2.6)	7
EQUATION (2.8)	8
EQUATION (2.9)	9
EQUATION (2.10)	11
EQUATION (2.11)	12
EQUATION (2.12)	12
EQUATION (2.13)	13
EQUATION (2.14)	16
EQUATION (2.15)	18
EQUATION (2.16)	19
EQUATION (2.17)	19
EQUATION (2.18)	21
EQUATION (2.19)	22
EQUATION (4.1)	47
EQUATION (4.2)	48

1 Introduction

Heat pumps have become a common way to heat up and cool down houses. A heat pump attached to a wall compresses a fluid with outside temperature to increase the temperature. As the fluid temperature is increased, the fluid is transported inside where heat is diffused through the house. The fluid in the heat pump is then transported outside where the pressure is released, and the fluid draws energy from the outside and restarts the cycle. Higher outside temperature demands less compressor energy from the heat pump. A lower outside temperature requires increased work by the heat pump, leading to reduced energy efficiency. Most heat pumps have a minimum temperature for which they can operate, typically -5, -10 or -20 °C. Resultingly, here in Norway, a regular heat pump can not function during the coldest days of the year.

Meanwhile, the temperature a some hundred meters under the surface holds a constant temperature of 5-15 °C. By extending the loop of the heat pump from the outside of the building to a depth of 200 meters, the source of heat obtaining is kept constant, and the heat pump can deliver heat even during the coldest days. Utilizing the warmth of the underground by geothermal wells is becoming normal either by use of one or several wells, depending on the heat demand. The new high school in Bryne, Bryne Videregående Skole has 34 geothermal wells for heating and cooling. The geothermal wells in combination with two heat pumps provide heat to the school, used for warm water and heat radiators. Although the geothermal system provides the school with a considerable amount of heat, relatively little is known as to how the heat is obtained.

The objectives of this thesis were tripartite, based on a collaboration with Bryne Videregående Skole and the University of Stavanger (UiS) starting January the 13th 2019.

- The collaboration included UiSs examination of the geothermal wells, and hence an objective is to obtain information about the geothermal system
- Secondly the aim was to investigate the boundary conditions of the system
- The last objective was to create a small-scale laboratory model to investigate and visualize effects which can not be seen at Bryne

Efforts to explore these objectives were made through theory, experimental results and novel information about the geothermal system operating at Bryne Videregående Skole.

2 Theory

2.1 Thermal Fluid Science

Heat transfer, thermodynamics and fluid mechanics are referred to as thermal-fluid science. Interactions between energy and matter occurs in all fragments of the nature, accordingly thermal-fluid science can be studied in all spectra of the nature. Whereas thermodynamics is defined as the science of energy, fluid mechanics deals with fluid behavior and fluid interaction; heat transfer focuses on heat, as the rate of energy transferred from a warmer system to a colder one (Çengel, 2017).

2.1.1 Heat transfer

A bottle filled with cold tap water in a room will experience a temperature increase towards room temperature, the same way a cup of hot coffee will experience a temperature decrease to reach the same room temperature. This is explained by the desire to reach thermodynamic equilibrium, where all fragments of a system have the same temperature. This is done by energy transfer in the form of heat, from the warmer to the colder body (Çengel, 2017).

2.1.1.1 *Types of heat transfer*

Heat can be transferred by three mechanisms: conduction, convection and/or radiation. Conduction implies energy transfer from the most energetic to the less energetic particles of the fluid. Convection is energy transfer between a solid and a gas or fluid in motion, and radiation is the energy caused by electromagnetic wave emission. All types of heat transfer involve energy transfer from a high temperature to a lower temperature, and thus occurs when there is a temperature difference between substances (Çengel 2017). For the purpose of this paper, the focus will be regarding conduction and convection.

2.1.1.1.1 Conduction

Conduction occurs in gases and liquids as heat is spread by the molecules with their random movements collide and diffuse, and in solids the vibrations in the mesh cause the conduction. Geometry is of great importance for the heat conduction rate, along with the thickness, material and temperature difference:

$$Q_{cond} = kA_0 \frac{T_1 - T_2}{\Delta x} \quad (2.1)$$

k = Thermal Conductivity

A_0 = Cross section of the surface area

$T_{1,2}$ = temperature at either side of the wall of which heat is conducted

Δx = thickness of the material

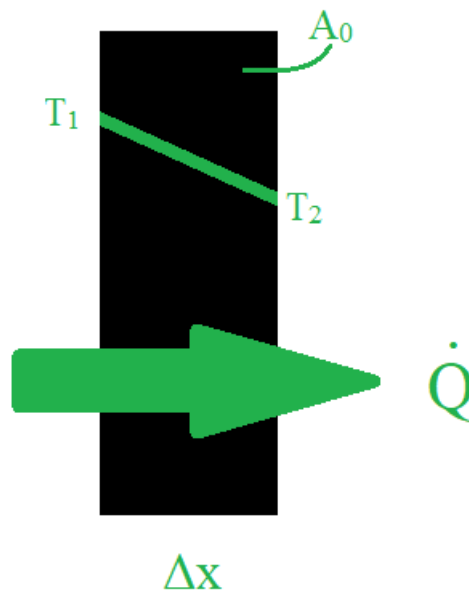


Figure 2.1.1 Heat conduction through a wall

Equation (2.1) is named after Jean Baptiste Joseph Fourier as he published the correlation in 1822, namely Fourier's law of heat conduction (Çengel, 2017) (Negash, 2017).

Conduction is often interchanged with diffusivity, which also describes molecular movements. Diffusivity is a measure of heat transfer rate in a material, and is given by conductivity divided by density and specific heat (Crank, 1975).

2.1.1.1.1 Thermal conductivity

Specific heat or heat capacity, c_p , defines a material's ability to store thermal heat. A large heat capacity value is consistent with the ability to store energy. For example, water with $c_p = 4.17 \text{ kJ/kg}^\circ\text{C}$ can store almost 10 times more energy than iron with $c_p = 0.45 \text{ kJ/kg}^\circ\text{C}$. On the contrary, the **thermal conductivity** gives information about the ability to conduct the heat, which for water and iron are, $k_{\text{water}} = 0.607 \text{ W/m}^\circ\text{K}$ and $k_{\text{iron}} = 80.2 \text{ W/m}^\circ\text{K}$ at 20°C . Hence iron conducts heat faster than water.

Resultingly, water is a poor heat conductor, but terrific for thermal energy storage. The conduction term refers to the transfer of energy as a result of interaction between particles (Çengel, 2017).

Material	Thermal conductivity at 20°C [W/mK]
Quartz	9
Granite	2-4
Marble	2-3
Limestone	2
Shale	1-2
Schist	2.5-4.5
Sandstone	2
Iron	80.2
Water	0.6
Air	0.03
Copper	400
Acrylic	0.2
PEM–Polyethylene Muffler	0.4

Table 2.1.1 List of thermal conductivity for some materials

2.1.1.1.2 Convection

Whenever a fluid is in motion over a solid and there are temperature differences between the fluid and solid, the convection heat transfer is activated. Convection is transfer of heat due to bulk movement. Conduction enhanced by convection will increase the rate of heat transfer. Convection is divided into two, based on the reason for the fluid movement. If the movement is caused by external forces (fan, pump) the convection is considered forced, whereas natural convection is caused by buoyancy forces encouraged by temperature/density difference.

The rate of heat convection is expressed by Newton's law of cooling:

$$Q_{conv} = hA_s(T_s - T_\infty) \quad (2.2)$$

h = Convection heat transfer coefficient [W/m²K]

A_s = Surface area [m²]

T_s = Temperature at the surface [°C]

T_∞ = Temperature of the fluid sufficiently far from the surface [°C]

Advection is transport of a substance by bulk motion, and thermal advection is often confused with convection. Generally, a fluid convects heat in one direction, whereas the heat by thermal advection spreads heat in all directions (Incropera, DeWitt, Bergman, & Lavine, 2007).

2.1.1.2 Combined Convection and Conduction Heat Transfer

Heat transferred to the internal fluid from the external fluid through the cylinder wall is calculated from equation 2.3 (EngineersEdge, 2019). The equation combines heat transferred by convection through the fluid layers and conduction through the cylinder tube.

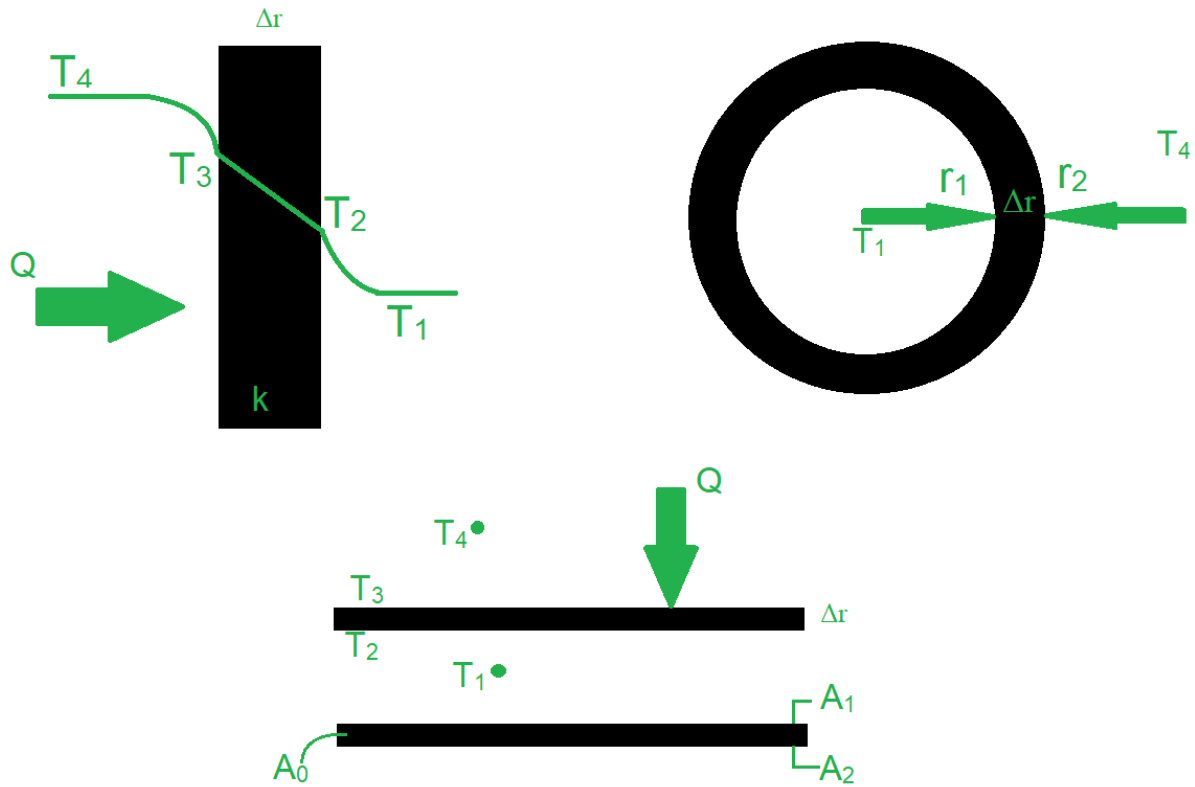


Figure 2.1.2 Cylindrical heat transfer

$$Q = UA_0\Delta T \quad (2.3)$$

$$\Delta T = (T_1 - T_2) + (T_2 - T_3) + (T_3 - T_4) = T_1 - T_4 \quad (2.4)$$

$$U = \frac{1}{\frac{A_0}{h_1' A_1} + \frac{A_0 \Delta r}{k A_{tm}} + \frac{A_0}{h_2' A_2}} \quad (2.5)$$

A_0 = Cross section area

ΔT = Temperature difference

U = Overall heat transfer coefficient

A_1 = Inner Area

A_2 = Outer Area

A_{lm} = Logarithmic mean surface area

Δr = radius ($r_2 - r_1$)

h'_1 = Convective heat transfer coefficient internally

h'_2 = Convective heat transfer coefficient externally

k = Thermal Conductivity of the material.

A measure of the heat energy obtained internally throughout the loop can be calculated by help of the specific heat

$$Q = \dot{m}c_p\Delta T \quad (2.6)$$

\dot{m} = mass travel per time

c_p = Heat capacity

$\Delta T = T_{out} - T_{in}$

2.1.2 Fluid Mechanics

To gain heat from the underlying rock layers, a pipeline is submersed into the ground and back. Fluid at a low temperature flows through the tube and reach returns to the surface at a higher temperature. In the pipe, the fluid can flow by different patterns, and this influences the amount or rate of heat conducted from the ground. To obtain information about the internal and external fluid behavior, this chapter uncovers methods of analyzing.

2.1.2.1 *Equation of state*

Equations relating a fluids pressure, temperature and specific volume are called equations of state. The most famous equation of state is perhaps the ideal gas law, founded by J. Charles and J. Gay-Lussac in 1802:

$$PV = znRT \quad (2.7)$$

P = Pressure

V = Volume

z = Compressibility factor

n = Number of molecules

R = Gas constant

T = Temperature

Where $z = 1$ for ideal gases. From the equation, the relation of pressure and temperature is obtained. A change in pressure will cause a change in the same direction for temperature. I.e. an increase in pressure will cause the particles to move at a higher rate and thus increase the temperature in the matter. This is important for the working cycle of heat pumps.

2.1.2.2 Dimensionless Numbers

Different dimensionless numbers helps obtain information and evaluate properties and mechanisms of flow and heat transfer (Kreith, 2000).

2.1.2.2.1 Reynolds number

An “ideal” flow, where water particles flows linear is laminar flow, and flow where particles moves in all directions is turbulent. Flow patterns in between are transient. To categorize if the flow has dominant inertial or viscous forces, the dimensionless Reynolds number is used, given by

$$Re = \frac{\rho v D}{\mu} \quad (2.8)$$

ρ = Density of fluid

v = Velocity of fluid

D = Diameter of pipe

μ = Dynamic Viscosity of fluid

Inserting valid numbers in the equation and comparing to the bellow table gives the flow regime, where

$Re < 2300$	Laminar flow – predictable, slow mixing
$2300 < Re < 4000$	Transitional, turbulent outbursts
$Re > 4000$	Turbulent – unpredictable, rapid mixing

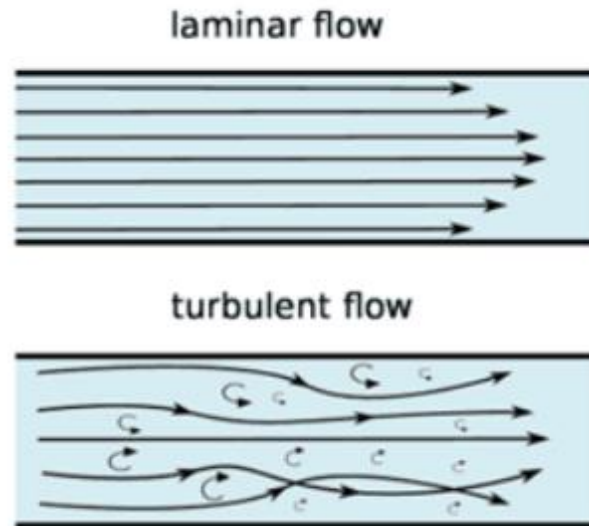


Figure 2.1.3 Laminar and turbulent flow regimes

Accordingly, ordered motion of linear streamlines have the lowest Reynolds number. High viscosity and low density increase the probabilities of having laminar flow, where the viscous forces suppress random fluctuations and maintains the fluid in lines. In the case of a high Reynolds number, $Re > 4000$, the fluid will undergo disordered motion and velocity fluctuations without patterns. For turbulent flow, which is most often encountered in the nature, the inertial forces are too large for the viscous forces resulting in fluctuations. Over a region, the flow can be transitional as it alters between laminar and turbulent until it reaches fully turbulent flow. The geometry, surface roughness, flow velocity, temperature and type of fluid affects the transitional period. Whether the fluid is laminar or turbulent reflects its uniformity. A layered flow is more likely to obtain temperature gradients than turbulent flow where the molecules are constantly mixing (Çengel, 2017).

Some flow patterns consist of a combination of laminar and turbulent flow. The smoke from a cigarette starts as a laminar flow and develops into turbulent flow creating plumes. The pattern result from a combination of several factors. From the cigarette, the smoke has a high temperature and has thus lower density than air and rises in a laminar flow. Smoke rising in a laminar pattern will have temperature gradients, where the center of the smoke holds the highest temperature. Heat transfer to the surroundings will decrease the outer temperature, consequently the flow acquires a nonuniform velocity. The velocity variation causes turbulence and change of flow pattern. The surrounding air will typically involve bulk flow or other disturbances which the laminar smoke may collide with. The collision will disturb the smoke pattern and resultingly the transitional or turbulent flow is obtained (Çengel, 2017).

2.1.2.2.2 Grashof number

Although the fluid flowing in the tube is under the influence of forced convection, the surroundings are influenced by natural. Natural convection flow regime is presented by the Grashof number, a dimensionless number describing the ratio of buoyancy force to the viscosity force (Monteith & Unsworth, 2013).

$$Gr_L = \frac{g\beta(T_s - T_\infty)D^3}{\nu^2} \quad (2.9)$$

g = Gravitational Acceleration, m/s^2

β = Coefficient of volume expansion, $1/K$

T_s = Temperature of the surface, $^\circ C$

T_∞ = Temperature of the fluid sufficiently far from the surface, $^\circ C$

D_C = Characteristic diameter of geometry, m

ν = kinematic viscosity of the fluid, m^2/s

A Grashof number larger than 10^9 indicates turbulent flow regime.

As well as being influenced by forced convection, natural convection can occur also inside of the pipeline. For determination of which forces are dominant, the value of Gr_L/Re_L^2 can be calculated, where

$$\frac{Gr_L}{Re_L^2} \gg 1 \quad \text{natural convection dominates}$$

$$\frac{Gr_L}{Re_L^2} \ll 1 \quad \text{forced convection dominates}$$

$$\frac{Gr_L}{Re_L^2} \approx 1 \quad \text{Both natural and forced convection effects must be considered}$$

2.1.2.2.3 Prandtl number

Prandtl number is another dimensionless number describing the fluid behavior, by the relationship of momentum/viscous diffusivity to thermal diffusivity (Çengel, 2017). In addition to informing about the type of fluid, it says something about the hydrodynamic boundary layer thickness.

$$Pr = \frac{c_p * \mu}{k} \quad (2.10)$$

c_p = heat capacity

μ = viscosity

k = heat conductivity

A higher Prandtl number corresponds to the momentum diffusivity being higher than the thermal diffusivity. Measurements done by X. Yang and S.C. Kong in late 2017, states the dependency of Prandtl number for Rayleigh number in transition from stable to unstable flow in addition to its influence on the flow pattern. Where the viscous diffusivity is small compared to the thermal (low Prandtl number) the flow structures are discovered to be more complex. For a heated tube in a cold-water tank, the stability or symmetry of the heated water increases with higher Prandtl number (Yang & Kong, 2017). A high Prandtl number is normal for heavy oils, where heat diffuses very slowly relative to momentum, and the thermal boundary layer is thinner than the velocity boundary level. Liquid metals have a higher heat diffusivity rate and a thicker thermal boundary layer than velocity boundary layer (Çengel, 2007).

2.1.2.2.4 Peclet number

A relation of heat transfer by advection and diffusion is given by the Peclet number. This is helpful for estimation of the importance or impact of the different heat transfer processes.

$$Pe = \frac{vD}{\alpha} = Re \cdot Pr \quad (2.11)$$

v = Fluid velocity

D = Characteristic length

α = Thermal diffusivity of the fluid

Where the resulting Peclet number demonstrates the fluid transport dominating;

Pe < 1	Diffusion dominates
Pe > 1	Advection dominates
Pe = 1	Similar influence

As a product of Reynolds and Prandtl number, the Peclet number is similarly not a material constant, nevertheless it is often calculated to find the type of heat transfer in geological settings (Shires, 2011) (Rapp, 2017).

2.1.2.2.5 Nusselt Number

Named after Wilhelm Nusselt, the Nusselt number is a heat rate coefficient representing the relation of conductive and convective heat transfer mechanism through a layer of fluid (Çengel, 2017).

$$Nu = \frac{h'D}{k} \quad (2.12)$$

h' = Convective heat transfer coefficient

D = Characteristic diameter

k = Thermal conductivity

Nu < 1 Conduction dominates

Nu > 1 Convection dominates

Nu = 1 Similar influence

2.1.3 Other types of flow

Internal/external

Depending on the flow area, it is determined whether it is internal or external. In a pipe, the fluid flow is typically internal, as the flow is in a confined space. Unbound fluid flow over a plate or a wire, where the flow travels over a surface, is external flow (Çengel, 2017).

Natural/forced

Based on the working force of the flow, it is decided whether the flow is natural or forced. A natural

flow is enforced by natural or internal causes such as the buoyancy effect. Forced flow is influenced by a fan, pump or other external forces (Çengel, 2017).

Steady/unsteady

Where a flow has constant velocity, temperature and other properties at the same point with time, the flow is considered steady. Unsteady flow is the opposite. Unsteady flow has usually inconstant volume, mass and/or total energy content within the same section (Çengel, 2017).

Dimensional flow

Fluid flow can be one-, two- or three-dimensional, depending on the flow pattern. Three dimensional is most often encountered, i.e. in a pipe where the particles can move in all directions. Nonetheless, if the movement in some directions are small compared to the other direction(s), the flow can be considered two- or even one-dimensional (Çengel, 2007).

Newtonian fluids

Sir Isaac Newton defined another way of dividing fluids depending on the relation of shear stress to the rate of deformation. Newtonian fluids have a deformation rate linearly proportional to the shear stress. Non-Newtonian fluids have a nonlinear share stress and rate of deformation. Common Newtonian fluids are water, and air where the viscosity is independent of shear stress applied (Çengel, 2017).

2.1.4 Density Dependence of Temperature

The density of a substance tends to decrease with temperature. For water, the highest density is reached at 4 °C, where on either side the density decreases (Lumen; Shapley, 2011). Resultingly, for a container containing fluids of different temperatures, the fluids of highest temperature will hold the lowest density and is thus found at the top of the container. Increasing the depth of the container, the density will increase and temperature decrease. An approximation for the density (kg/m³) dependence of temperature (°C) is presented by the Kell formulation {Jones, 1992 #68}.

$$\rho = (999.83952 + 16.9455176T - 7.9870401 \times 10^{-3}T^2 - 46.170461 \times 10^{-6}T^3 + 105.56302 \times 10^{-9}T^4 - 280.54253 \times 10^{-12}T^5)/(1 + 16.897850 \times 10^{-3}T) \quad (2.13)$$

ρ = Density

T = Temperature

Table 2.1.2 presents the density of water for some temperatures.

Temperature (°C)	Density (kg/m ³)
100	958.4
60	983.2
30	995.65
20	998.207
10	999.703
4	999.972
0	999.84
-10	998.117

Table 2.1.2 Water density vs. temperature

As explained by M.P.M Reddy regarding the ocean, the density in a column may well not increase linearly downward (Reddy, 2001).

Normally density increases with depth in the ocean as a natural tendency towards gravitational stability. However, the density does not increase uniformly with depth in the ocean. In the low latitude equatorial and tropical regions, there is a thin layer of low and uniform density in the upper zone, then there is a layer of rapid increase in density with depth [...] in the deep zone there is a very slow increase of density with depth.

The extract refers also to the temperature distribution due to the coherence of temperature and density.

2.1.5 Flow Visualization

A fluid undergoing natural convection has a flow pattern difficult to obtain. The movement occurs generally only in parts of the fluid, so flow meters are of no good use. A method to visualize the flow pattern is described by Baker (1966), whom discovered a valuable method of visualizing flow pattern by use of electrodes in a solution containing a pH indicator (Baker, 1966) (Focke & Knibbe, 1986).

2.1.5.1 Electrolysis

By use of two electrodes connected to a power supply, the system undergoes electrolysis. The electrons in the electrodes starts to flow towards one side, namely the cathode. The cathode will attract positively charged cations in the fluid, whereas the other electrode, the positive anode, attracts anions. Between the electrodes and attracted atoms, electron exchange occurs. This electron exchange causes chemical changes which can form solids or gases.

Electrodes connected to a power supply placed in a water container, will thus attract water molecules; the negative oxygen is attracted to the anode while the positive hydrogen atoms are attracted to the cathode. On the cathode, the hydrogen atom in the fluid can receive an electron and is thus no longer attached to the oxygen. The single neutral hydrogen can form a bond with a positive hydrogen atom, resulting in H_2^+ in the gaseous form. This hydrogen binding appears as a small gas bubble attached to the cathode. As the bubble grows larger (by more of the similar reactions) the bubble may disperse and flow towards the top of the water container. The amount of H^+ in the liquid solution is thus reduced, and the concentration of OH^- increased (FuseSchool, 2016).

2.1.5.2 pH

pH is a measure of the amount or concentration of H^+ and OH^- ions present in a solution. The pH scale is logarithmic and ranges from 0-14, where the pH number indicates the negative exponential value.

$$pH = -\log[H^+] \quad (2.14)$$

$[H^+]$ = concentration of hydrogen

Hence, an increase in H^+ will decrease the pH value and make the solution more acidic. An increase of OH^- (resultingly a decrease in H^+) increases the pH value and makes the solution more basic or alkaline (Grønneberg, 1997). pH is measured by electrodes (pH Meter), pH paper or use of fluid pH-indicators. By applying a fluid pH-indicator to a solution, an idea of the pH value can be obtained. The table below presents the color appearance for different pH indicators at given pH values.

Universal indicator components			
Indicator	Low pH colour	Transition pH range	High pH colour
Thymol blue (first transition)	Red	1.2 – 2.8	Yellow
Methyl orange	Red	3.2 – 4.4	Yellow
Methyl red	Red	4.8 – 6.0	Yellow
Bromothymol blue	Yellow	6.0 – 7.6	Blue
Thymol blue (second transition)	Yellow	8.0 – 9.6	Blue
Phenolphthalein	Colourless	8.3 – 10.0	Fuchsia

Table 2.1.3 (Wikipedia, 2019)) The color range of pH indicators

Where the addition of a fluid pH indicator allows an easy method of determining the pH, the pH paper allows a more precise indication as more pH indicators are used. The use of a pH meter is considered the most accurate measurement, where the pH value can be displayed with two decimals.

2.1.6 Thermodynamics

The study of energy transfer, often in terms of heat and work, is known as thermodynamics. The essentials of thermodynamics are stated through two laws (Michaud, 2005). The first law of thermodynamics states the principle of energy conservation, how energy is transferred and not be created. The second law states energy with properties of quality and quantity, and the fact that energy is always transferred to the substance containing the least of it, i.e. heat transfer from a room to an ice cube (Çengel, 2017).

2.1.6.1 Enthalpy

A way to define a substance internal energy is by enthalpy. Enthalpy (h) is the sum of a systems internal energy and the product of its pressure and volume, given by

$$h = u + PV \quad (2.15)$$

h = Enthalpy

u = Internal energy

P = Pressure

V = Volume

The enthalpy of a system is difficult to measure directly, and a table for the exact fluid must be provided to calculate the value (OpenStax, 2016). A table typically provides enthalpy in [kJ/kg] for a given fluid at a given temperature. The enthalpy for temperatures in-between can be found by interpolation.

2.1.6.2 Entropy

Entropy describes the disorder of a system. It is an amount of possible microscopic states, which (at constant pressure) increases with temperature for fluids, and decreases with temperature increase for gases (Michaud, 2005). A change of entropy can be caused by mass flow, heat transfer or irreversibility, and the entropy is therefore commonly used for calculations of those properties. Entropy, S , is defined as

$$dS = \left(\frac{dQ}{T}\right)_{int\ rev} \quad (2.16)$$

S = Entropy

Q = heat

T = Temperature

This applies for internally reversible cycles (int rev).

By use of the Boltzmann constant, k , and the number of possible microstates of the system, the Boltzmann relation presents the entropy as

$$S = k \ln N \quad (2.17)$$

S = Entropy

K = Boltzmann constant

N = Number of microstates of the system

The value of both enthalpy and entropy is commonly found from tables or graphs.

2.1.6.3 *Heat Pump*

A heat pump is a device working against the normal heat transfer pattern, where they essentially transfer heat from low temperature areas to warmer. Clausius' statement for the second law of thermodynamics states the transformation of heat from a colder to a warmer body can only occur with input from an external power source. An engine for this process can be the reversed Carnot cycle.

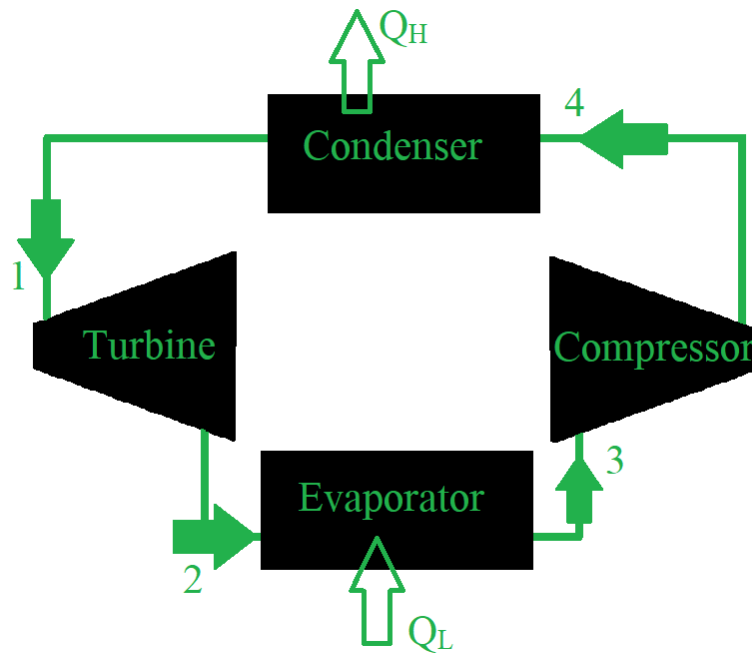


Figure 2.1.4 A typical reversed Carnot cycle

Where the Carnot Cycle creates work while transferring energy from warm to colder places, the reversed Carnot Cycles/ refrigerator/heat pump requires work to convert energy in the form of heat from cold elements to warmer. (Boelter, Karr, Klemp, & Sternitske, 2018). The stages of the Carnot Heat Pump (Reverse Carnot Cycle) involves:

- 1 → 2: Isentropic Expansion
- 2 → 3: Isothermal Expansion
- 3 → 4: Isentropic Compression
- 4 → 1: Isothermal Compression

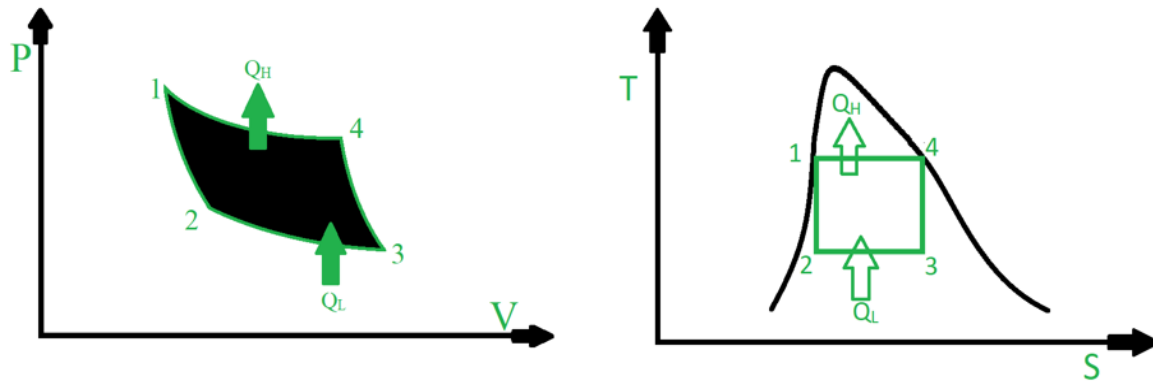


Figure 2.1.5 Plots providing pressure vs. volume and temperature vs entropy for a reversed Carnot cycle

In the turbine, undergoing isentropic expansion, the pressure of the fluid decreases, resultingly, so does the temperature. This is stated by the equation of state and seen by the above graphs, as the volume is barely increasing compared to the pressure drop. Exiting the turbine, the fluid receives heat in the evaporator while volume is increased, hence the system undergoes isothermal expansion. Passing the compressor, the pressure and resultingly the temperature is increased, while volume is decreased. In the condenser, heat is withdrawn at constant temperature while the volume decreases and pressure increases (Shet, Sundararajan, & Mallikarjuna) (Sherwin & Horsley, 1996) (ur Rehman, 2015). The work required for the cycle is generally given by

$$W = -Q_H - Q_L \quad (2.18)$$

W = Work

Q_H = Heat Supplied (value is negative)

Q_L = Heat Delivered

The efficiency of the cycle is calculated by:

$$COP = \frac{\text{Heat Absorbed}}{\text{Work Supplied}} = \frac{T_1 (s_4 - s_1)}{T_1 (s_4 - s_1) - T_2 (s_3 - s_4)} = \frac{T_1}{T_1 - T_2} \quad (2.19)$$

$T_{1,2,3,4}$ = Temperature at the different stages

$S_{1,2,3,4}$ = Entropy at the different stages

2.2 Geothermal Heat

At the time the earth was formed 4.6 billion of years ago by colliding meteorites and debris, the kinetic energy from the movement was converted to heat energy. As an enlarging amount of matter collided, the energy increased and remained somewhat trapped in the center due to insulation of the matter. As a result of the energy transfer in the form of convection and conduction, a constant outwards flow of heat from the center through the mantle up to the crust spreads the internal heat. Radioactive decay which transmits heat contributes to earth heating, mainly in the crust and mantle. The radioactive decay originates from uranium, rubidium, potassium and other sources as radioactive elements dissolves into other elements and thus creates energy. A third source of heat descends from gravitational pressure; toward the center of the earth, pressure increases, and the substances are consequently heated.

The inner core is at present calculated to be 5-6000 °C, but then the temperature decreases with each layer outwards (Boden, 2017). The general geothermal heat gradient from the surface is approximately 25 °C/km, depending on the underlying rock layers (Finger & Blankenship, 2011). Old tectonic plates with low permeability can have temperature gradients as low as 7 °C/km, whereas geographical areas along tectonic plate boundaries tend to have higher gradients, sometimes revealed by hot springs or volcanoes (IEA 2011).

2.2.1 Geothermal Rock Differences

By use of geological maps, testing of local water sources and analysis of the elements in the soil, sites appropriate for geothermal heat usage can be found (Budd, Gerner, & Suzanne). The underlying rock type will influence the characteristics of geothermal reservoirs. The rock types can be divided into three: igneous, metamorphic and sedimentary, where the latter is normally found as a thin overlying layer at the surface covering the two former which originates from the earth interior (crust and mantle). Rock and mineral composition affects thermal parameters as conductivity and other physical properties. Sandstone and limestone (sedimentary rocks) generally serves as excellent geothermal reservoirs. Quartz-rich sandstone have virtuous conductivity capacity and permeability which makes it preferred over granite, as heat exchange can occur by convection not solitary conduction. Where there is fluid flow in the ground, an increase of permeability in low-permeable matrix' can however be done by applying forces (fracking) so the rock obtains fractures for fluid flow. This is desired as fluid flow in the ground results in convection of heat transfer in addition to the conduction, and thus increases the total heat transfer to the tube (Balkan Pazvantoğlu, Erkan, & Şalk, 2017).

The thermal conductivity in rocks varies, in addition to permeability and porosity, with composition, anisotropy and the fluid filling of pores. Whereas some minerals have excessive heat conductivity properties (quartz, hematite), others have rather poor (clay, gypsum, organic material). Characteristically, metamorphic rocks contain high quartz contents and low schist and gneiss contents,

thus they are often great heat conductors. The texture and grain size of the minerals along with the anisotropy also affects the conductivity. For a horizontally layered rock (i.e. schist), the horizontal conductivity is expected to be enlarged compared to the vertical. As fluids have lower conduction capabilities than solid matrix, an increase in porosity of the rock will result in a decrease in bulk conductivity. (Balkan Pazvantoğlu et al., 2017).

2.2.1.1 *Local Geology*

The overall subsurface in Norway consists of old, hard rocks. The bedrock can be divided in three; Basement, Caledonian Orogeny and Oslo Graben. The Basement is the oldest, containing rocks older than 600 million years, made up mainly by granite or gneiss. The Caledonian orogeny, originating 350-600 millions of years ago, contains mainly schist, slate, marble and greenschist. 280 million years ago volcanic activities created Oslo Graben, which accordingly contains volcanic and igneous rock (Gjølberg, 2011). Rogaland county is built up by both Basement (southeast) and Caledonian Orogeny (northwest). In the Jæren region, the subsurface commonly consists of a layer of drift and phyllite above the Basement (Thorsnæs, 2019, 5th of February). In Bryne, the metamorphose of the phyllite continued converting the rock into mica with layers of quartzite and schist, and migmatite, which is located below a 15-20 m thick layer of moraines sediments (NGU, 2019). The subsurface in the area is thus appropriate for heat extraction.

2.2.2 *Utilization of Geothermal Heat*

The inner heat in our planet can be utilized by three principal methods by the use of one or several drilled pipelines: power generation, direct use and geothermal heat pumps. The former is dependent of high temperatures above 100 °C and is the least common way of applying geothermal heat. Direct use of the higher temperature is the most efficient method as there are no conversions where energy can be lost. The temperature underground should in this case range from 50 to 100 °C and the heat is in this case normally used for heating of houses or food drying. Easier to get use of, is the geothermal heat pumps which can be used for heating and cooling by use of underground wells in combination with a heat pump. Considering Earth as a thermal “bank”, heat can be deposited underground during summertime when the surface temperature is high, and one desires colder indoor temperature. This submersed heat energy along with prior elevated underground temperature can be withdrawn during colder seasons for heating of houses. The idea behind drilling down for heat gains stems from the reason that heat transportation demands less energy than heat generation (Boden 2017).

Although temperature and rock conductivity varies around the globe, the temperature in the ground can in most places be utilized for some sort of heating and/or cooling. Although the temperature obtained often increases near or along tectonic plates, at hot spots or volcanoes, the content of the magma may be of acidic substances which can cause damage on equipment. Accordingly, several aspects have to be considered when planning a geothermal system. There are to this date no projects in Norway regarding

geothermal power generation, direct use or deep geothermal heat, however shallow geothermal heat utilization is commonly found in both private housing, industry buildings and municipal facilities.

2.3 Geothermal systems

There are different ways of extracting the geothermal heat, where the main categorizations are: Open or closed loops, deep or shallow depths.

2.3.1 Deep or Shallow

Ref chapter 2.2, the temperature increases towards the center of the earth. Thus, drilling deeper into the earth will result in encountering higher temperature than shallow. Anyhow, drilling deeper is more expensive and requires more materials resistant to the higher pressure, which is why shallow systems are more commonly used. Shallow geothermal heat is placed higher than 500 m down, where the temperatures are close to mid-atmospheric, typically 8-10 °C (Sharma, Shukla, & Aye, 2018) (Straalberg, 2013). A heat pump is needed to transform the obtained temperature into higher temperatures for heating purposes. Deep geothermal systems, at a depth of typically 1-2 km, will withdraw severely higher temperatures with possibilities of direct usage of the heat, or power generation.

2.3.2 Open or Closed

Open or closed systems describes the tube system collecting the heat. Most common is the closed loop, where a U-tube is immersed into a hole in the ground, a fluid is pumped down one end to gain temperature while traveling to and from the bottom, and returns to the surface in the other end, at a higher temperature. Open systems can be placed where there are underground water reservoirs. One pipe immersed in the water extracts the reservoir water to the surface, where heat is extracted. Another pipe transfers the now colder ground water back to the reservoir. The reinjection should preferably be located at a distance and/or at a level beneath the pipe sucking up the water.

Open loops are considered to bring a larger impact on the nature as the water reservoir is altered, whereas the closed systems influences the ground environment only by drilling the hole where the U-tube is to be set. Due to the direct use of the underground water source, the efficiency of open loop systems are generally larger than for closed loops, where the heat have to be transferred through rocks and tube layers. As the subsurface water contains substances (minerals or organic particles), corrosion is likely to occur in the pipelines, leading to need of special tubing material. (Egg & Howard, 2010).

Ground water reservoirs could also be an environment for closed loops, as the water conducts heat to the U-tube. Flow of ground water can often increase the rate of heat transfer, as the convection forces will enhance the heat transfer. Additionally the flow provides a constant temperature as it is unaffected by heat energy drawn from the reservoir to heating of the U-tube. Without water flow providing constant inflow of new water with a constant temperature, the reservoir temperature could decrease as the heat is transferred from the ground to the indoor. On the other hand, closed loops located where there is no water flow can utilize the ground as heat storage during summertime. By transporting heat down during the summertime, this heat can be transported up during colder days.

2.3.3 Drilling and sizing

There are several methods of drilling geothermal wells. In Norway where the continental shelf contains relatively hard crystalline rocks, the DTH, down-the-hole hammer, is commonly used. The DTH is an efficient way of drilling, as it can drill down to a depth of 100 meters in 1-2 days. Other kinds of lithology requires other types of drilling methods. This method consists of a bit attached to a tungsten carbide buttons, entrenched on a rotating hammer. A stream of compressed air from the drilling string delivers compressed air to the slowly rotating hammer. Drilling cuttings from the rock is removed through the annulus by the airflow. Selections of well sizing and material is crucial to obtain high heat conduction and low pressure drop and friction. The diameter of the casing varies as it depends on the yield of the well, but a diameter of 100-200 mm is normal, large enough to fit an appropriate pump (Banks, 2012; Erdogan, 2010).

When the drilling hole is finished, the U-tube allowing for heat transport to the surface is submersed. The U-tube should be small enough in diameter for all of the inside fluid to be affected by the heat transfer, and large enough for a great amount of heat to be transferred; typically between 19 and 38 mm. The rest of the borehole may be filled with grout or ground waterter (Erdogan, 2010). Traveling through the u-tube, the fluid will experience friction caused by internal forces and drag against the tube walls, and resistance caused by heat exchangers, trapped air bubbles, bends or other constrictions. The pressure drop applied must be outbalanced by a pump adjusted for the concrete pressure drop to ensure fluid flow (Banks, 2012). The pump can be placed above or below the surface.

3 The Geothermal System at Bryne VGS

The geothermal heat system at Bryne VGS consists of 34 energy wells ranging from the surface down to a depth of 200 m. Starting in August 2014, the shallow, closed wells have since provided the school with heat for warming of water and the indoor. The NGU (Norwegian Geology Exploration) map of the area proves a layer of moraines laying above phyllite undergoing metamorphose. The metamorphose turns the phyllite into mica with quartzite and schist, whereby the primary is known to have a high heat conductive capacity (table 2.1.1) (Ramstad, 2012).

3.1 Operation Planning

In conjunction with the merge of the two high schools Time and Bryne, the new Bryne VGS in consent with the TEK rules (building code) was built including internal renewable energy sources. The system includes 34 geothermal wells, two heat pumps, four windmills, 86 m² of sunlight collectors (both flat-plate collectors and vacuum tube collectors), two gas boilers and 40 m² photovoltaic cells. The main amount of energy was to be gained from the geothermal wells by use of the heat pumps, which is the abundant energy source system at the school. The heat pumps were to distribute heat to water tanks and radiators. The electricity needed for the geothermal system, should be gained by the other renewable energy sources (Nilsen, 2015).

To map the subsurface of the area for the geothermal wells, a test well was drilled at the accurate site in December 2011. Drilling to a depth of 200 m, they encountered different layers of sediments and rock, as well as water precipitations throughout the whole zone. The subsurface consists of a moraine layer down to a depth of about 15 m. Below is the rock layer consisting of micaceous schist with layers of quartzite and mica schist. For the test well, they used a well diameter of 140 mm, and casing with 17.50 m length. Information of the system is obtained from reports, sketches and online information (DNF, 2013) (EngineeringToolBox, 2003; PipeLife, 2007).

Figure 3.1.1 presents a sketch of the system, whit wrong dimension, only for informal use. All sketching is designed in Autodesk Fusion 360 and/or Paint. With the integration of CAD, CAM and CAE software, Autodesk Fusion 360 allows for 3D design, and is used for the 3D images in this paper (Autodesk).



Figure 3.1.1 A miniature model of the subsurface in Bryne

The miniature visualizations of the subsurface shows the inserted U-tube (black) and casing (green) in the moraine (brown with black dots) and rock layer (black with white dots). Dimensions are not correct.

A thermal response test in the well gave an effective heat capacity of 3.7 W/m·K. The test also proved the ground as unaffected by ground-water flow. The measurement of ground-water flow was done by drilling of 4 more wells. All five (including the test well) were emptied of water by pressurized air. Measurements of the time used for the underground to re-fill the wells and the height of the water/air boundary (measured in meters above the sea level) would reveal the impact of water flow. The test proved the area to be without impacts of ground-water flow, nevertheless, the developers states there may be some groundwater movements. As no ground water flow was found, the subsurface was considered to be a heat storage where heat could be withdrawn during the winter and delivered during the summer. The temperature in the ground was obtained by inducing a temperature sensor down the collector tube. The underground temperature vs. depth is displayed in figure 3.1.2. The temperature ranges from 8.1 to 8.8 °C, the overall mean temperature was calculated to be 8.4 °C. The test was executed in December 2011.

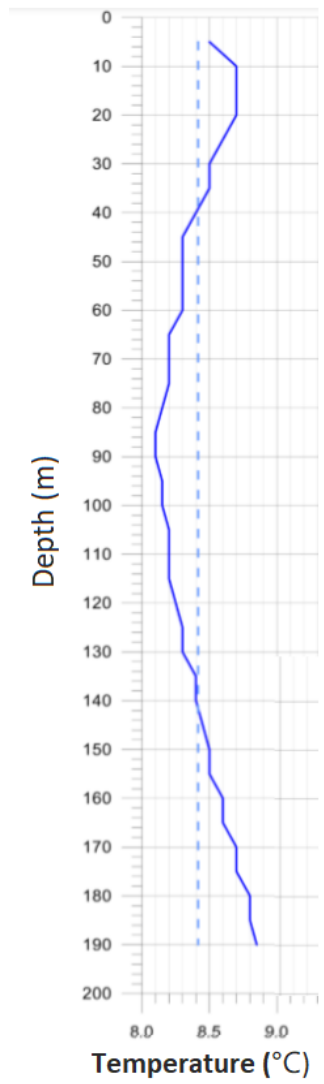


Figure 3.1.2 Temperature vs. depth, measured in the test well at Bryne VGS

3.2 Bringing the system to life

29 new wells were drilled, a total of 34, with a diameter of 115 mm, 18 m casing length and a distance of 7 m between each well. The casing runs through the moraine layer and a few meters into the solid rock. The casing is secured by bentonite in the crossing between the moraine and rock, and provides support to avoid collapse and avoids water fallout into the above layer, as infiltrating of water is common in case of overpressure. Below the casing depth, the drilling occurs without stabilizing casing, as boreholes in hard rock at this depth maintain its stability. As the water conveying capacity tends to be high in the area and found to be more than 1000 l/h, the drilled wells in the rock was quickly filled with water.

The test well proved the ground water level similar to the surface levels. Well covers are placed on the top of each well to prevent flood for the underground. The U-collector Muoci Tech turbo collector (PEM 40x2.4 PN8 SDR 17) was installed in each well, and propylene glycol was chosen to be the working fluid in the U-tube, containing 30 % glycol. Returning from the ground, all wells have proper isolation to avoid temperature loss at the surface. The pressure loss of each well was calculated to be maximum 107.6 kPa.

A sketch of a geothermal well I displayed in figure 3.2.1, and further on is a visualization of the geothermal energy system at Bryne.

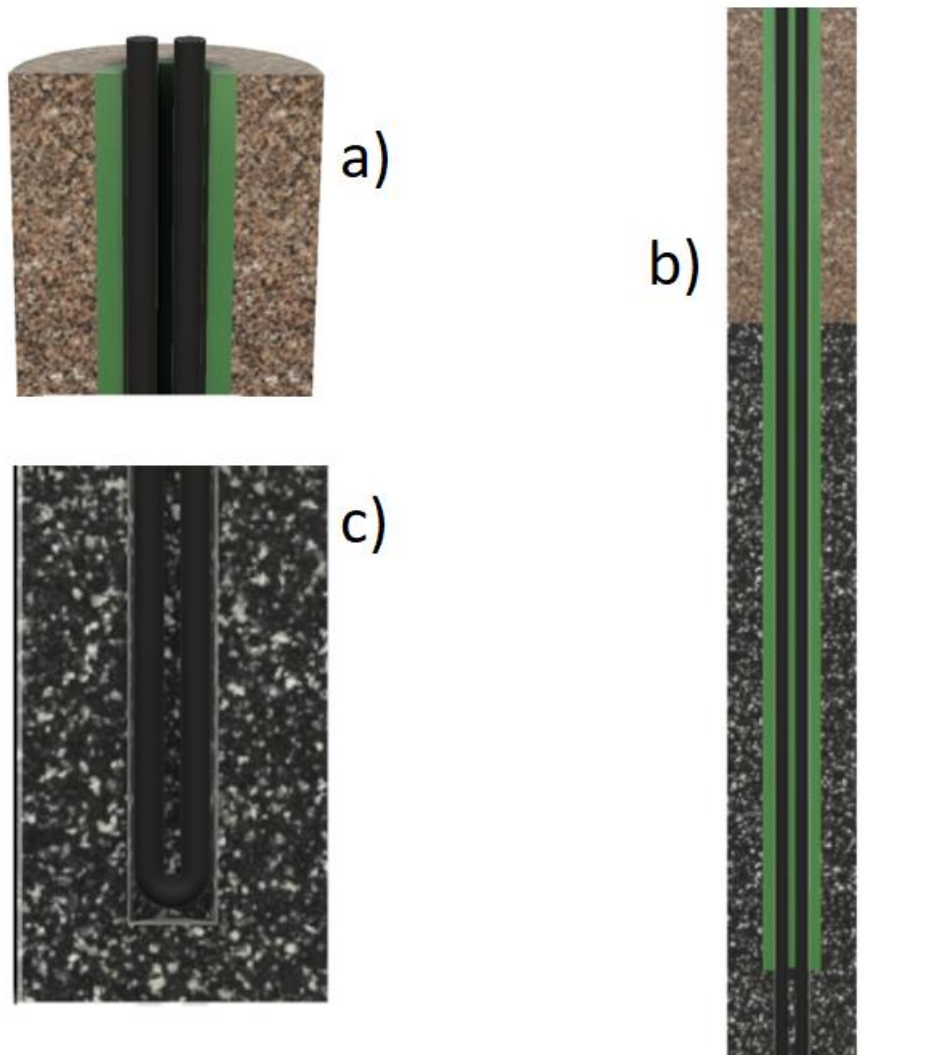


Figure 3.2.1 A model of the geology, U-tube and casing in Bryne

In figure 3.2.1,

- a) shows the top of the well, with the PEM U-tube (black) placed inside the casing (green) in the moraine laier (brown).
- b) displays the transition from moraine to rock, with the casing is set two meters further down than the moraine/rock boundary.
- c) displays the bottom part of the well; the bend of the U-tube and the surrounding micaceous schist

IWMAC is a digital tool providing live information from tools in the geothermal system. The webpage allows monitoring of different parts of the cycle, displays the temperature and pressure several places along the way.

An overview of the geothermal system is presented in figure 3.2.2, and is further described in chapter 3.2.1.

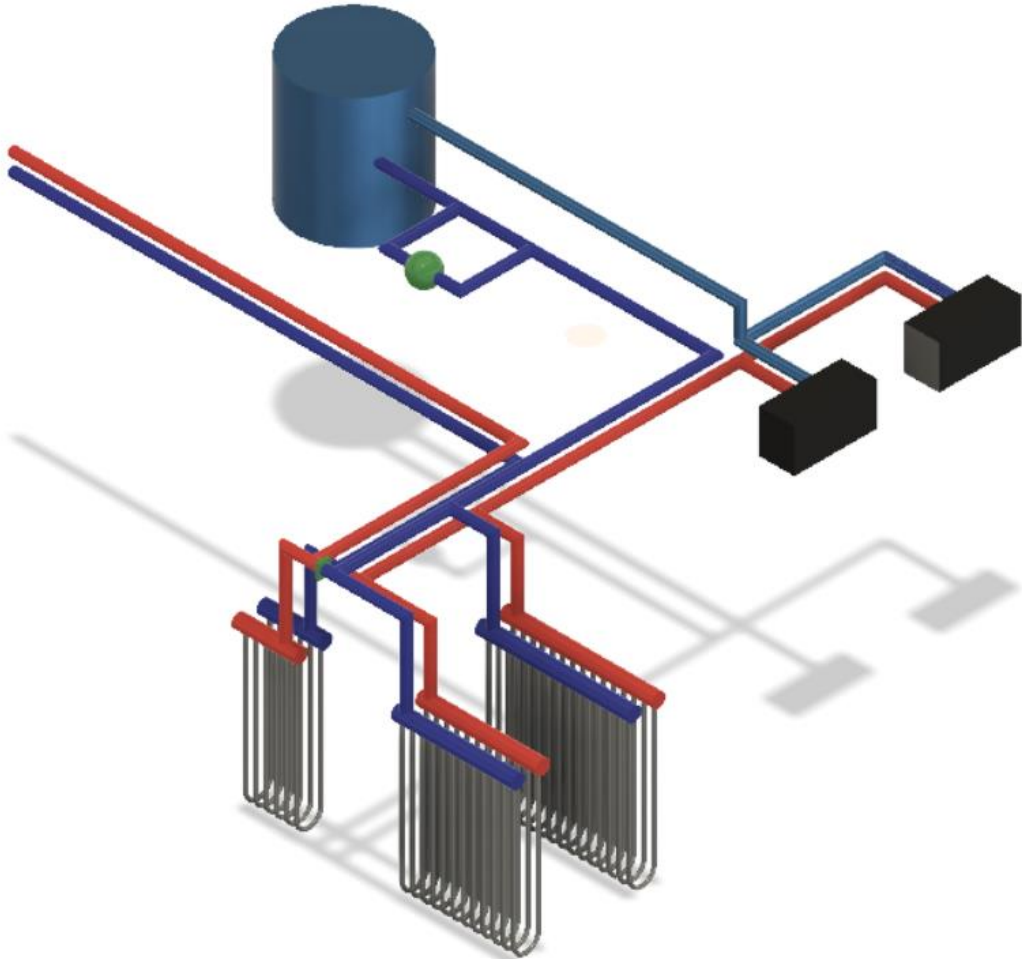


Figure 3.2.2 An overview of the geothermal system at Bryne VGS

3.2.1 Heating Cycle

As the building requires both heating and cooling, 6 wells are reserved for cooling, while the remaining 28 are used for heating. For the 28 wells for heating, the cold propylene glycol is submersed down the wells to the ground, where heat is conducted from the ground to the fluid in the U-tube. The heated glycol mix reaches the surface and is transferred to a larger tube. 12 and 16 wells leading to each tube. These two tubes are connected to transport heat to the heat exchangers. The transport of heat from the lowest part of the well is toward the heat pumps is illustrated on figure 3.2.3.

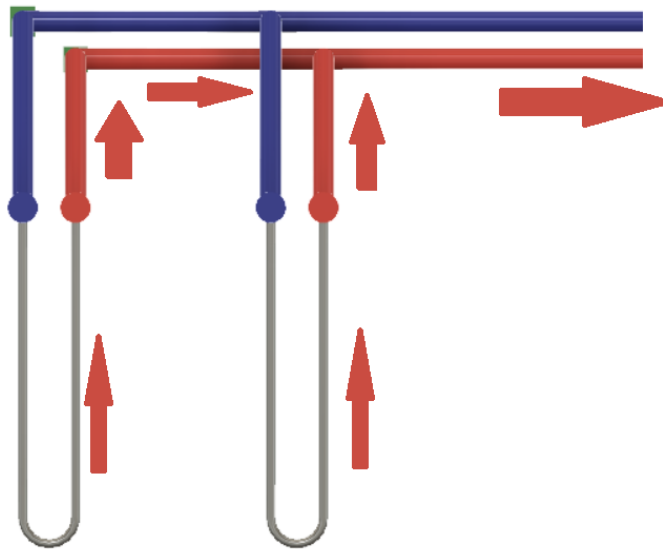


Figure 3.2.3 Visualization of the heat transport from the wells

Ongoing from Figure 3.2.3, the propylene glycol enters the heat pump working a reversed Carnot cycle. The heat obtained from the geothermal wells is transferred to the evaporator, where the heat is transmitted to the cooling agent of the heat pump for further use. The KFC cooling agent enters the evaporator from the heat pump side, at a low temperature, and leaves with a higher as heat has been transferred from the glycol. In three compressors, the KFC is compressed to reach a higher temperature, and ends up with a temperature around 80 °C when compressed to approximately 15 Bar. The fluid at that point enters the condenser, where heat is delivered to two water circuits for warm water and heating purposes. The KFC, after transferring the intended heat, is run through a valve (turbine) decreasing the pressure and the cycle is restarted. Figure 3.2.4 is delivered by DNF and presents schematically the heat pump system.

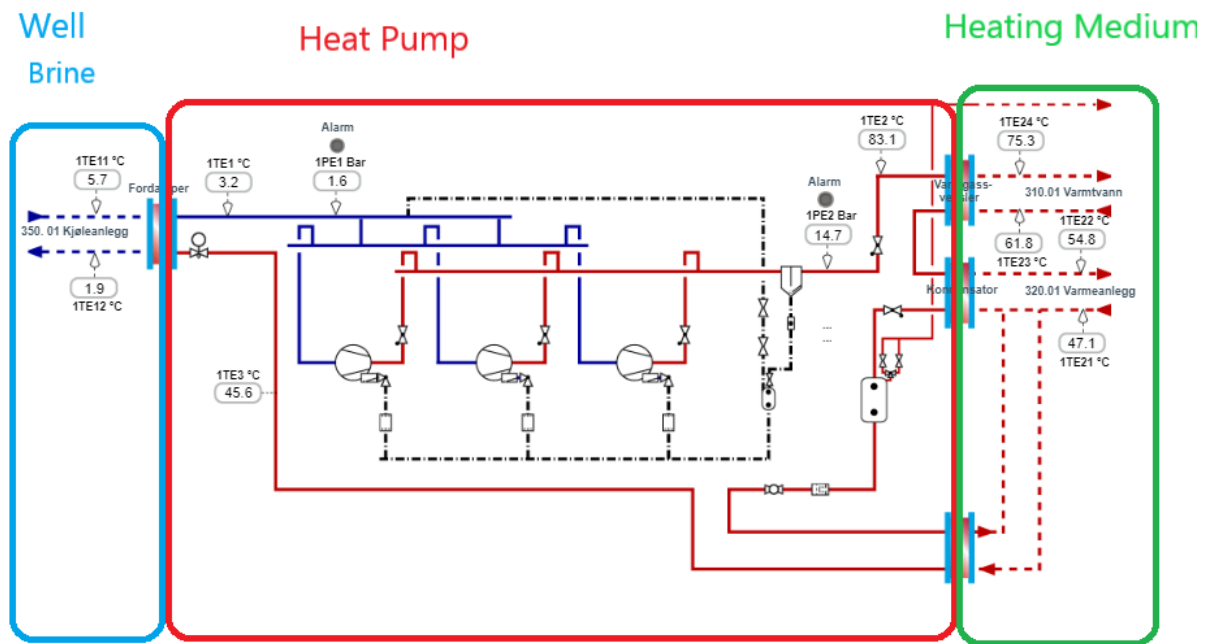


Figure 3.2.4 Heat Pump 1 (13.03.19 10:00), showing heat transfer from the wells (blue) through the heat pump (red) to the heating medium spreading the heat energy (green).

After passing on heat energy in the heat exchanger, the propylene glycol is transferred to the accumulator. The accumulator stores and may filter the fluid and maintains the of 30-70 glycol – water ratio for the cycle. The overall figure of the heat pump is presented in figure 3.2.5.

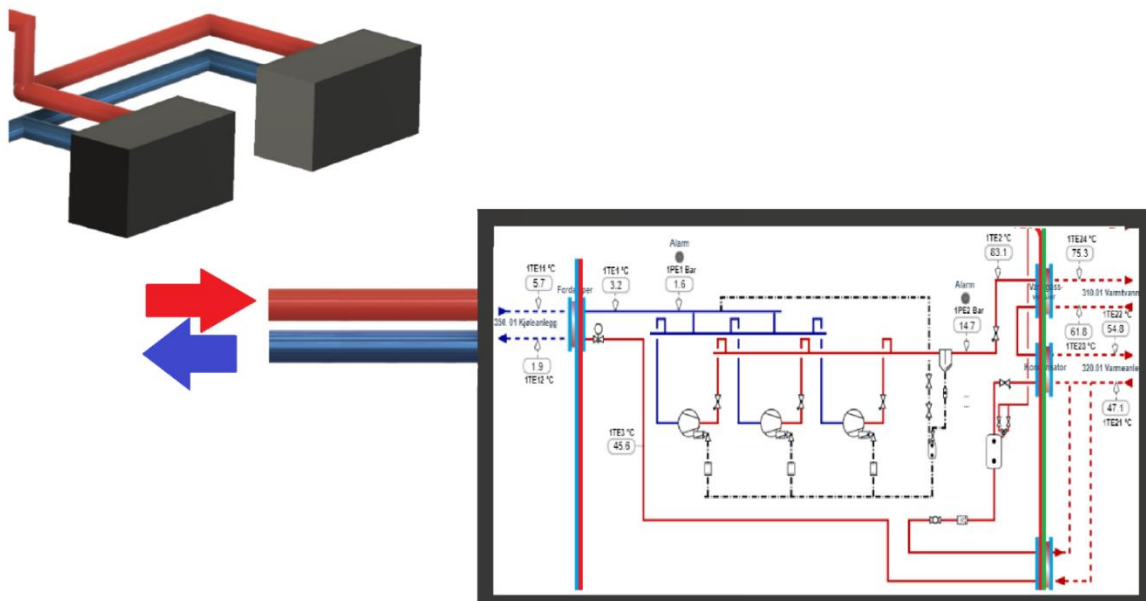


Figure 3.2.5 Transportation of the fluid to and from the heat pump

From the accumulator, a portion of the fluid travels through a pump providing pressure (indicated with a green sphere) before joins the rest of the fluid to the geothermal wells to restart the cycle.

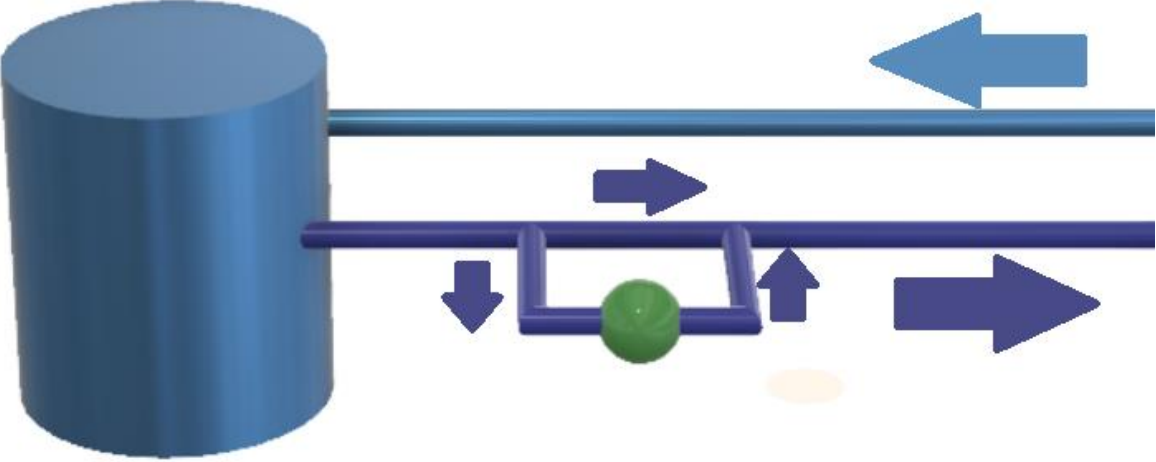


Figure 3.2.6 Fluid transport to and from the accumulator

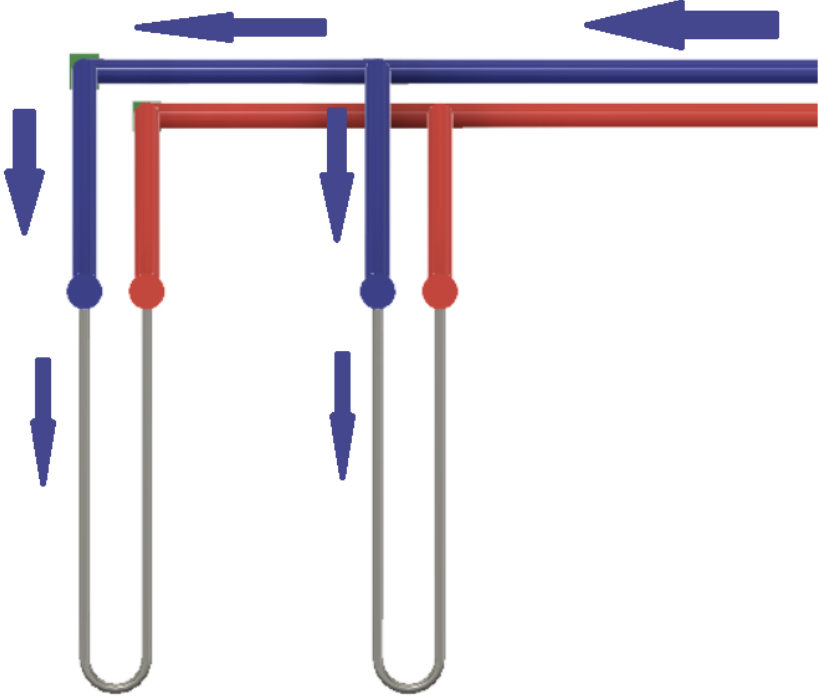


Figure 3.2. Fluid transport to the ground

3.2.2 Refrigeration and Combination

Excess heat from rooms in need of cooling (computer lab, refrigeration rooms etc.) is transferred via propylene glycol to the ground in order to return at a lower temperature. Resultingly, heat is not only gained but also transferred to the ground. To enhance the system at cold days, a valve (green) can be opened for the cooled down propylene glycol returning from the ground to be mixed with the tube exporting the glycol from the wells to the housing, for both the heating and cooling cycle, including the valve (green) allowing the mixing. Even though the fluid from the cooling side has undergone refrigeration, it will be warmer than the fluid returning from the ground on the heating side and thus improve the total temperature in the tube resulting in higher temperatures delivered to the heat pumps.

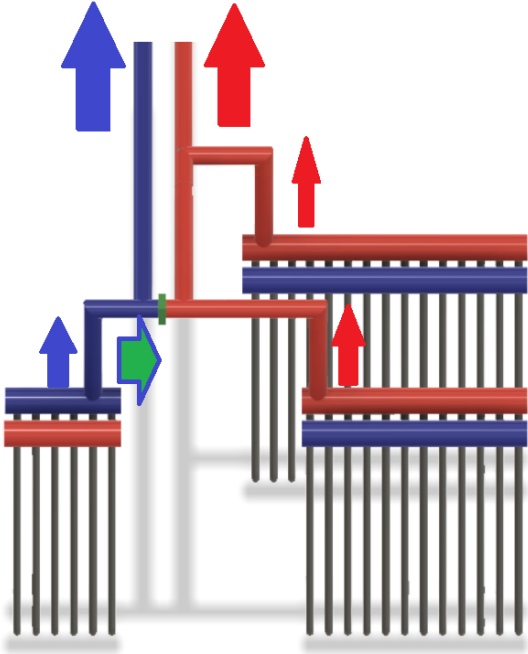


Figure 3.2.7 The Combined heating and cooling cycle, flow from the wells

Similarly, as the fluid is transported from the accumulator, it may, in addition to being transported to the wells for heating, be mixed with the warm fluid from the overheated rooms. This will enhance the cooling of the propylene glycol on the left side.

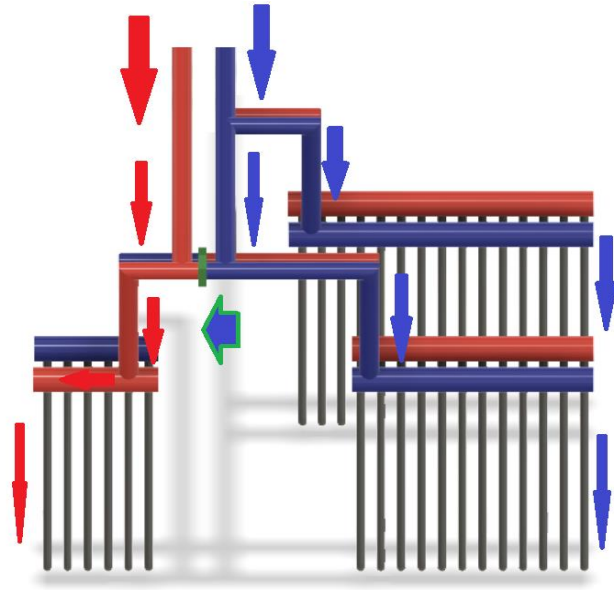


Figure 3.2.8 The Combined heating and cooling cycle, flow to the wells

The whole schematic design is visualized anew as more information about the details has been obtained by the reader.

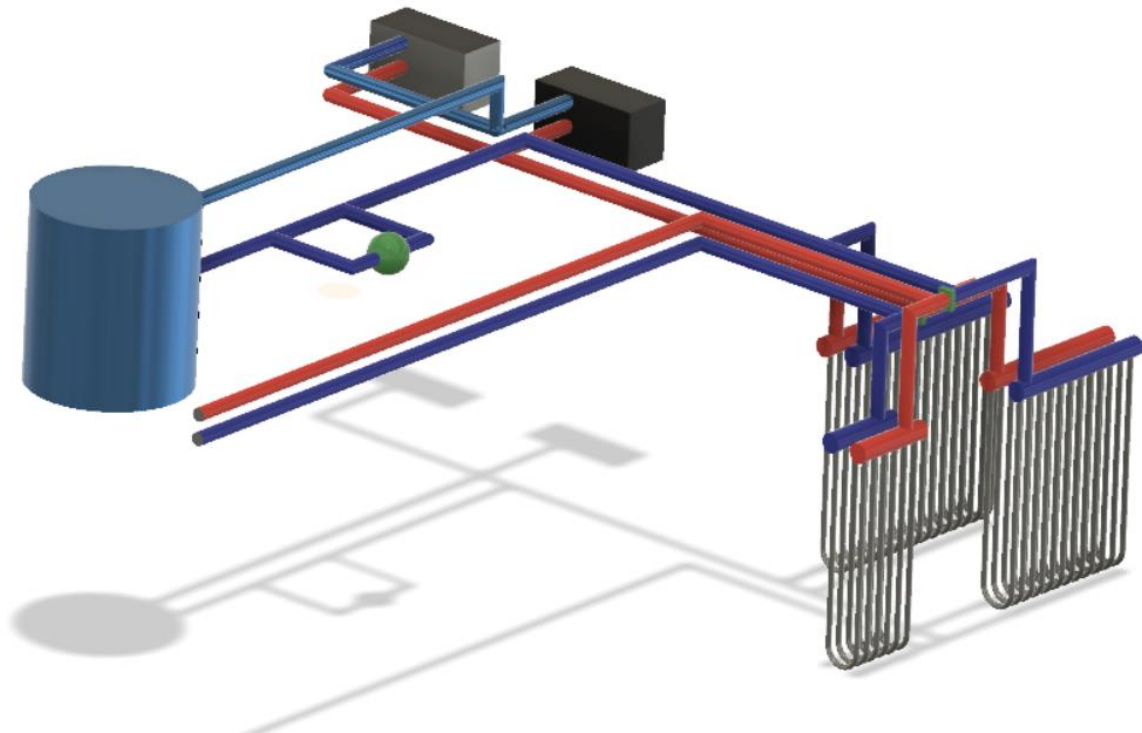


Figure 3.2.9 Presentation of the schematic design of the geothermal system at Bryne VGS

3.3 Application of the Geothermal system

From the time the system was applied in August 2014, the combined results of the renewable system have been above expectations. The windmills and vacuum tube sun collectors gives a lower output than expected, but the geothermal wells gives a higher. The geothermal wells in combination with the heat pumps are delivering so much heat energy they make the gas boiler superfluous. The solar panels supports the geothermal system with energy for the pumps, and the total produced energy for the last year (07.03.18-07.03.19) was 1'035'000 kWh for the whole renewable energy system {IWMAC, 2019 #69}.

The temperature in the ground seems unaffected by the heat induced during summertime, which implies the subsurface below Bryne is unsuitable for energy storage. Despite the advance measurements stating no flow of ground water, a plain reason for the lack of energy storage efficiency underground is in fact the presence of flow carrying the excess heat onward.

3.3.1 Display of Heat Production

For a variation of dates, the following temperatures were displayed from the live information delivered by IWMAC, along with the calculated heat obtained (from the ground) and heat delivered (Heat Pump 1 & 2). The days displayed is chosen as a fair representative of the seasonal temperature variations. The numbers are calculated by us of equation 2.6 and data presented by IWMAC, attached in Appendix 3.

		Ground	Heat Pump 1	Heat Pump 2
14th of January	Tin	0.9	4.6	3.4
	Tout	4.3	-0.1	-1.0
Calculated Q [kW]		224.06	154.86	144.98
1st of March	Tin	1.1	4.7	3.5
	Tout	4.2	0.1	-0.4
Calculated Q [kW]		204.29	151.57	128.50
6th of May	Tin	5.8	7.9	7.5
	Tout	7.2	3.6	5.5
Calculated Q [kW]		92.25	141.68	65.90
7th of June	Tin	14.2	14.8	14.8
	Tout	12.5	11.7	14.8

Table 3.3.1 Calculated heat obtained from the geothermal wells

3.4 External and Internal Effects of Geothermal Usage.

The geothermal system at Bryne VGS have proven to be an effective method of obtaining heat, but more information about the occurrences inside and outside the geothermal wells is desired. However, study of the subsurface is tricky, and the system at Bryne providing heat to the school should not be adjusted for experiments. Therefore, to investigate this, a model is built. A model of a geothermal well allows testing and studying of internal and external effects of contracting heat from the ground.

4 Experimental method

To understand the heat transfer pattern and the impacts of the subsurface surroundings in Bryne, a model of the system was built by students at Bryne VGS. A basic system setup consists of a cylinder with an immersed copper U-tube connected plastic tubes transporting the fluid between the copper tube and water reservoir. The water reservoir is a Julabo machine providing flow of constant temperature. Places along the cycle, temperature sensors will indicate the temperature, along with a flow meter displaying the flow. By observing the temperature differences over time with different flow rates, enhancement and decrease of efficiency will be studied along with the reservoir impacts.

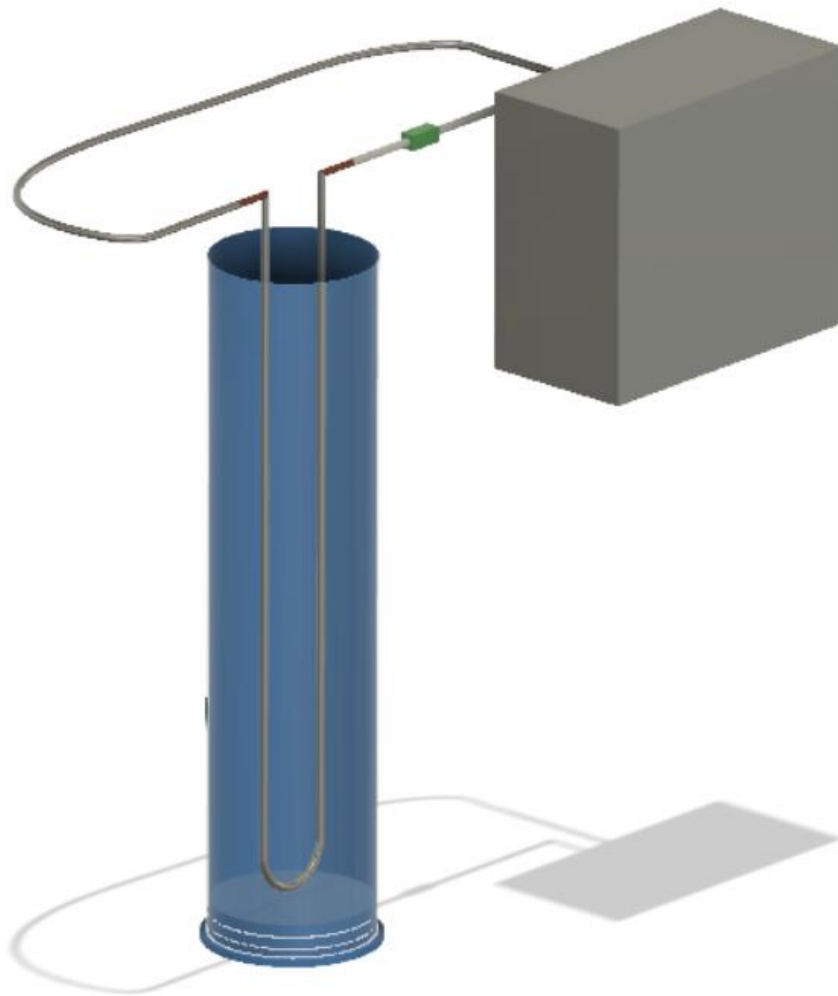


Figure 4.3.4.1 The Laboratory Setup

The grey box presents the Julabo heat exchanger, the green box presents the valves and flow meter

This chapter will list the methods used to investigate the behavior of the fluid in the internal flow and external reservoir, along with the method to achieve an optimal flowrate. Results can be found in chapter 5.

4.1 Experimental Setup

The acrylic tube has a diameter of 20 cm and 85 cm height. This is connected to PVC cylinder with a height of 4 cm and a diameter of 25 cm, milled out to fit the acrylic tube. Two O-rings and three screws secure for leakage and stability between the two cylinders. A copper U-tube is submerged in the cylinder, connected to the PVC at the bottom with a screw for stabilization. Both ends of the U-tube is connected to a Julabo device which provides quite stable temperatures for the loop. From the Julabo device, water is pumped out through a Gardena Flow Meter displaying the flow before entering the copper U-tube. On either side of the flow meter, a spherical valve allows for adjustment of the flow. For some of the measurements, an external flow meter is attached between the last valve and the copper U-tube. From the U-tube, water is directly transported to the Julabo apparatus.

Five temperature sensors from Pasco were placed on the system after careful calibration by use of a Calibrator by Fluke, 9102S DRY-WELL. The placement was as follows, where h indicates height from the bottom of the cylinder:

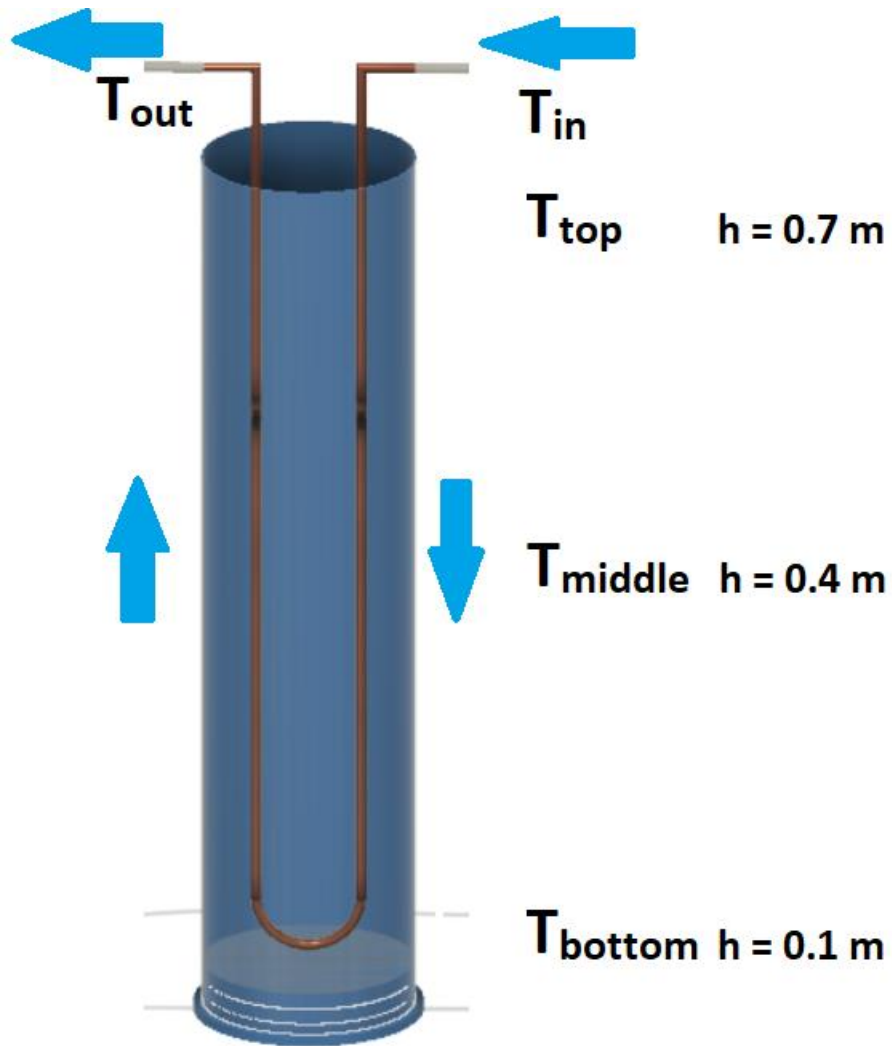


Figure 4.1.1 Placement of temperature sensors

Due to the large heat conduction of copper, the temperatures measuring T_{in} and T_{out} were placed on the outside of the copper with an isolating layer on the outside. The other three temperature sensors were attached to a stick submerged in the water cylinder, at heights given above.

4.2 Equipment

- Water Reservoir; Acrylic walls, $h = 0.77$ m $d = 0.2$ m, PVC bottom
- U-Tube; Copper, $L^{\text{total}} = 2$ m
- Isolation
 - Cotton
 - Isolation coat, thickness 2 cm.
- Plastic tubes
- Valves
- Julabo Machine
- Gardena Flow meter
- Electromagnetic Flow meter; Europik-567
- Computer with different software (PASCO Capstone + Excel)
- Pasco
 - Interphase
 - PasPort Sensors
 - Quadro Temperature Sensor
 - Absolute Pressure Temperature Sensor
 - Voltage Current Sensor
 - Temperature Sensors x5

4.2.1 Pasco

Pasco delivers a series of instruments for measurements, for example for measurement of temperature, pressure and voltage. For this experiment, Pasco 850 Universal Interface was used to receive data from the sensors. A Quadruple Temperature PasPort was connected to the apparatus, where four temperature sensors were attached to the experiment. An additional PasPort, Absolute Pressure Temperature, had the fifth temperature sensor connected to the experiment. The Pasco 850 was connected to the computer, running the program Pasco Capstone. This program displays the outlet values and allows for data exportation to other programs. Introducing the electromagnetic flow meter, the voltage sensors was connected to the interface by a Voltage Current sensor.

4.2.1.1 *Temperature Sensors*

The temperature sensors “Fast Response Probes” measures temperature in the range from -10 to 70 °C with a 0.0025 °C accuracy. The small temperature sensor is placed at the tip of a 1.2 m cable and covered with a thin layer of PVC for protection.

4.2.2 Software

To achieve, analyze and present the findings, different software was used.

4.2.2.1 *PASCO Capstone*

PASCO Capstone is the software achieving information from the Pasco 850 Universal Interface through a USB interface. The program displays the outlet values in the desired display, i.e. tables, graphs, oscilloscopes and more. The two first were used for the purpose of this thesis. In addition, the program allows for data exportation to other programs, i.e. Excel, for further analysis. It is by this software the sensors and measurements are started and the frequency of sampling is chosen. The software also allows for sensor calibration.

4.2.2.2 *Excel*

By Microsoft Office Excel the data captured by PASCO Capstone was analyzed, sorted, compared and displayed. The software was also used for several calculations, and with the Solver tool to find optimal solutions.

4.2.3 Julabo

Julabo delivers heat exchangers for temperature control. The Julabo F34-ME Refrigerated/Heating Circulator delivers fluid in desired temperature at a chosen flow rate. The machine is installed with a circulating pump system and has high heating and cooling capacities. With “Temperature Control Features” it provides optimization with a +/- 0.005 °C accuracy, and with the “Acting Cooling Control” it offers fast cooldown throughout the temperature range ranging from -30 to +150 °C. For this setup, the temperature was set to 5 °C, and the flow rates given by the adjustable pumps delivered rates between 7 and 10 liters/min. The heat exchanger uses some time to reach the desired temperature, and gets

affected by the temperature entering the machine, making the outgoing temperature slightly unstable. For this setup, the outgoing temperature ranges between 5 and 6.5 °C.

Four pump levels are available on the machine, giving the following flow rates (+/- 0.2 l/m)

Pump level 1 = 7.4 l/min	12.33E-05 m ³ /s
Pump level 2 = 8.3 l/min	13.83E-05 m ³ /s
Pump level 3 = 9.2 l/min	15.33E-05 m ³ /s
Pump level 4 = 10.1 l/min	16.83E-05 m ³ /s

The use of pump level 1 and adjustments of the valves on the plastic tube allowed lower flow rates. The flow rate was measured using a Gardena Water Smart Flow Meter for high rates, however as that flow meter was inaccurate at flowrates lower than 2 liters per hour, an electromagnetic flow meter was added for the lowest flowrates.

4.2.4 Gardena Water Smart Flow Meter

With an attached screen, the flow meter measures and displays the flowrate of the liquid flowing through the device. The device measures the flowrate mechanically by a propeller. The blades of the propeller is attached in a way making the propeller rotate at the speed proportional to the flowrate. Measurements of the propeller speed is used to calculate and display the flowrate. The tool runs on battery and has a +/- 5 % measurement tolerance within the flow area 2-30 l/min.

4.2.5 Electromagnetic flow meter

Based on Faraday's law of electromagnetic induction, the velocity and hence the flow of a tube can be measured based on the voltage induced across a conductor. Approximately 100 years after Faraday discovered that magnetic fields can generate electrical currents, Fader Bonnavon built the first electromagnetic flow meter. Inside an electromagnetic flow meter, two field coils are placed outside the tube on each side. They generate a magnetic field in the tube which, when there is liquid flow, applies a force to the charged particles. The particles will separate on each side of the tube, divided by charge. The electrical voltage formed depends on the velocity in the fluid, as a larger velocity will give higher voltages detected and measured by the electrodes on the side. A frame presented by Endress + Hauser is given below, visualizing the inside of an electromagnetic flow meter(Hauser, 2017).

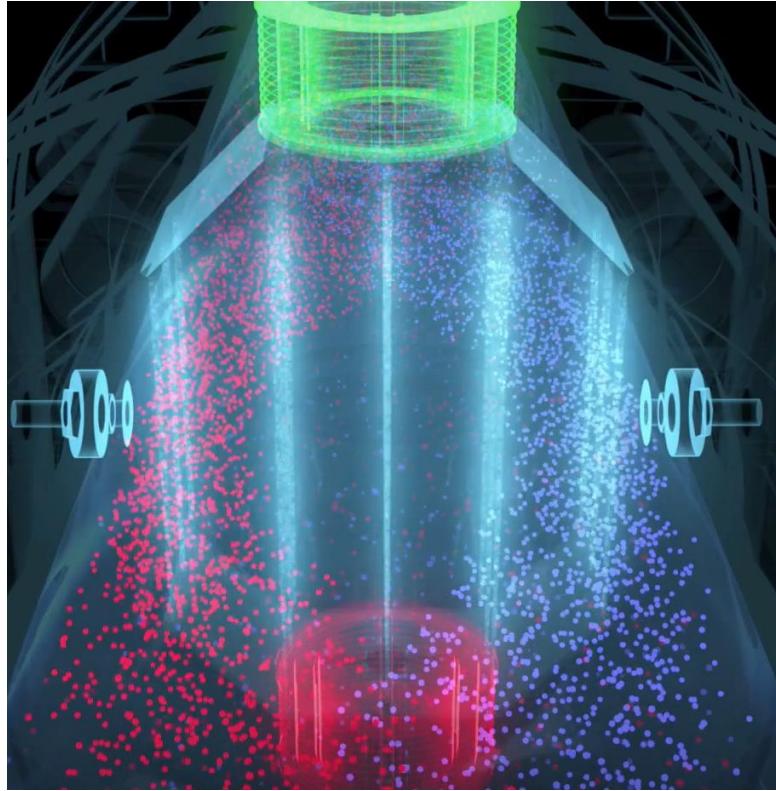


Figure 4.2.1 (Endress + Hauser) Electromagnetic flow meter

To avoid electrical shortcuts, a lining is fitted on the inside wall. To prevent noise from surroundings, the magnetic poles are constantly reversed so the constant interfering voltages can be disregarded, and stable and correct measurements are obtained.

The voltage across the electrodes is given by

$$E = BDv_{avg} \quad (4.1)$$

B = Magnetic field applied

D = metering tube diameter

v_{avg} = average velocity

Assuming the hole tube is filled with fluid, i.e. single-phase liquid flow, the equation is rewritten to include the flow (Bentley, 2005);

$$E = \frac{4B}{\pi D} Q \quad (4.2)$$

B = Magnetic field applied

D = metering tube diameter

Q = Fluid Flow, given by $Q = v_{avg} * \frac{\pi D^2}{4}$

The electromagnetic flow meter used for these experiments is Europik-567, delivered by Heinrichs Messgeräte. It was carefully calibrated prior to the experiment execution, the calibration technique is presented in Appendix 1.

4.2.6 Experimental Preparation

To prepare an experiment, the Julabo machine is turned on, and uses roughly one hour to cool down its water reservoir from room temperature. Meanwhile both valves are closed to prevent flow. When Julabo reaches the correct temperature and has the right pump rate, Pasco Interface 850 and the Pasco Capstone program is turned on, the experiment is started by pushing “Record” on Pasco Capstone, followed by adjustments of the valves allowing the water to flow.

At the end of an experiment, the fluid in the cylinder has a lower temperature than the room temperature. To ensure same initial conditions when several experiments were carried out on the same day, some of the cold water in the bottom of the cylinder were extracted with a siphon and replaced with the same amount of water of a higher temperature. By this, the temperature sensors in the water reservoir quickly displayed temperatures close to room temperature. However, the water inside the copper tubes remains cold for a longer time, hence a severe number of experiments are started while the Tin and Tout are lower than room temperature. Otherwise, if the next experiment is to be run the following day, the reservoir reaches room temperature by conduction of heat from the surroundings.

The above setup, equipment and preparation applies for the following experiments unless otherwise stated.

4.3 Internal Fluid Flow

The internal fluid transported in the U-tube through the water cylinder is explored in this chapter.

4.3.1 Equipment

As listed above in chapter 4.1.1.

4.3.2 Experimental Setup

With the general setup, the temperature difference of the inlet and outlet is examined as the flowrate is altered. The next part will be divided in three, as the tests were done with minor differences as to how the flow is adjusted. For the two first sections (high and medium flowrates), the flowrate was measured using a Gardena Flow Meter, whereas an electromagnetic flow meter was utilized for the lowest rates. The obtained tables were evaluated, and the temperature difference of the inlet and outlet at different time from start were collected in a table displayed in the results.

4.3.2.1 High Flowrates

The setup was first run with flowrates provided directly by the Julabo machine, with the valves open. The flow rate was given by the different pump rates of the Julabo machine. Each pump rate was tested two times, and both terminus (pump 1 and 4) were tested one additional time. The aim for these experiments were to analyze $\Delta T = T_{\text{out}} - T_{\text{in}}$ until the temperatures reached fairly constant temperatures. The experiments were run for approximately the same amount of time.

4.3.2.2 Medium Flowrates

To obtain lower flowrates, the valve connected to the inlet of the Gardena Flow Meter was adjusted to different degrees to obtain various flowrates. By observing the display on the flow meter, the valve was twisted until the desired flow rate was obtained. 9 different flowrates between 2.17 and 10.5E-05 m³/s were assessed. As for the previous, most of these experiments were run until T_{in} and T_{out} appeared constant. One run was left on for two days.

4.3.2.3 Low Flowrates

Due to the lack of accuracy for the Gardena Flow Meter on low flowrates, the Heinrichs Messgeräte Electromagnetic Flow meter was used to attain the lowest flowrates. As the flow meter was placed between the valve-Gardena-valve and the copper tube inlet, both valves were used to control the flowrate. The first valve encountered moving from the Julabo apparatus were used as a main adjuster, and the second valve were used for fine adjustments. As the flow meter had been calibrated and were connected to the computer displaying the voltage measured, the valves were turned until the preferred flow was achieved. As the intended voltage and hence flowrate was found, the experiment was running for more than five hours to analyze the impact of different flowrates over time.

4.4 External Fluid

As the impact on the subsurface area around the wells in Bryne is also a curiosity, the impact of the surrounding water reservoir was similarly investigated. For all the above experiments, temperatures in the water cylinder was measured. The impacts were studied by two main approaches. The first investigates the free convection in the cylinder, which to some extent leads over to the next approach where the temperature distribution in the cylinder over time is studied.

4.4.1 Free Convection in the Cylinder

When first pouring water into the cylinder, the warm water tap was used, providing a temperature close to 50 degrees. As the flow of cold water (5°C) started, a pattern of water flowing downwards close to the copper tube was visible. Although the main pattern was visible for the bare eye, capturing the movements with a camera was challenging. Running the experiments as the water in the cylinder had reduced to room temperature, the pattern was less- or non-visible. To present and study this fascinating movements, a study presented by Baker in 1966 proved the following method to be efficient. There were no literary study of use of this method for this exact purpose, but a feasibility test proved the method to be suitable.

4.4.1.1 Equipment

- Thymol Blue 250 ml, (0.1 g /100ml),
- Salt (300 ml salt mixed with 300 ml water, 100 % solved)
- Power Supply; Manson SPS 9602
- 2 Electrodes (cable)
- Camera NIKON D5500
- Pipette
- Small containers

Manson SPS 9602

With the maximum power of 900W, the DC regulated power supply offers an adjustable voltage output. Range: 1-30V, 30A.

NIKON D5500

The digital single-lens reflex camera (S-SLR) provides photographs of good quality, and is used for the images of the system.

4.4.1.2 *Experimental Setup*

Immersed in the water cylinder are two electrodes, one negative (cathode) and one positive (anode). As voltage is induced, the solution becomes basic or alkaline near the cathode, and acidic near the anode. Placed in pure water, perhaps with salt to increase the conduction, the only visible result of the acidic and basic inducement would be the accumulation of hydrogen bubbles at the cathode when the electrolytic currents are rather high. Introducing the thymol blue indicator, turning the reservoir yellow as it is neutral, the appearance of the basic solution around the cathode visualizes as blue. Pulsing the voltmeter, color will be emitted and transported with the flow in the reservoir.

The electrode wire of the cathode was enfolded around the copper U-tube, covering approximately 5 cm of the tube, 5-10 cm from the water surface on the inlet side. Pulsing the voltmeter, a blue color was visible close to the wires around the tube. As there were no temperature gradients in the reservoir, pulses of voltage induced caused a blue veil to form around the coil/tube with no other movement than slowly spreading by advection. The system with its contents was left alone for 443 hours, then when returning, the fluid in the cylinder had become multilayered. Samples from each layer was extracted and analyzed. More information is presented in Appendix 2.

The blue color gathered at the top ensured a terrific scene to visualize the flow pattern. As the internal flow was started, a set up camera shot frames along the cycle at different time intervals.

4.4.2 Temperature distribution over time

The temperature sensors placed in the center of the cylinder at different heights captures the temperature decrease over time. In addition, a thermographic camera was used to display the vertical temperature distribution.

4.4.2.1 *Equipment*

- As listed above
- Thermographic camera: FLIR C2

Thermographic camera

An overview of temperatures in the system can be obtained using a thermographic camera. Whereas a common camera captures 400-700 nanometer of visible light, thermographic cameras captures wavelengths up to 14'000 nm (14 μm). Resultingly they can capture infrared light with information about the temperature, as thermal radiation ranges from 7-14 μm . A thermographic camera makes thus the otherwise invisible heat energy visible on a screen. As all objects emits or reflects energy, the objects framed on a thermographic camera will emit a color expressing the temperature of the obstacle, different to a normal camera catching the actual color(USA-NASHUA).

The FLIR C2 camera will when pointing it towards an obstacle, display the temperature at the point in the exact middle of the screen (visualized with a circle on the screen) at the top left corner of the screen. A scale displaying the color from highest to lowest temperature of the frame is displayed on the right side along with the exact values of the highest and lowest temperatures found.

4.4.2.2 *Experimental Setup*

The temperature sensors placed vertically along the center of the acrylic cylinder indicates the temperatures at the desired time interval. The sensors are placed at a distance of 10, 40 and 70 cm from the bottom of the cylinder. As the system was turned on, the sensors indicate temperature variation and hence the impact of heat transfer from the reservoir vs. depth and time. The sensors are placed at a small distance from the copper tube and can be regarded as an equilateral triangle at a cross-section where the two tubes and the sensor indicate the corners. Due to the radial heat flow, the temperature measured will not represent the temperature throughout the whole cross-section but indicate an average. From experiments run both for short and long periods, the temperature variations over time is discovered.

In addition, a thermographic camera was used as a tool to display the temperature distribution in the cylinder. With the camera, the temperature scale was “locked” by pointing the camera lens toward temperatures in the right temperature range, making the temperature profile constant for all images. Frames were shot at different time intervals along a run.

4.5 Exploration of an optimal rate

The enthalpies (h) for a given temperature provides information about the amount of energy one kg of a fluid contains. With the enthalpy for the inlet and outlet temperature, Δh describes the energy gained by the water in the U-tube, in the form of kJ/kg. By calculating the mass delivered by the system per second from the flowrate, the energy delivery [J/s] = [W]. As the enthalpy between two fairly close temperatures is considered linear, the enthalpy values in between can be calculated by interpolation. The temperature interval typically ranges between 10 and 7 °C, hence, the value for the enthalpies were interpolated by use of h_1 (5 °C) = 21.020 kJ/kg and h_2 (10 °C) = 42.022 kJ/kg

Calculations of the obtained energy proved the severely low flowrates are providing the highest energy output. Hence, the data collected from the experiments in 4.3.2.3 *Low Flowrates* were utilized to find a coherence between ΔT ($T_{out} - T_{in}$) and the flowrate.

Since the temperature difference is solely dependent of the flowrate and the enthalpy is considered linear between two sufficiently near temperatures, an estimation of the flowrate providing the highest energy output can be found. As the similarities with a real system is highest as the system has reached equilibrium, the temperatures at time = 20'000 seconds were used for the calculations. First, a coherence between ΔT and the flow rate must be found, using the obtained values to create a trendline relating the two. The trend line allows calculation of ΔT from flowrate. Both a linear and quadratic trend line were inserted.

Also in Excel, writing the equation for Temperature difference (y) and clicking an empty cell for x, likewise writing values for Δh and masse dependent on the same empty cell, the command "Solver" will fill in the value for x creating the highest energy output. Running this command for both the linear and quadratic correlation creates a value for the flow leading to the highest energy output.

The same method was used to find an optimal rate based to equations 2.3 and 2.6.

A flowrate close to the calculated greatest value was tested the same way as described in 4.3.2.3.

5 Experimental Results

For each experimental run, a table of the set sampling interval displayed all the temperatures measured at the given time, and a graph demonstrated the same values. An external table and graph were inserted for the measurements with the electromagnetic flowrate. An interval of a table and the belonging complete graph is presented below.

Time (s)	T_{in}	T_{out}	T_{bottom}	T_{middle}	T_{top}
17	21.69	21.48	20.81	21.07	21.52
17.5	21.62	21.49	20.81	21.07	21.52
18	21.48	21.51	20.81	21.07	21.52
18.5	21.26	21.54	20.81	21.07	21.52
19	20.99	21.55	20.81	21.07	21.52
19.5	20.68	21.52	20.81	21.07	21.52
20	20.34	21.45	20.81	21.07	21.52
20.5	19.99	21.33	20.81	21.07	21.52
21	19.62	21.15	20.81	21.07	21.52
21.5	19.25	20.94	20.81	21.07	21.52
22	18.88	20.68	20.81	21.07	21.52
22.5	18.52	20.41	20.81	21.07	21.52
23	18.16	20.12	20.81	21.07	21.52
23.5	17.82	19.82	20.81	21.07	21.52
24	17.48	19.5	20.81	21.07	21.52
24.5	17.15	19.19	20.81	21.07	21.52
25	16.84	18.87	20.81	21.07	21.52
25.5	16.53	18.55	20.81	21.07	21.52
26	16.24	18.25	20.81	21.07	21.52
26.5	15.95	17.94	20.81	21.07	21.52
27	15.68	17.64	20.81	21.07	21.52

Table 4.5.1 Temperature vs. time for flow rate = 4.17E-05 m³/s

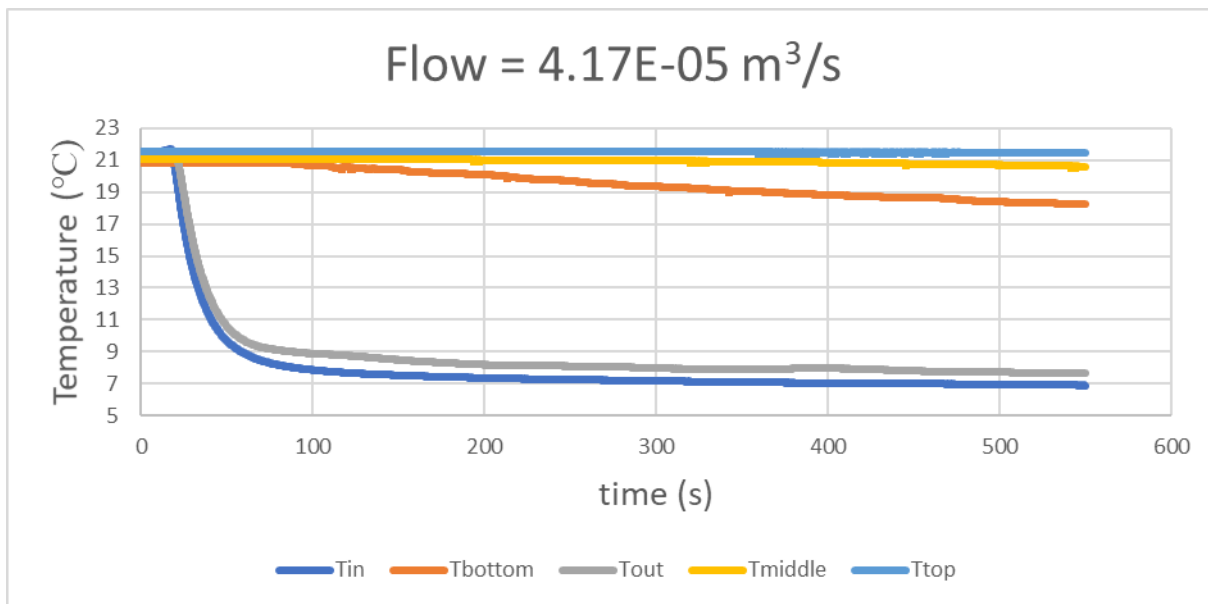


Figure 4.5.1 Temperature vs. time for flow rate $4.17E-05 \text{ m}^3/\text{s}$

The impact of the cold-water flow is presented with sensors both internally and externally. The entire system held room temperature as the system was started. The small temperature variations measured at the start is caused by natural variations in the room. In water as well as in air, the warmer molecules are lighter than cold, so the cold molecules will gather at a lower height in the room. The recording was for this experiment started approximately 15 seconds prior to the internal flow. As the flow is started, the inlet temperature gradually decreases as the water already in the tube (room temperature) is replaced with the cold water from the Julabo machine. The set flowrate leads to a retention period of about 2 seconds, which is why the outlet temperature experiences a slight increase of temperature before beginning to decrease at time = 19 seconds.

The next chapters present the results for different flowrates, separating the internal and external fluid. The perspicuous way to present the data for the internal temperature differences is by tables providing the difference of inlet and outlet temperature vs. time at different flowrates. For the external flow, a graph providing the patterns was considered the best option to present the data obtained by the Pasco products.

5.1 Internal Fluid Flow

The tables presented in this chapter demonstrates the temperature difference at the inlet and outlet with varying flowrates vs. time in seconds. As the time from the measurements start to the time the fluid starts flowing in the inner cycle varies, the time listed in the tables for fast and intermediate flowrates represent the amount of seconds from a given temperature was reached. The table presents thus series of experiments based on as comparable circumstances as possible.

5.1.1 Fast Rate

By use of the flowrate provided directly by the Julabo pump, the following table presents the data found. The time given indicates the time in seconds from the inlet temperature reached 18 °C. One experiment with pump rate = 3 is extracted as the temperature difference indicated bad isolation.

Flow (m ³ /s)	50	100	150	200	300	400	500
12.33E-05	0.21	0.24	0.24	0.19	0.15	0.14	0.11
12.33E-05	0.4	0.35	0.37	0.32	0.28	0.28	0.26
12.33E-05	0.41	0.43	0.37	0.31	0.22	0.21	0.17
13.83E-05	0.31	0.33	0.25	0.2	0.22	0.2	0.2
13.83E-05	0.2	0.2	0.17	0.21	0.14	0.13	0.14
15.33E-05	0.2	0.22	0.19	0.16	0.3	0.08	0.06
16.83E-05	0.13	0.17	0.23	0.19	0.13	0.05	0.12
16.83E-05	0.14	0.17	0.16	0.13	0.09	0.05	0.03
16.83E-05	0.11	0.1	0.08	0.07	0.04	0	-0.01

Table 5.1.1 Temp difference vs. flowrate, fast rates

5.1.2 Intermediate flowrates

The time listed in the table indicates the time from the temperature at the inlet reached 14 °C.

Flow (m ³ /s)	50	100	150	200	300	400	500
3.83E-05	0.87	0.86	0.9	0.86	0.77	0.73	0.73
4.17E-05	0.94	1.05	0.87	0.86	0.78	0.85	0.73
6.00E-05	0.87	0.82	0.78	0.74	0.72	0.68	0.65
7.00E-05	0.77	0.8	0.73	0.65	0.58	0.59	0.53
7.67E-05	0.64	0.61	0.57	0.54	0.51	0.45	0.46
8.50E-05	0.67	0.65	0.59	0.5	0.46	0.42	0.4
8.67E-05	0.56	0.57	0.52	0.43	0.4	0.36	0.4
10.5E-05	0.48	0.54	0.51	0.48	0.36	0.25	0.19

Table 5.1.2 Temperature difference vs. flow rate, intermediate flow rates

5.1.3 Low flowrates

The time indicates time from the measurements was started.

Flow (m ³ /s)	500	1000	2000	5000	7500	10000	12500	15000	17500	20000
0.706E-05	5.36	5.32	5.05	3.98	3.52	2.92	2.68	2.55	2.3	2.24
1.006E-05	5.1	5.02	4.8	3.82	3.27	2.81	2.52	2.32	2.13	2.1
1.468E-05	5.04	4.86	4.39	3.3	2.75	2.31	2.01	2.52	1.66	1.57
1.929E-05	3.37	3.19	2.98	2.33	2.01	1.71	1.52	1.38	1.34	1.28
2.506E-05	1.72	1.58	1.37	0.85	0.67	0.5	0.44	0.38	0.37	0.36

Table 5.1.3 Temperature difference vs. flowrate, low flowrates

5.2 External Fluid

The information acquired by investigation of the water cylinder is presented in the subchapters.

5.2.1 Free Convection in the Cylinder (Thymol Blue)

The separation in the cylinder works as a terrific scene to visualize the effect of the internal flow on the external reservoir. As the internal flow was started, a set up camera shot frames along the cycle at different time intervals. With an interval of three seconds, figure 52.1. illustrates the movement of the basic layer as it is cooled down. Figure 5.2.2 presents the water temperature at larger time differences.

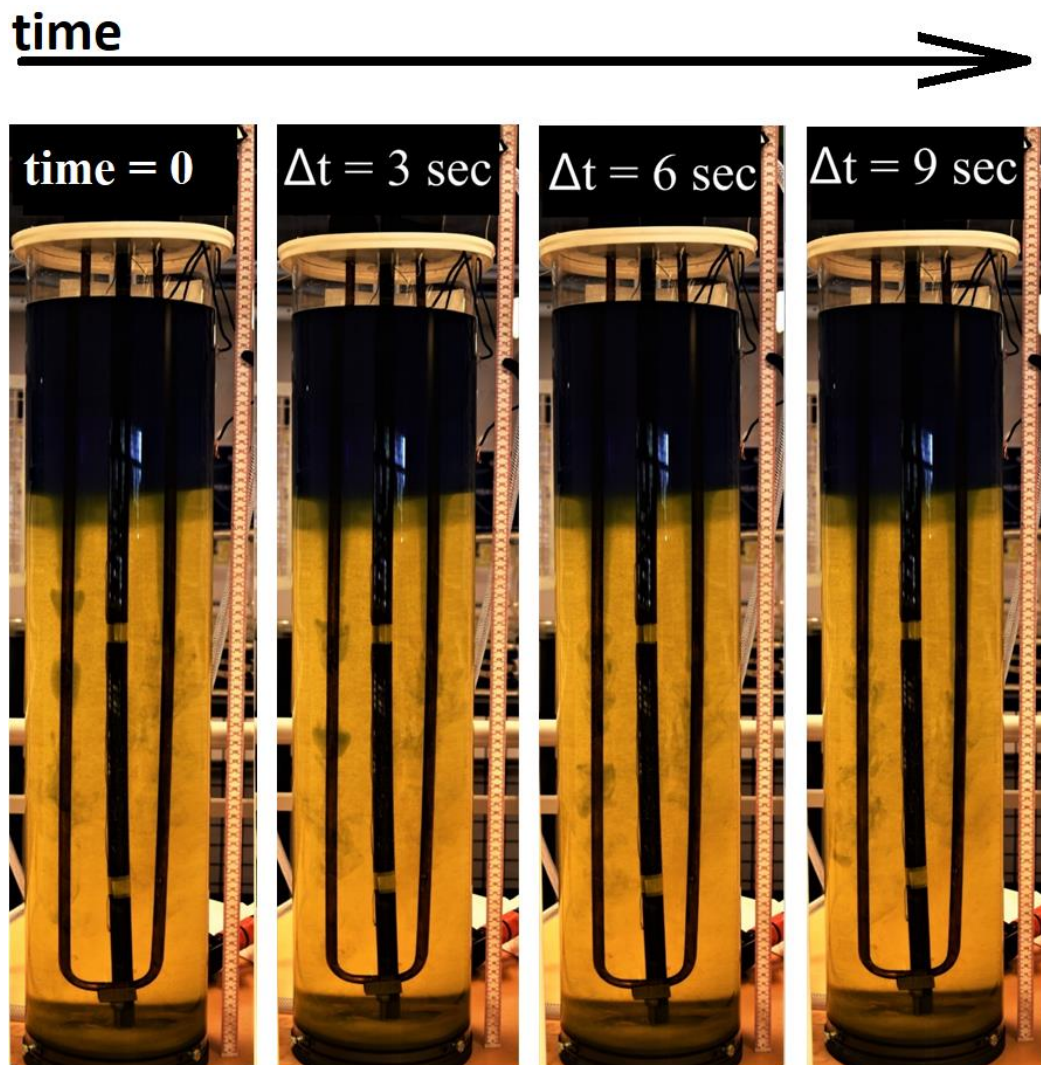


Figure 5.2.1 Visualization of the flow patterns close to the U-tube

time

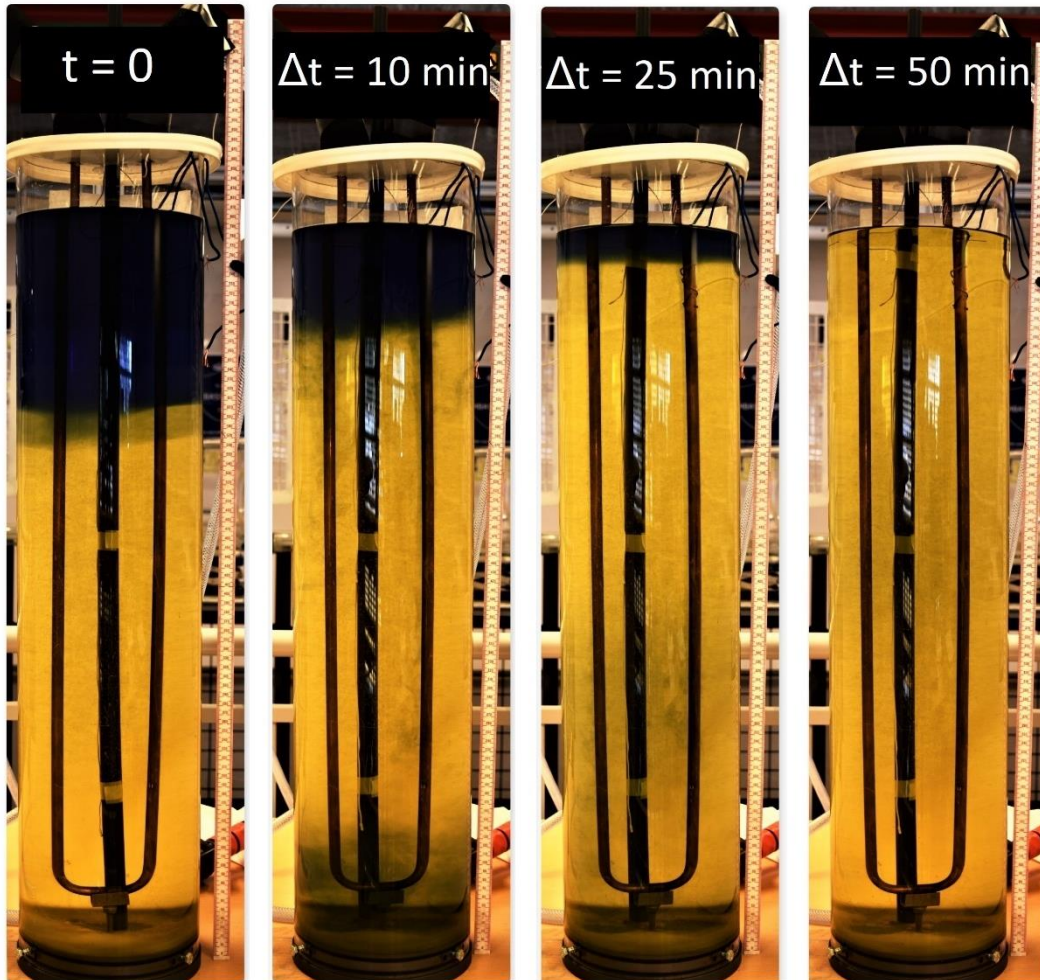


Figure 5.2.2 Presents the free convection occurring in the cylinder over time

5.2.2 Temperature distribution over time

As the water in the cylinder transfers heat to the inner cycle through the copper tube, the temperature decreases. Due to the density difference, the cold water falls to the bottom, and the warmest water remains or rises to the top. To indicate this, three temperature sensors and a thermographic camera was used.

5.2.2.1 Temperature Sensors

When starting the experiment, the temperature sensor placed in the bottom of the water cylinder indicates a change of temperature first. This is proven by the figure 5.2.3, measurements from a run of flowrate $8.50E-05 \text{ m}^3/\text{s}$. The temperature at the bottom decreases already after approximately 1 minute (60 seconds), the temperature in the middle starts decreasing at the similar rate after 5 minutes (300 seconds). The temperature is slightly affected after 10 minutes (600 seconds).

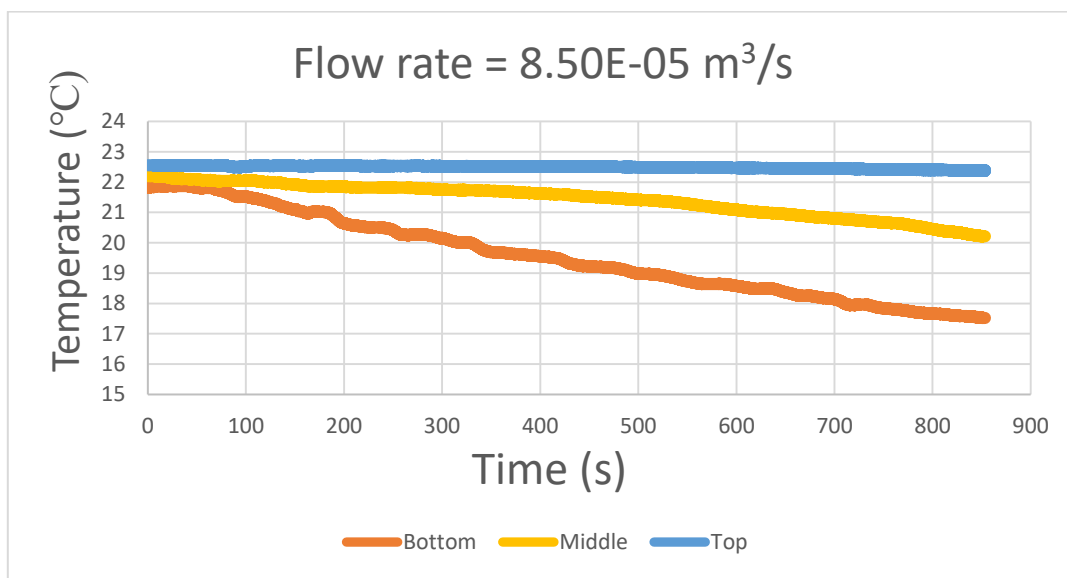


Figure 5.2.3 Temperature vs. time. Flow rate = $8.5E-05 \text{ m}^3/\text{s}$

The same pattern is observed for all rates, demonstrated by two examples in figure 5.2.4 and 5.2.5. The graph for all flowrates tested is attached in Appendix 5.

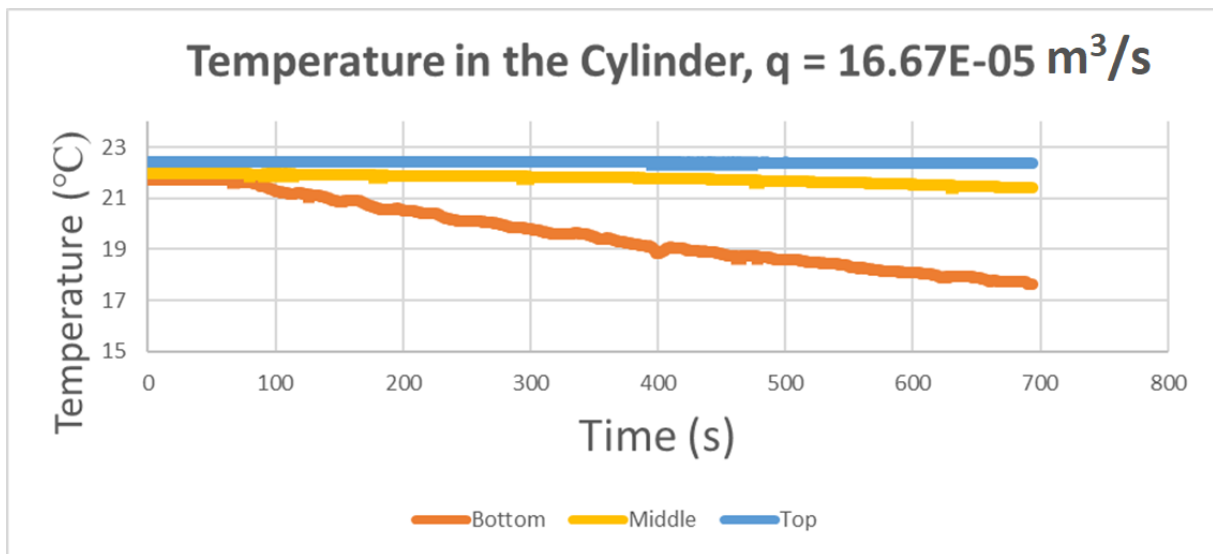


Figure 5.2.4 Temperature vs. time, flow rate = $16.67E-05 \text{ m}^3/\text{s}$

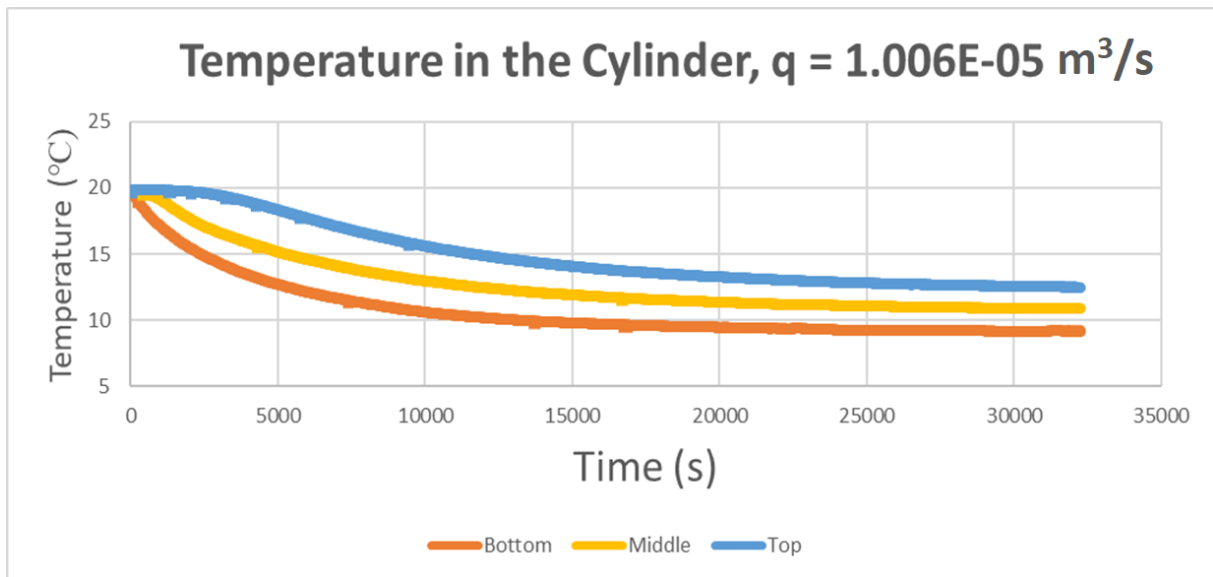


Figure 5.2.5 External temperature vs. time for flow rate = $1.006E-05 \text{ m}^3/\text{s}$

Measurements from the 44-hour experiment is displayed in figure 5.2.6.

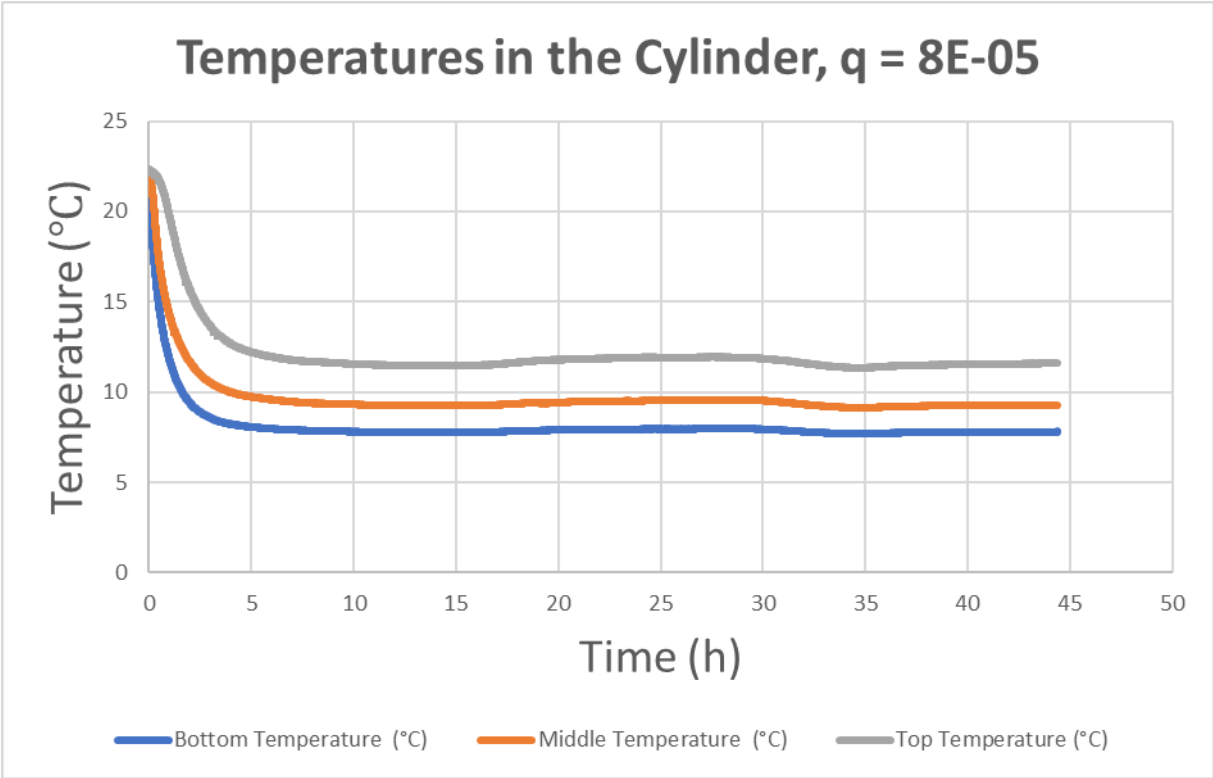


Figure 5.2.6 External temperature vs. time, 44-hour run

As the system seem to reach equilibrium after six-seven hours, a segment of experiments was performed over that time period.

5.2.2.2 Thermographic Camera

By application of a thermographic camera, the temperature profile in the cylinder is captured. Images capturing the temperature profile at different times presents the temperature difference undergone in the cylinder. A sequence for a run is presented below.

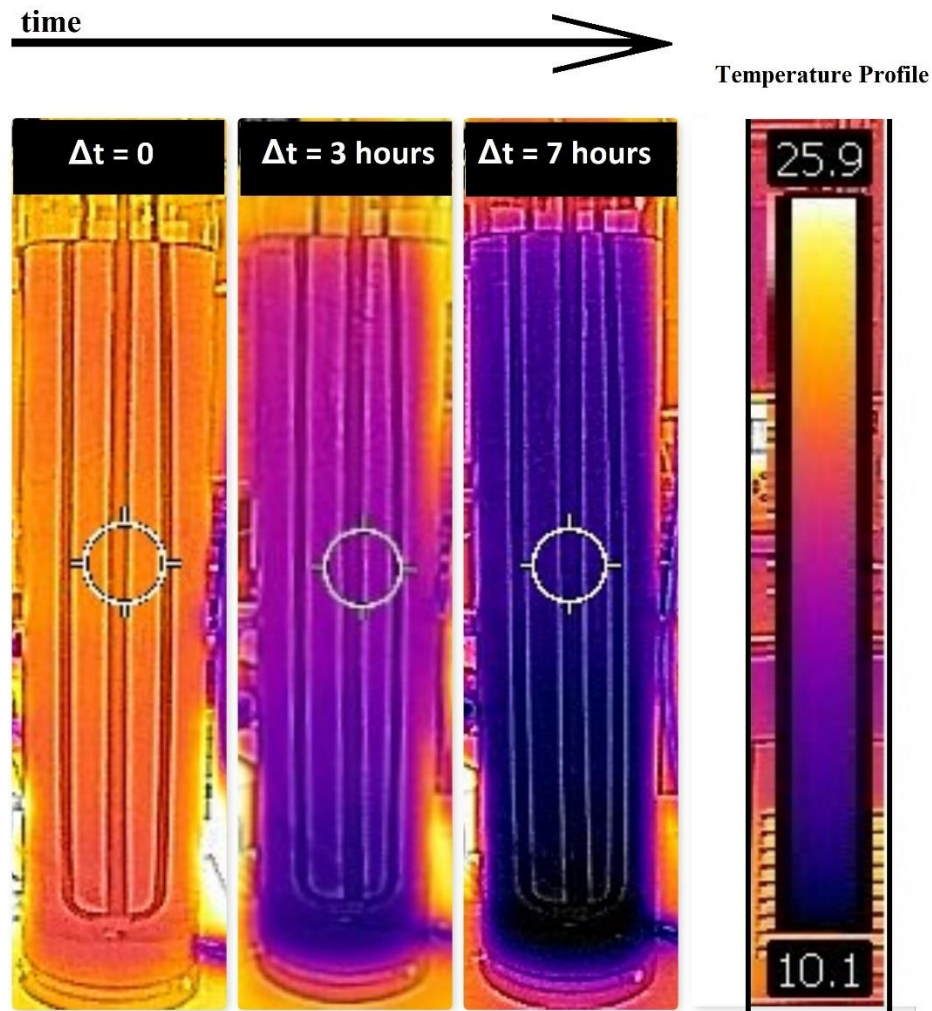


Figure 5.2.7 Temperature in the cylinder captured by a thermographic camera. The temperature profile is displayed at the right.

The figure presents the temperature difference in the vertical section of the cylinder at different Δt from start. The temperature profile scale is shown to the right. For the first frame, $\Delta t = 0$, the marginally darker color at the bottom presents the gravitational forces of the heavier cold water, even as the cylinder has been left alone with no fluid in the U-tube for 15 hours. During the experiment, the temperature in the whole cylinder decreases, additionally the temperature in the bottom is severely lower than the temperatures above, indicated by the less blue color upwards.

5.3 Calculations of Obtained Heat

5.3.1 Laboratory

By use of enthalpy, the energy obtained by the fluid in the u-tube through the water reservoir is presented on the right side.

		h (5°C)	h (10°C)		ρ vann 7.5 °C (kg/m³)
		21.02	42.022	kJ/kg	999.85
Flow	Temperature	Enthalpy	delta h	masse	Energy
m ³ /s	T *C	h (kJ/kg)	Δh (kJ/kg)	m (kg/s)	(J/s) = (W)
7.06E-06	7.67	32.24			
	9.91	41.64	9.41	7.06E-03	66.42
1.01E-05	6.65	27.95			
	8.75	36.77	8.82	10.06E-03	88.72
1.47E-05	7.2	30.26			
	8.77	36.86	6.59	14.68E-03	96.79
1.93E-05	6.94	29.17			
	8.22	34.55	5.38	19.29E-03	102.70
2.51E-05	6.84	28.75			
	7.2	30.26	1.51	25.06E-03	37.89

Calculations by use of equation 2.3 involves uncertainties connected to the overall heat transfer coefficient value. Assumptions were made regarding the external heat transfer coefficient (h_2) as the value was not found from the experimental setup. The assumption of h_2 is based on still water and thus solitary conduction from the outside fluid.

A0	A1	Alm	A2	delta r	h2	k
m ²	m ²	m ²	m ²	m	W/m ² K	W/mK
7.85E-05	0.0377	0.04224	0.04712	0.001	400	400
Flow	Tinside	Toutside	ΔT outside-inside	h1	U	Q
m ³ /s	°C	°C	°C	W/m ² K	W/m ² K	W
7.06E-06	8.79	11.32	2.53	802.19	1.48E+05	29.36
1.01E-05	7.70	10.85	3.15	1143.28	1.67E+05	41.28
1.47E-05	7.99	11.45	3.46	1668.04	1.84E+05	50.16
1.93E-05	7.24	11.01	3.78	2192.79	1.95E+05	57.94
2.51E-05	7.58	11.08	3.50	2848.73	2.04E+05	56.12

Equation 2.4 presents energi outputs similar to the energy calculated from enthaly calculations.

		Cp		
		4170		
Flow	m	deltaT	Q	
m ³ /s	kg/s	°C	W	
7.06E-06	7.06E-03	2.24	63.57	
1.01E-05	10.06E-03	2.1	85.85	
1.47E-05	14.68E-03	1.57	94.38	
1.93E-05	19.19E-03	1.28	101.57	
2.51E-05	25.06E-03	0.36	37.22	

5.3.2 Bryne VGS

Due to lack of enthalpy information for a 30 % propylene glycol mix, the energy could not be found by use of enthalpy. The energy is found by equation 2.6. Equation 2.3 presents too many unknowns for calculation.

	ρ	m	cp	ΔT	Q
	kg/m ³	kg/s	J/kg	Tout-Tin °C	kW
Total	1022	17.374	3793	3.1	204.29
1 well	1022	0.511	3794	3.1	6.01

5.4 Exploration of an optimal rate

The plot of the energy obtained vs. flow for the measurements of the lowest flowrates are presented below.

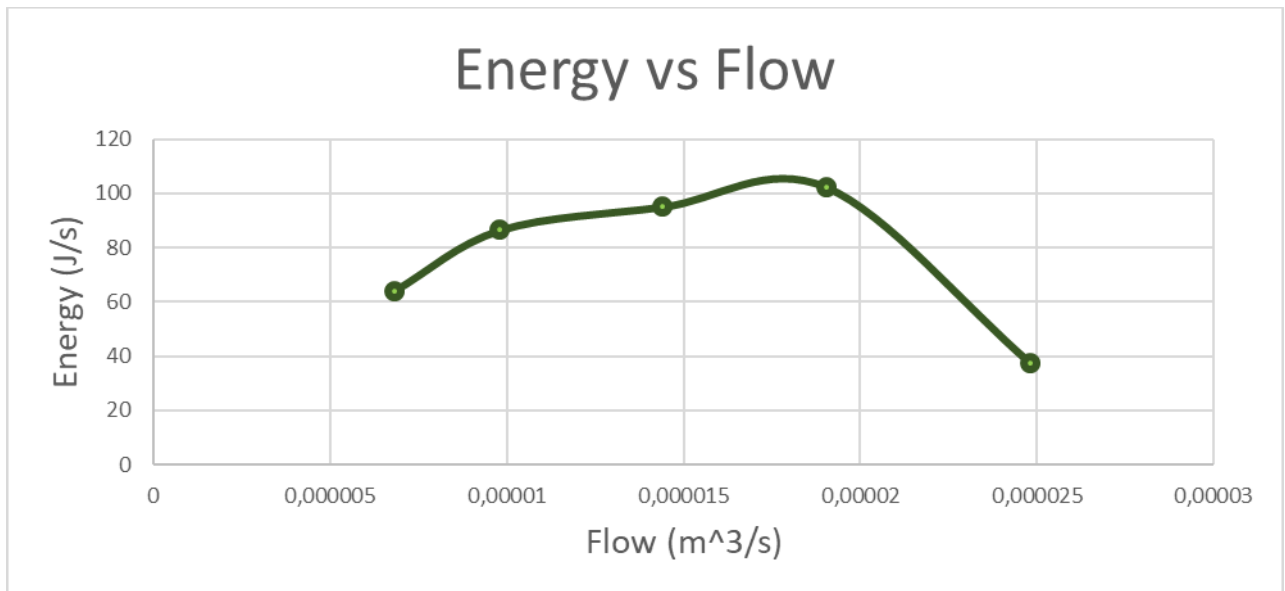


Figure 5.4.1 Energy output vs. flowrate

Figure 5.4.1 visualizes that the highest energy output is obtained when the flow is somewhere between $1.47\text{E-}05$ and $2.5\text{E-}05$. The linear and quadratic trendline for the coherence of temperature difference and flow are given below. The R^2 describing the fit of the curve is closer to 1 for the quadratic fit.

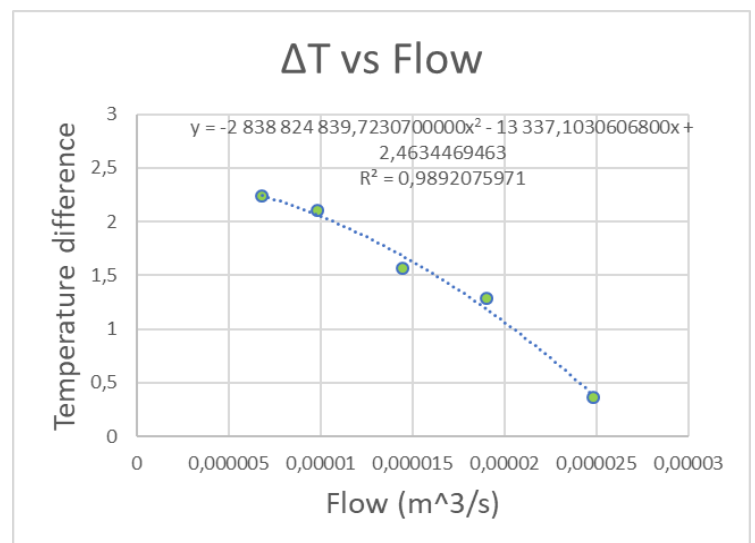
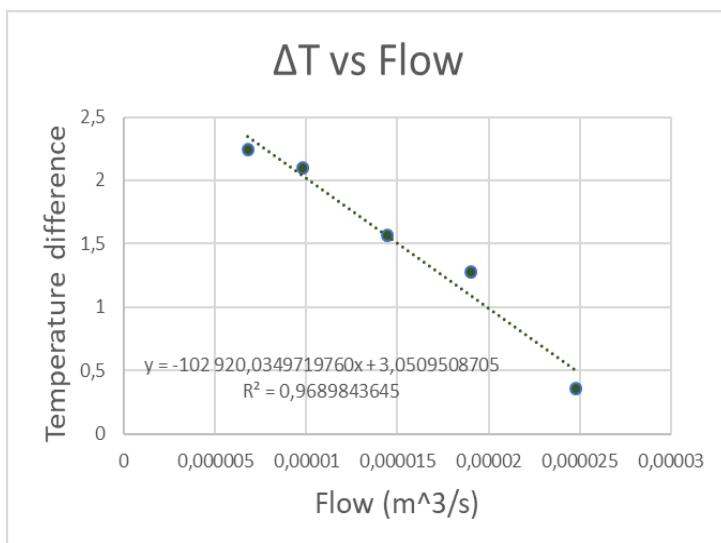


Figure 5.4.2 Temperature difference vs. flow rate with linear (left) and polynomial (right) fit

The use of Solver for the optimal flowrate gave the following table.

	Flow m ³ /s x	ΔT Tout-Tin °C y	Δh J/kg	Mass kg/s	Energy W
Linear	1.48E-05	1.53	6.41	14.8E-03	94.96
Quadratic	1.53E-05	1.59	6.68	15.3E-03	103.49

Due to the higher R² value for the Quadratic approximation, and as the maximum energy output for the linear approximation is lower than already obtained, the equation obtained by the Quadratic approximation was further investigated. By use of the correlation between flowrate and voltage, the calculated voltage needed to obtain the desired flowrate of 1,5339E-05 m³/s was 1.1540 V. The required flowrate was difficult to achieve, however a flowrate quite close to the intended was obtained, and the experiment followingly carried out gave the results:

Flow m ³ /s	Temperature °C	Enthalpy, h kJ/kg	Δh kJ/kg	masse kg/s	Energy (J/s) = (W)
1.58E-05	6.44	27.07			
	8.03	33.75	6.68	15.8E-03	105.22

By use of equations 2.3 and 2.6 The optimal rates at the laboratory were found to be

Flow	h	U	Temp diff inside/outside	Q
m ³ /s	W/m ² K	W/m ² K	°C	W
2.15E-05	2448.96	1.99E+05	3.70	57.93

Flow	Mass	deltaT	Q
m ³ /s	kg/s	°C	W
1.57E-05	15.68E-03	1.58	103.47

5.5 Comparison of dimensionless numbers and properties in Bryne and at the Laboratory

	Bryne	Laboratory
Fluid		
Cp fluid [J/kgK]	3793	4170
k fluid [W/mK]	0.419	0.609
ρ [kg/m ³]	1037	999.85
μ [Poise]	0.00820	0.0014
q [m ³ /s]	5.00E-04	RANGE: (0.007-1.7)E-04
velocity [m/s]	0.514	RANGE: 0.14-3.3
Travel time [s]	805.20	RANGE: 0.45-10.77
β		1.10E-04
Tube		
din [m]	0.0352	0.008
dout [m]	0.04	0.01
k [W/mK]	0.4	400
L [m]	400	1.5
Surroundings		
Heat transfer [w/m*K]	3.7	0.026
Initial temp	8.5	22
Temp at eq.	-	11
Twall		9.00
Tfluid		12

Table 5.5.1 Properties of the geothermal system in Bryne and at the laboratory setup

Laboratory Bryne	Pr 9.59 74.77	Gr 5573596.23		
Flow	Velocity	Re	Nusselt	Peclet
7.06E-06	0.14	802.19	11.96	7689.98
1.01E-05	0.20	1143.28	15.88	10959.74
1.47E-05	0.29	1668.04	21.49	15990.14
1.66E-05	0.33	1890.19	23.75	18119.76
1.93E-05	0.38	2192.79	26.74	21020.54
2.51E-05	0.50	2848.73	32.97	27308.54
3.38E-05	0.67	3845.77	41.92	36866.30
3.83E-05	0.76	4357.16	46.32	41768.67
4.17E-05	0.83	4736.05	49.51	45400.73
6.00E-05	1.19	6819.91	66.28	65377.06
7.00E-05	1.39	7956.56	74.98	76273.23
7.67E-05	1.53	8714.33	80.64	83537.35
8.50E-05	1.69	9661.54	87.58	92617.50
8.67E-05	1.72	9850.98	88.95	94433.53
1.05E-04	2.09	11934.84	103.71	114409.85
1.23E-04	2.45	14014.91	117.94	134349.85
1.38E-04	2.75	15719.89	129.28	150694.11
1.53E-04	3.05	17424.87	140.39	167038.38
1.68E-04	3.35	19129.84	151.27	183382.64
BRYNE				
5.00E-04	0.51	1745.58	56.13	130517.07

Table 5.5.2 Dimensionless numbers

6 Discussion and Observations

6.1 Properties

Table 5.5.1 displays the dimensions of the two systems side by side. The fluid properties are overall in the same order, the same applies for the dimensionless numbers. The flow in Bryne is higher than all flowrates at the laboratory, but due to longer travel distance and increase of tube diameter the fluid spends severely longer time underground. From the heat conductivity of the u-tubes, it is seen that copper can transfer much more heat from the surroundings than PEM, which, as it is a type of plastic, is typically associated with isolation. If the system in Bryne had replaced the U-tube with copper, a higher temperature may have been obtained during the coldest periods of the year, or a shallower drilling depth may have been sufficient. The use of PEM to obtain heat is supported by the long subsurface travel distance. As a U-tube length of 400 meter is required to reach the constant temperatures at the depths of 200 meters, and the traveling time through the U-tube is 13 minutes, the conductivity of the PEM tube is considered sufficient for heat obtaining.

Another difference is the surroundings of the U-tube. Where the U-tube at the laboratory is placed in a water column with a diameter of 20 cm, the real system is placed in a water column with a diameter of 11.5 cm. Surrounding the laboratory water cylinder is an acrylic wall with air on the outside with low conductivity, whereas the real structure is surrounded by a rock layer with a severely higher conductivity.

There are thus some dimensional differences between the two systems. If a system was to be made proportional to the real system, with a cylinder of 0.8 meters, the U-tube inside diameter must have been 0,14 mm, and the flowrate in the power of negative 11 m³/s. Anyhow, the large heat conductivity in the U-tube used in the laboratory provides a similar temperature difference for the inlet and outlet for low flowrates as the real system at Bryne does. The laboratory setup is accordingly considered to give valuable information about the real geothermal system.

6.2 Internal Flow

The flow in the tube at the laboratory for low flow rates is according to the Reynold number laminar, but most of the experiments are considered turbulent or at least transitional, implying the inertial forces are too strong for the viscous. The three turns in the copper tube (one entering, two at the bottom) will result in mixing of the fluid along the travel distance. Laminar regime indicates one-dimensional flow, transitional and turbulent flow indicates two- or more likely three-dimensional flow. One-dimensional flow can result in a temperature gradient in the copper tube, where the warmest fluid is located close to

the tube wall. The method used to measure the inlet and outlet temperature may thus not reflect the overall temperature in the fluid, only the temperature of the warmest fluid close to the wall. In addition to the fluid close to the tube wall receiving more heat, the velocity close to the wall is considered lower than the middle velocity due to frictional forces. The water molecules close to the wall spend thus longer time in the tube and consequently have more time to attain heat. The Reynolds number for the flow in Bryne also indicates laminar flow. The vertical distances here are so long the fluid will travel laminarily and temperature gradients within the tube will occur.

The Grashof number indicates the ratio of buoyancy forces to viscous forces in the external flow, implying the buoyancy forces are significantly larger. The driving force in the internal flow is forced convection. The Prandtl number informs about the viscous/momentum diffusivity vs the thermal diffusivity for both the internal and external flow. It indicates the momentum diffusivity to be larger, which implies a temperature symmetry around the copper tube, and a larger velocity boundary layer than thermal boundary layer. The same applies in Bryne.

The Nusselt number implies the working principle of heat transfer internally to be convection for the flow in Bryne and for all flowrates at the laboratory. The Peclet number for all flow rates indicates that advection heat transfer forces dominate over diffusion. The bulk transfer of heat is thus larger than the molecular transport of heat, meaning the heat is mainly transported by bulk movements in the cylinder, and at a smaller scale by molecules close to the warmer area diffusing heat. Hence the flow pattern and ways of heat transfer is similar for the real geothermal system in Bryne and the laboratory setup. Both systems are run with non-Newtonian fluids, and the constant change of flow pattern and temperature input makes the flow unsteady.

At the laboratory, the use of isolation outside the copper tubes were inconsistent. For the fast flowrates the only isolation was the 2 cm isolation layer, which from the thermographic images proved not to be completely isolating. Seen from the table for the fast rate, one value is even negative, which must be due to different isolation on the inlet and outlet. After this discovery, the cotton was added, where upon the thermographic camera proved the isolation layer to be OK.

For all the tables displaying ΔT , the travel time is not considered. Where the inlet temperature is noted at time t' , the outlet temperature should be noted at $t' + \Delta t$, where Δt = travel time through the copper tube. However, for the fast rates, the travel time is about 0.5 seconds, and the temperature difference does not change severely during half a second, at least not as the time from start exceeds 100 seconds and the graph starts to even out. However, even if the true ΔT is slightly smaller than accounted for, the same method is used for all the flowrates and the comparison is thus true anyhow. For the low flowrates, the travel time is more significant, where the water uses about 11 seconds to travel through the whole tube for the minimum flowrate. Still, for the lowest flowrates, the temperature is considered quite stable as the system is running for a long time, so the temperature of the outlet does not change much during

those 11 seconds. The same method was used for the system in Bryne in table 3.3.1, where the travel time is not considered.

For the highest flowrates, first carried out at the laboratory, the experiment was stopped when the temperature difference of the inlet and outlet appeared constant. Yet, running the system a longer period proves that the temperature difference continues to decrease after 500 seconds. The low flowrates running for a longer period experiences temperature difference even from time = 17500 to time = 20000. To investigate the temperature difference over time, the experiments could be run for a longer period for the fast flowrates. The temperature sensors appear to lose calibration memory after a while, hence, they were re-calibrated three times during the overall experimental period, and will not be 100 % correct for all experiments. However, as the temperature sensors are not completely correct, temperature differences less than 0.10 °C can be caused by isolation differences or poor calibration, and thus a longer period of measurements is not considered to give relevant or correct results. If the temperature sensors at the inlet and outlet is perhaps differing with 0.05 °C, a displayed ΔT of 0.1 °C could imply true ΔT in the range between 0.05 and 0.15, which is a large difference. For the larger flowrates, a ΔT increase or decrease by 0.05 would not cause tremendous changes to the overall presentation. The intermediate flowrates could perhaps have been run for a longer period, but then again the ΔT difference for time = 400 and 500 seconds is small, and an assumption for the pattern to come can be made based on the patterns for the slow flowrates.

By sole use of the Julabo machine for flow adjustment (fast flowrates), ΔT for the same flowrate varies almost as much as for different flowrates, and a solid coherence between flowrate and delta T is difficult to obtain. For the intermediate flowrates, a stronger pattern is obtained for ΔT vs. flowrate for time = 500 s. ΔT decreases as the flowrate increases. Looking at ΔT as less time has gone by, the same overall pattern is observed. For the lowest flowrates, all temperature differences are clearly affected by the flowrate. The temperature difference between ΔT for time = 500 and time = 20000 are much larger for the lowest flowrates. This indicates that low flowrates need more time before reaching equilibrium temperatures.

All experiments experience a decrease of temperature difference between the inlet and outlet with time. This is perhaps because it takes for the system to transfer the heat initially in the copper tube to the internal fluid. This is seen for both the inlet and outlet temperature; however, the inlet temperature seems to stabilize first. This is conceivably because the total length from the source of the cold water is shorter for the inlet temperature, so there is less material to withdraw heat from. In addition, the heat conducted from the air through the plastic tube is smaller than from the water through the copper, resultingly the stable or equilibrium outlet temperature takes more time to reach.

6.3 External Flow

The temperature sensors placed vertically in the middle of the water cylinder proves the density dependence of temperature. The coldest temperature is measured at the bottom, and the bottom temperature starts decreasing first. Where the temperature 10 cm from bottom typically starts decreasing after one or two minutes, the temperature at the top appears unaffected for the first 10 minutes or more. At this time, the thermal advection and diffusion from the top layer starts to transfer heat to the colder layer below, and the temperature is thus released. The temperature sensor in the middle of the water cylinder is affected after the bottom sensor and prior to the top. The heat transfer from the water seems independent of the flowrate as the reservoir temperature pattern is similar for all flowrates, which can be seen in appendix 5.

A measure of room temperature in the laboratory proves the temperature is varying; the temperature in the room is warmer during daytime (Appendix 6). The laboratory is a large room with many windows (pointing towards west) and machines. The use of the machines and/or sunlight will increase the temperature in the room. This will also lead to an increase of the temperature in the water cylinder. The experiments are normally run during daytime, however the experiments running with low flowrates are sometimes run until late in the evening. The surroundings at the laboratory varies with up to 2.3 °C from day- to nighttime, causing the temperatures in the water cylinder to vary about 0.5 °C. As the reservoir is affected by the changes, so is the U-tube. The 44 hour test proves there is an equilibrium to be reached where heat transferred to the copper tube is the same as heat transferred to the water cylinder.

The external fluid behavior was visualized at the laboratory. The innovative experiment with thymol blue proves the impact of the water reservoir; the flow of cold water downwards in the close vicinity of the well. The experiment is performed while there is a large difference between the temperature in the copper tube and the rest of the reservoir (beginning of an experimental run), however, the same pattern will assumingly appear when equilibrium is reached. A smaller difference of the inlet and outlet temperature would assumingly result in a thinner boundary layer than earlier. The effect of less temperature difference internally and externally can be determined at the laboratory with adjustments of the temperature delivered from the Julabo machine.

The cold film and flow outside the U-tube affects the heat transfer from the reservoir to the tube, as the surrounding liquid has a lower temperature than the average temperature at each depth. The temperature measured in the reservoir at different depths does not represent the temperature in close vicinity of the U-tube as the sensors are placed at a distance from the U-tube. The constant radial heat transfer contributes decreases of the local temperature. Similarly, heat is constantly transferred from the surrounding room through the acrylic cylinder to the water. Resultingly, the temperature in the water close to the cylinder wall holds a higher temperature than the measured value.

As visualized with the pH indicator, the radial flow on the outside of the well develops from laminar into turbulent flow. As long as the flow is laminar, the blue color presents a measure of the velocity boundary layer. This movements can be described the same way as smoke from a cigarette. The randomness of the turbulent flow explains how the temperature sensor in the reservoir does not display the exact same temperature pattern for experiments with similar starting points, and why the temperature sensor at times displays small spikes. As the cold water sinks, the whole cross-section in the bottom part is cooled down. This results in a large temperature difference at the top and bottom part of the cylinder, even as the temperature at the top is also reduced due to diffusion and as colder water flows towards the bottom. A typical temperature difference of the upper and lower temperature sensor as the system has reached equilibrium is $5\text{ }^{\circ}\text{C} \pm 1\text{ }^{\circ}\text{C}$. This is visualized also from the thermographic camera displaying the overall temperature change in the cylinder over time (figure 5.2.7).

Whereas the temperature at the laboratory is coldest at the bottom, a real geothermal system may have a different pattern, as the lowest part of the system is closes to the warmer inner core of the earth. Exactly how the temperature profile in the ground will be is challenging to determine. The water in the close vicinity of the U-tube is cooled and descends towards the bottom. The fluid at the bottom is heated and travels upward due to the buoyancy effect. To investigate this at the laboratory, a small heat source could be introduced at the bottom of the cylinder.

6.3.1 Ground-Water Flow

The blue alkaline layer flowing downward indicates the geometric symmetry of the boundary layer of cold surrounding water. Introduction of ground water flow would shift the pattern of the boundary layer and ensure warmer water closer to the copper tube at one side. The ground-water flow-measurements in Bryne proved no flow, however the test could not confirm the flow with 100 % accuracy. If there is groundwater-flow in the area, the transportation of heat down during the summer would be a waste. On the other hand, the underground water would remain more constant throughout the year and result in enhanced heat transfer to the U-tube, with convection in addition to conduction. An introduction of a temperature sensor in one or more wells could reveal whether the temperature is dependent of internal fluid temperatures which are seasonal dependent, or by the external temperature flowing by. Several temperature sensors immersed close to the circumference of the well could reveal if one side holds a higher temperature than the other. If there is a difference, the ground-water flows in the direction from the warm side to the low. Analyzing measurements by temperature sensors in several of the wells would give a new indication of the subsurface environment and confirm/invalidate the current insinuation of the subsurface as a reheatable energy storage.

6.3.2 Temperature in the ground

The uppermost parts of the geothermal wells are affected by the seasonal temperature variations. During the winter when the need for heat is greatest, the temperature in the U-tube may experience cooling in the uppermost part of the U-tube. If the fluid does not anyway reach the outside temperature, this will not make a big effect, however if the fluid is heated up to a temperature higher than the temperature at a depth of i.e. 10 meters, heat will be transported from the internal fluid. This can be avoided by attaching an isolating layer on the exiting tube from the surface down to a suitable depth.

The temperature obtained from a sensor in the collector tube (Figure 3.1.2) displayed an interesting profile. The measurements were done in December when the average temperature in the area is 3-7 °C. The measurements proved an increase from 8.5 to 8.7 °C the first 10 meters, and a decrease of the same amount from 20-30 meters down. The temperature at this depth is highly affected by the season, however at a slight delay. The temperature increase may therefore be caused by a warm autumn. The temperature is from this point slightly decreasing until the depth is 90 meters. At this depth, the seasonal variations are negligible, as the temperature from that depth appears to increase at a constant rate. This proves the temperature gradient is found, and indicates the temperature found above 90 m depth is affected by seasonal variation. The temperature increase from depth = 90 to 190 meters, with a temperature difference of 0.7 °C can be used to estimate a mean temperature in the top layer. The method results in an average surface temperature of 7.47 °C, with a variation of +/- 0.7 °C based on the displayed pattern. This analogy implies the average subsurface temperature throughout the year is equal to the temperature in the middle (due to the linearity), $T_{\text{avg}} = T(100\text{m}) = 8.15 \text{ °C}$.

The water underground must be, like at the laboratory, reduced after some time of heat transfer to the immersed U-tube. The conductivity from the surrounding rock in Bryne is higher than the conductivity from the surroundings at the laboratory. Hence, more heat is transferred to the underground water reservoir. Assuming no ground-water flow; the use of several geothermal wells located close to each other in Bryne may result in a local temperature reduction. Still, the use as “storage” during summertime increases the underground temperature, along with the possible underground water flow. Table 3.3.1, where the temperature of the fluid exiting the well the 6th of May is 7.2 °C, implies the subsurface temperature must be 7.2 or probably higher.

6.4 Internal Flow, Energy output

Calculations of heat obtained by the underground loop was based on different methods. The calculations depending exclusively on the temperature change internally offers a true presentation of the obtained energy. It is called true as the only variation are the measurable mass flow and temperature differences, associated with tiny uncertainties. The equation presenting heat transferred to the inner fluid by convection and conduction from the outside is based on uncertainties connected to the overall heat transfer coefficient and presents a less accurate result. Heat transfer through a wall is a complex process, and accurate calculation depends on several properties. The equation, however, states the importance of the properties and presents a method of calculating heat transfer from the surroundings if more properties are present.

From the coherence of flowrate and temperature difference through the enthalpy, the optimal flowrate was calculated to be $1.53\text{E-}05 \text{ m}^3/\text{s}$. As this was to be tested, the exact intended flowrate was not obtained, as fine tuning of the valves is tricky, and the voltage (flowrate) tend to vary somewhat over time. The flowrate tested was $1.576\text{E-}05 \text{ m}^3/\text{s}$, which did prove a higher energy output than earlier tests, in addition to a higher value than the calculated supreme flowrate. It is difficult to say whether the calculated supreme flowrate would have resulted in a higher or lower energy output. The fact that the obtained energy output was higher than what was calculated may be caused by a false coherence obtained for ΔT vs. flowrate. It can also be caused by a different pattern for energy vs. flowrate for rates close to the supreme rate. As a flowrate close to the calculated supreme resulted in the highest energy output obtained, the method of calculations proved to give appropriate solutions.

The flowrate is hence of great importance for amount of heat gained. A flowrate increase by 50 % from the laboratory optimal, i.e. increase of $0.75\text{E-}05 \text{ m}^3/\text{s}$ results in a 50 % reduction of heat obtained in the reservoir. Running the system with a higher rate will thus result in less obtained energy and more energy usage for the pump. The U-tube conductivity and surrounding temperature influences the optimal rate, and hence the optimal rate of a geothermal system may be affected by seasonal variations in the top layer. Heat delivered divided by internal volume for the system at Bryne is $3859.977 \text{ W}/\text{m}^3$. The same at the laboratory for flow = $1.576\text{E-}05 = 348'870 \text{ W}/\text{m}^3$ and flow = $2.506\text{E-}05 = 125'628 \text{ W}/\text{m}^3$. With the optimal rate, the laboratory setup is almost 100 times more volume effective. With the rate $2.506\text{E-}05$ the laboratory is about 30 times more volume effective. This is highly affected by the difference of the U-tube conductivity and the undiscovered subsurface temperature.

As the geothermal system at Bryne VGS has other dimensions and properties than the laboratory setup, the obtained optimal rate for the laboratory is likely not the optimal rate in Bryne. However, a method to calculate the optimal rate provided allowance of flow rate adjustments is found. By this, the system could be enhanced. Another way of enhancing the system could be by changing the combined heating

and cooling system. Whereas the fluid transporting excess heat from cooling rooms etc. is transported directly into the wells for cooling before merging with the heating part of the cycle on the way to the heat pumps, the excess heat could have been transported to the heating cycle without entering those geothermal wells. Likewise, the fluid from the accumulator leading towards the wells could have been directly transferred to the tubes transferring cold fluid to the rooms with excess heat.

If a geothermal system is running with an optimal rate, but a less amount of energy is needed, a higher COP for a heat pump can be obtained by lowering the flowrate. The following increase of the temperature in heat pump fluid implies the compressor in the heat pump can work at a lower power demanding less electricity. If a higher volume is needed than the supreme amount, the compressor must work harder to compress the fluid to a higher temperature, and will therefore work at a lower COP.

7 Conclusion

The geothermal heat system at Bryne Videregående Skole is a practical and interesting way of producing heat. As the system provides the school with energy, a model of a geothermal well was built to explore internal and external effects of geothermal heat transport by flow rate adjustments. The dimensions and relations of the real and laboratory system is incomparable, however the materials and flow rates at the laboratory provides valuable information about the characteristics of the real system. By experiments, calculations and estimations, helpful information about the complex heat transportation from the ground is obtained. Additionally, the operating system in Bryne and the wish for a simple schematic model demonstrated how a closed, shallow geothermal system can be operated.

The dimensionless numbers prove the internal flow in Bryne is laminar, whereas most of the laboratory experiments show transitional or turbulent internal flow. The major internal heat transfer is caused by convection, the velocity boundary is larger than the thermal, and more heat is transferred by advection than diffusion. Testing high flowrates in combination with the somewhat inaccurate temperature sensors make it challenging to present accurate temperature differences of the inlet and outlet, as the outlet temperature is close to the inlet. By decreasing the flowrate, the temperature difference is increased and a pattern between temperature difference and flowrate is found.

The laboratory setup developed by the students at Bryne VGS works flawlessly, but the additional setup could have been performed in a better way. The isolation around the temperature sensor attached to the copper tube should have been tested so could have been run with a supreme isolation. The temperature sensors' lack of accuracy and calibration memory makes the obtained temperatures and temperature difference vaguely inaccurate. Further, variations in room temperature influence the temperature in the water reservoir; hence the experiments were not all run with the same surrounding temperature. As the travel time is not taken into consideration, the displayed temperature difference for the inlet and outlet is slightly inaccurate for some of the measurements.

The impact of the surrounding liquid is swiftly displayed by use of pH indicator and thermographic camera. The visualization proves that the fluid in the close vicinity of the u-tube is cooled down after transferring heat to the tube, as the density increases, and it sinks to the bottom. The flow pattern varies between laminar and turbulent flow as it sinks. This pattern reduces the temperature primarily at the bottom, then gradually upwards in the reservoir until an equilibrium with the surroundings is reached. The temperature sensors in the water column demonstrates the same temperature profile. As the temperature sensors are placed at a distance from the copper tube, the measured temperature will present the mean temperature at the given depth while the temperature close to the U-tube is colder. Where the water reservoir at the laboratory receives heat from the measurable room temperature, the real system is affected by more factors. The geothermal wells are affected by heat transfer from the bottom due to the

warm center of the earth, heat induced during summertime, surrounding temperature diffusion and possibly ground water flow. The average surrounding temperature in the geothermal wells is assumed to be between 7 and 8.15 °C.

By decrease of the flowrate, a higher temperature difference was obtained, but less volume of the increased temperature fluid was delivered. Considering the mass flow rate and temperature difference of the inlet and outlet allowed calculations of obtained heat. With a coherence of flowrate, mass flow and temperature difference, the optimal rate for the laboratory system was found to be 1.53E-05 m³/s. An experiment with a flowrate close to the optimal, 1.57E-05 m³/s, proved the calculations to be successful, as more energy is obtained from this flowrate than earlier rates. This method of discovering an optimal flowrate presents a technique possibly increase the efficiency at Bryne VGS.

The findings at the laboratory thus presents internal and external occurrences related to the heat transfer applicable to the real system at Bryne Videregående Skole.

Further Research

The findings of this thesis should be strengthened by more tests for all the flowrates.. As the experiments were run for a different time length, it is recommended to run the experiments for a longer time, preferably 7-8 hours to ensure constant temperatures obtained by all the sensors. If leakage is avoided, the setup can also run overnight. A continual running of the system will keep the temperature in the water cylinder cool and resultingly the equilibrium temperatures at new flowrates will be reached faster.

To investigate the external flow pattern further, the test with the pH indicator should be done for different flowrates. As an example, it would be interesting to see how the external pattern changes if the internal flow decreases. To investigate the radial temperature in the reservoir, several (for example 5) temperature sensors could be attached to a stick. The stick should be placed horizontally in the tube touching the U-tube at two places and have the ability to be placed at different places along the depth.

The method discovered in this thesis to discover an optimal flowrate could be tested at Bryne VGS. As the system is providing the school with heat, this test should be run during summertime. If the optimal flowrate proves to be lower than the present, less energy will be needed for the pump.

To investigate ground-water flow further, temperature sensors could be induced in several of the wells over a time period to analyze the differences, or several sensors could be placed different places along the circumference of the well. Temperature sensors should also be used to

As there may be ground-water flow in Bryne, it would be interesting to investigate the impact of flow or mixing caused by other impacts than forced convection in the laboratory reservoir.

The energy system at Bryne Videregående Skole is put together by more components than illustrated in the 3D sketch. A model including the other devices delivering energy to the school could be added in the sketch. The connection between and significance of each component would then be illustrated.

References

- Autodesk. Autodesk Fusion 360. In *Autodesk Homepage*.
- Baker, D. J. (1966). *A technique for the precise measurement of small fluid velocities* (Vol. 25).
- Balkan Pazvantoğlu, E., Erkan, K., & Şalk, M. (2017). *Thermal conductivity of major rock types in western and central Anatolia regions, Turkey* (Vol. 14).
- Banks, D. (2012). *An Introduction to Thermogeology : Ground Source Heating and Cooling*. New York, UNITED KINGDOM: John Wiley & Sons, Incorporated.
- Bentley, J. P. (2005). *Principles of Measurement Systems* (Vol. Fourth Edition): Pearson Prentice Hall.
- Boden, D. R. (2017). *Geologic fundamentals of geothermal energy*. In *Energy and the environment* (Boca Raton, Fla.).
- Boelter, K., Karr, C., Klemp, S., & Sternitske, S. (2018). Refrigerator. Retrieved from <http://blog.uwgb.edu/chem320b/author/klemsh23/>
- Budd, A., Gerner, E., & Suzanne, O. R. Feeling the heat: Geothermal Energy. Retrieved from <https://www.science.org.au/curious/technology-future/feeling-heat-geothermal-energy>
- Çengel, Y. A. (2007). *Heat and mass transfer : a practical approach* (3rd ed. ed.). Boston: McGraw-Hill.
- Çengel, Y. A. (2017). *Fundamentals of thermal-fluid sciences* (Fifth edition]. ed.). New York, N. Y.: McGraw-Hill Education.
- Crank, J. (1975). *The mathematics of diffusion* (2nd ed. ed.). Oxford: Clarendon Press.
- DNF. (2013). Flowchart, Brynde Videregående Skole. In B.-V. F. D. 1&2 (Ed.): Rogaland Fylkeskommune.
- Egg, J., & Howard, B. C. (2010). *Geothermal HVAC*: McGraw-Hill Professional.
- EngineeringToolBox. (2003). Propylene Glycol based HEat-Transfer Fluids. Retrieved from https://www.engineeringtoolbox.com/propylene-glycol-d_363.html
- EngineersEdge. (2019). Combined Overall Heat Transfer Coefficient Equation. *Heat Transfer Engineering, Thermodynamics*. Retrieved from <https://www.engineersedge.com/heat-transfer/overall-heat-transfer-coef.htm>
- Erdogan, B. (2010). *The Sizing of Vertical Single U-Tube Ground Heat Exchanger For Ground Source Heat Pump*. Paper presented at the International Scientific Conference, Trakya University, Mechanical Engineering Department, Edirne, Turkey.
- Finger, J., & Blankenship, D. (2011). *Handbook of Best Practices for Geothermal Drilling*.
- Focke, W. W., & Knibbe, P. G. (1986). Flow visualization in parallel-plate ducts with corrugated walls. *J. Fluid Mech*, 156, 73-77.
- FuseSchool (Writer) & F.-G. Education (Director). (2016). What is Electrolysis | Chemistry for All | FuseSchool. In: Youtube.
- Gjøølberg, M. (2011). *Dyp Geotermisk Varme - Noe For Norge?*, Universitet for Miljø- og Biovitenskap, Retrieved from <https://brage.bibsys.no/xmlui/bitstream/handle/11250/188684/Masteroppgave%20-%202011%20-%20Mari%20Gj%C3%B8lberg.pdf?sequence=1>
- Grønneberg, T. (1997). *Kjemien stemmer* (Nynorsk [utg.]. ed.). Oslo: Cappelen.
- Hauser, E. (2017). Electromagnetic Flow Measuring Principle. *Flow Measurement*.
- Incropera, F. P., DeWitt, D. P., Bergman, T. L., & Lavine, A. S. (2007). *Fundamentals of heat and mass transfer* (6th ed. ed.). New York: Wiley.
- Kreith, F. (2000). *The CRC Handbook of Thermal Engineering*: CRC Press LLC.
- Lumen. Volume and Density. <https://courses.lumenlearning.com/introchem/chapter/volume-and-density/>
- Michaud, G. (2005). A Brief Introduction to Thermodynamics. In.
- Monteith, J., & Unsworth, M. (2013). *Principles of Environmental Physics : Plants, Animals, and the Atmosphere*. Jordan Hill, UNITED KINGDOM: Elsevier Science & Technology.

- Negash, T. (2017). Heat Transfer. In D. M. U. M. E. Department (Ed.), *Slideshare*.
- NGU (Cartographer). (2019). Geologien i min kommune. Retrieved from <http://geo.ngu.no/kart/minkommune/>
- Nilsen, D. A. J. (2015). Energisentral+Bryne+Videregående[3096]. In *PowerPoint Presentation*
- OpenStax. (2016). *Chemistry*.
- PipeLife. (2007). Rørhåndboka. In *Initio*: Pipelife Norge AS.
- Ramstad, R. K. (2012). Beskrivelse K202 Energibrønner og Rør - Generell del. In A. Viak (Ed.).
- Rapp, B. E. (2017). *Microfluids: Modelling, Mechanics and Mathematics* (Vol. Chapter 9, Péclet Number).
- Reddy, M. P. M. (2001). *Descriptive Physical Oceanography*: A.A. Balkema Publishers.
- Shapley, P. (2011). Temperature effects on Density. Retrieved from <http://butane.chem.uiuc.edu/pshapley/GenChem1/L21/2.html>
- Sharma, A., Shukla, A., & Aye, L. (2018). *Low Carbon Energy Supply : Trends, Technology, Management*. In *Green Energy and Technology*.
- Sherwin, K., & Horsley, M. (1996). *Thermofluids*: Chapman Hall.
- Shet, P. U. S. P., Sundararajan, P. T., & Mallikarjuna, P. J. M. Reversed Carnot Cycle. *Refrigeration Cycles*.
- Shires, G. L. (2011). Peclet Number. *Thermopedia*.
- Straalberg, E. A. (2013). *Energieffektivitet i Grunne Geotermisk Systemer*. (Master), University of Bergen, Bora. Retrieved from <http://bora.uib.no/bitstream/handle/1956/7109/109343997.pdf?sequence=1&isAllowed=y>
- Thorsnæs, G. (2019, 5th of February). Rogaland. Retrieved from <https://snl.no/Rogaland>
- ur Rehman, M. (2015). vapour compression cycle. In (pp. 21).
- USA-NASHUA. Flir C2: Powerful, Compact Thermal Imaging System. In FLIR (Ed.).
- Wikipedia. (2019). Universal Indicator. In t. f. E. Wikipedia (Ed.).
- Yang, X., & Kong, S.-C. (2017). *Numerical study of natural convection states in a horizontal concentric cylindrical annulus using SPH method*.

Appendix 1,2,3,4,5

Appendix 1 - Calibrations	ii
Appendix 2 – Test of pH and Salinity.....	vi
Appendix 3 Enthalpy Table and Data from IWMAC	ix
Table of enthalpy	ix
IWMAC	x
Data for table 3.3.1.....	xiii
Appendix 4 – other calculations of optimal rate	xix
Equation 2.3	xix
Equation 2.6	xxi
Appendix 5 Experimental Graphs.....	xxii
Flow = 0.7056E-05	xxii
Flow = 1.006E-05	xxiii
Flow = 1.45E-05	xxiv
Flow = 1.576E-05	xxv
Flow = 1.929E-05	xxvi
Flow = 2.506 E-05	xxvii
Flow = 3.83E-057	xxviii
Flow = 4.17E-05	xxviii
Flow = 6.00E-05	xxix
Flow = 7.00E-05	xxix
Flow = 7.67E-05	xxx
Flow = 8.50E-05	xxx
Flow = 8.67E-05	xxx
Flow = 10.50E-05	xxx
Flow = 12.33E-05	xxxii
Flow = 13.83E-057	xxxiii
Flow = 15.33E-05	xxxiv
Flow = 16.83E-05	xxxv
44 Hour Test, Flow = 8.33E-05 m ³ /s	xxxvi
Room Temperature, 27 Hours.....	xxxvi

Appendix 1 - Calibrations

pH

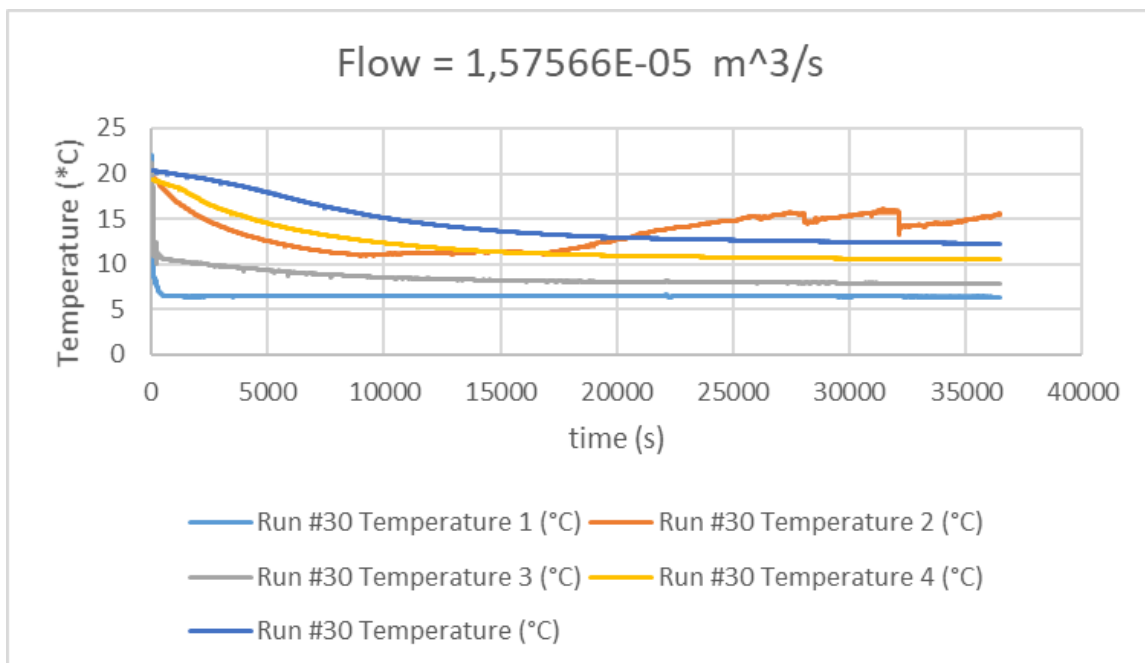
The pH indicator had been used by others not too long ago hence the only type of calibration used was by checking if a neutral solution of water had a neutral pH value.

Salinity

Small bags containing solutions with a given salinity comes with the apparatus for calibration. The solution was poured into a small container where upon the pH dipstick was immersed. To solutions with different salinity came with the machine and so both solutions were used for the calibration.

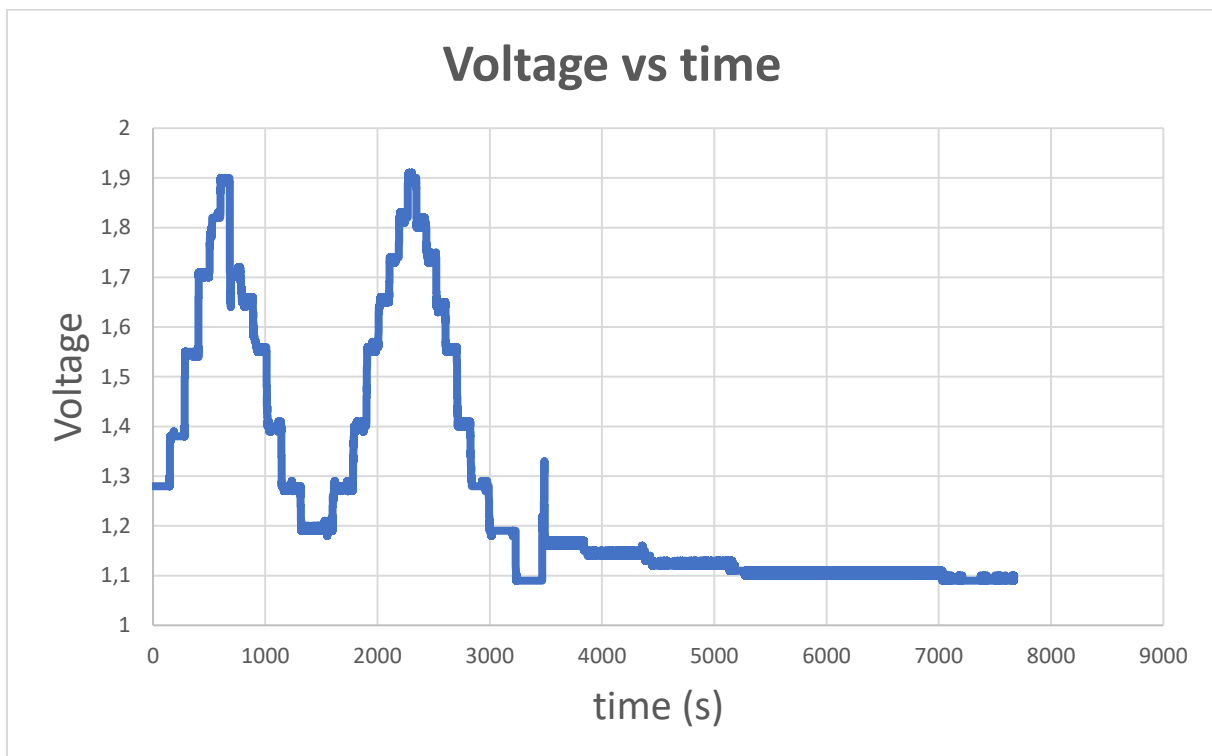
Pasco temperature sensors - Calibrator Dry Well

Before starting the experiment, all five temperature sensors were tested and calibrated. The calibration was done using a Calibrator by Fluke, 9102S DRY-WELL. The apparatus provides the desired temperature and works with the accuracy of 0,01. The sensors were calibrated by dual calibration, where the sensors were placed inside the Calibrator, and calibrated by the Pasco Capstone software using two different temperatures. As there more than one time were uncertainties regarding the temperature sensors, they were tested using and same device multiple times, in addition to being re-calibrated as it appears the calibrations slip out over time. Furthermore, two of the sensors may have turned bad after being submerged in water for a large period, or due to the addition of thymol blue or salt, as they at one point decided to not react to the real temperature anymore. This is displayed in the below graph, for temperature 2.



Calibration of the Electromagnetic flowmeter:

By use of the water tap, a loop through the flowmeter fills a container with a fixed volume. A constant stream from the tap runs through the flowmeter connected to the Pasco device for the voltage to be displayed on the Pasco Capstone Software. By measuring the time it takes to fill the container, a graph matching voltage to flow is made. On the graph, a linear trend line is put in along with its formula in order for flow rates to be calculated from the voltage measured. For a visualizing effect, the flow used for the calibration started slow and stepwise increased to the maximum, before the similar steps was taken to reduce the flowrate down to a minimum. The hole experiment was then repeated. This way the approximately similar flow/voltage was measured multiple times with different impacts in the meantime to ensure stability and continuity in the system. To finish, four tests was made with flowrates closer to zero. The obtained curve is presented below.



The voltage measured as the fluid was still was 1.09 volt.

Based on the measured time and volume (5 liters), the flowrate for each flow was calculated. A plot of the calculated flowrates vs the measured voltage with addition of a trend line proves the correlation is linear. The trend line slope and equation enables a tool for calculation of flowrates from voltage.

Given in the graph underneath, $y = 13,85x - 15,047$, where y = flowrate (l/min) and x = measured voltage (v). The R^2 value describing the accuracy fit is $R^2 = 0,9991$, resultingly the linear fit represents a decent approximation. Moreover, it appears to be even more accurate for the lower flow rates, which is where most of these measurements are to take place.

Reasons for the inaccuracy can be inaccurate time measure; hard to put the exact time for stop and start. The voltmeter is slightly inaccurate as it gives a step jump of 5.19 mV.

time (h:m:s)	Volt	Q (l/min)
00:27:25	1,1013	0,18
00:11:03	1,12208	0,45
00:06:41	1,14	0,75
00:04:43	1,16364	1,06
00:03:31	1,18961	1,42
00:03:20	1,19481	1,50
00:01:55	1,27792	2,61
00:01:54	1,27792	2,63
00:01:53	1,27792	2,63
00:01:53	1,27792	2,65
00:01:15	1,37662	4,00
00:01:10	1,3974	4,29
00:01:09	1,3974	4,35
00:01:09	1,4026	4,35
00:00:47	1,54805	6,38
00:00:46	1,55844	6,52
00:00:46	1,55844	6,52
00:00:45	1,56364	6,67
00:00:40	1,63636	7,50
00:00:38	1,65195	7,89
00:00:38	1,65195	7,89
00:00:35	1,7039	8,57
00:00:34	1,7039	8,82
00:00:33	1,72306	9,09
00:00:33	1,72987	9,09
00:00:30	1,80779	10,00
00:00:30	1,81818	10,00
00:00:30	1,82338	10,00
00:00:27	1,8961	11,11
00:00:27	1,9011	11,11

Tabell 1 Time for filling 5 liters vs voltage vs calculated flow in sorted order by time.

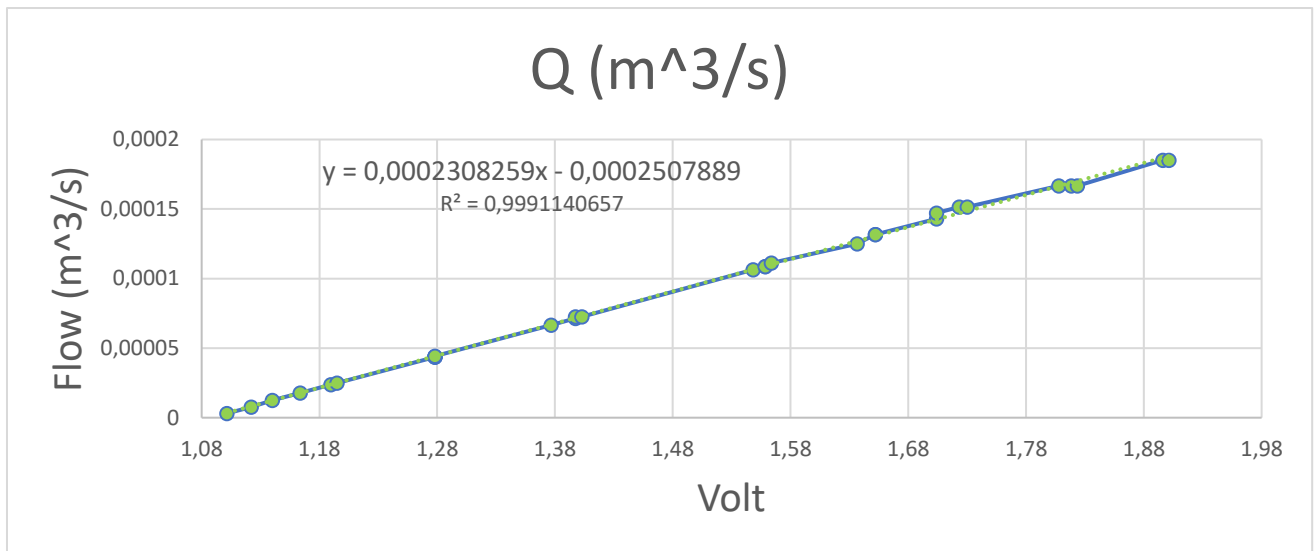
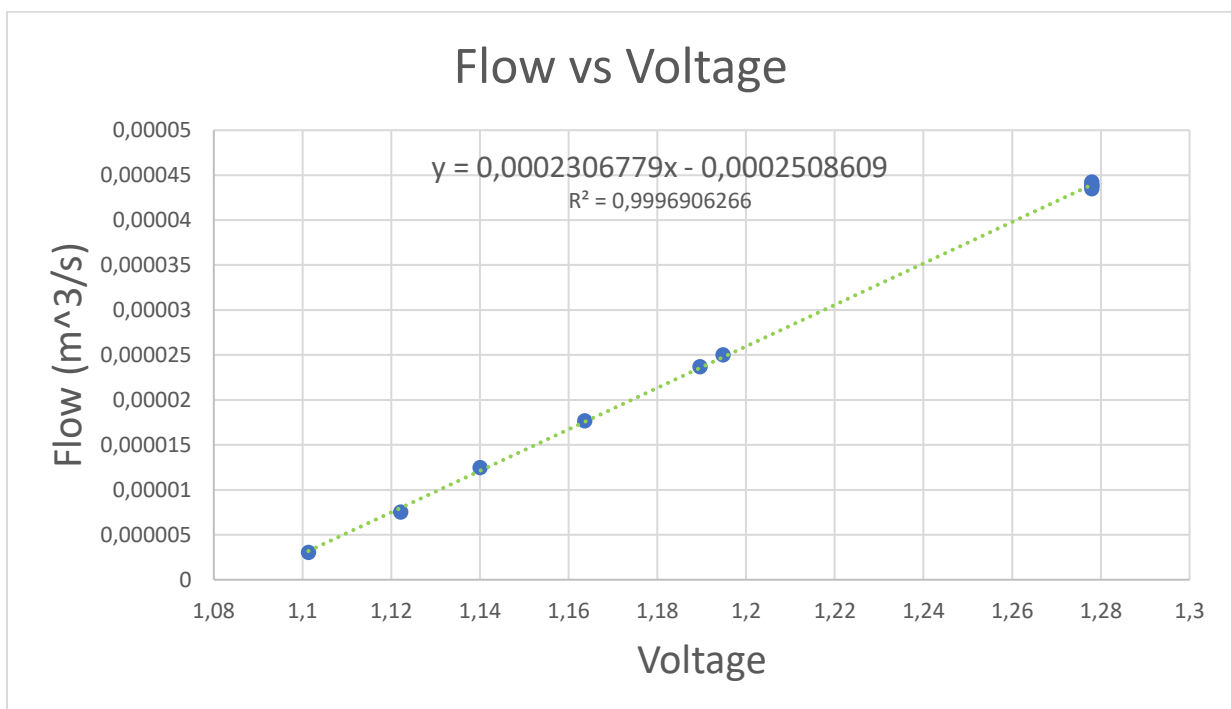


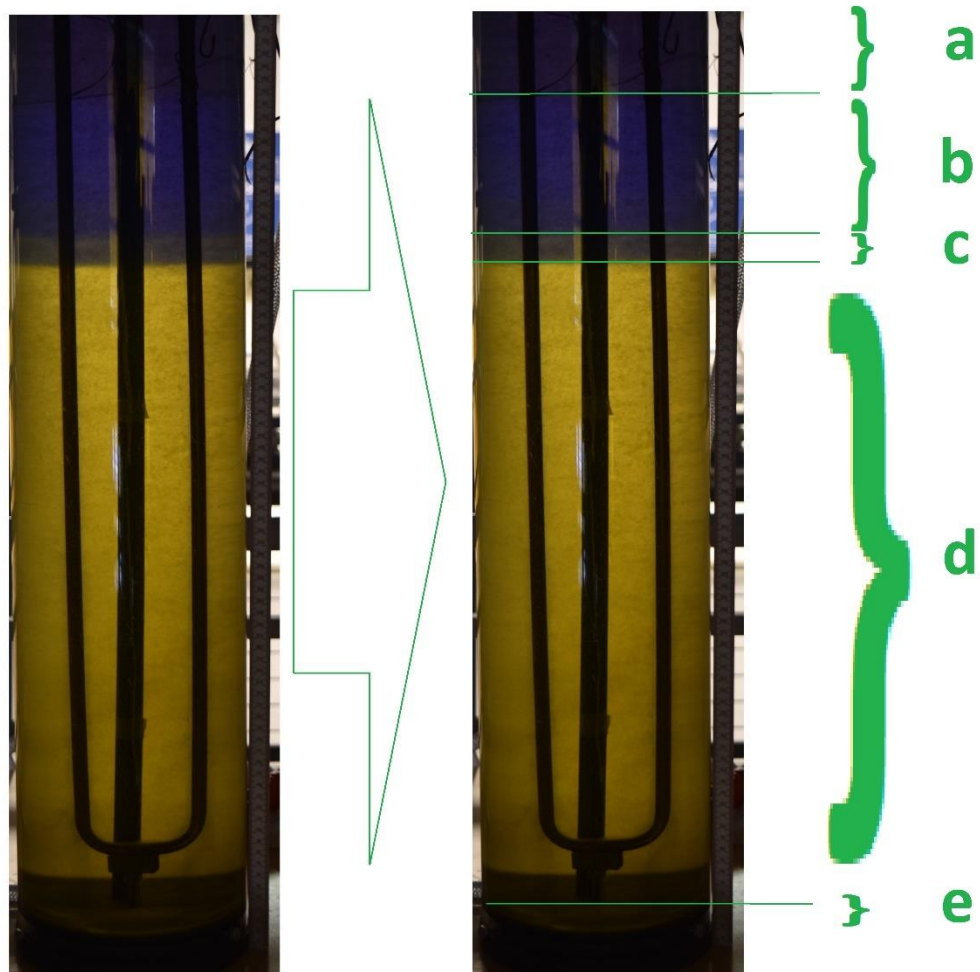
Figure 2 Calculated Flow vs Voltage for the calibration rounds with the trend line and its formula

As the experiments to be performed using the electromagnetic voltmeter will occur at low flowrates and the accuracy is assumed to be larger for the lowest flowrates (as the time for exact filling of the volume is easier to capture when the flow is low), the lowest rates are used to create the trendline.



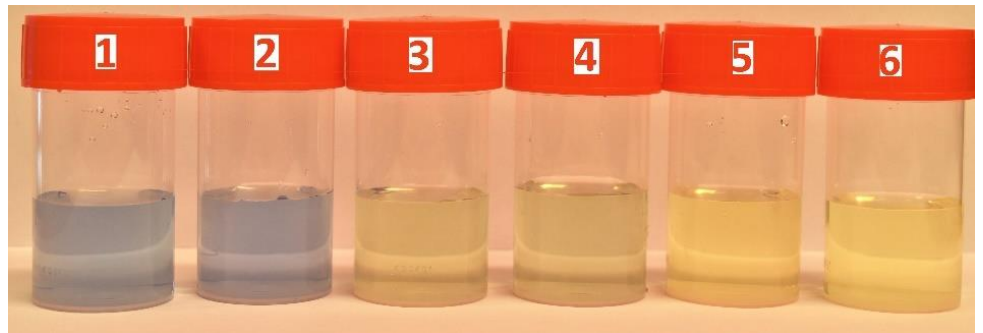
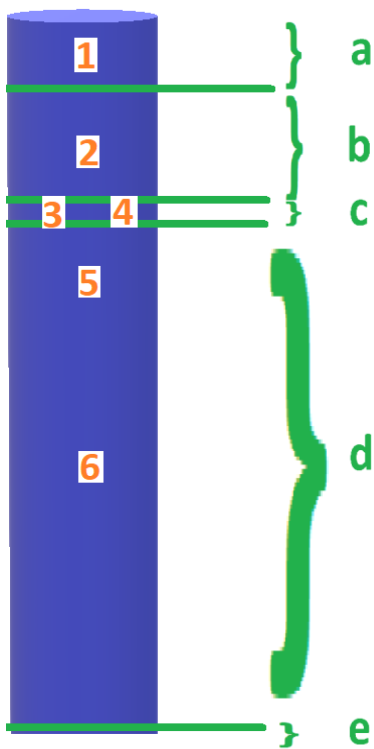
The equation given for the flow (y) can thus be used by filling in the voltage for x.

Appendix 2 – Test of pH and Salinity



The five layers are separated by color, where the first four, a-d, are fluid and the last, e, consists of bottom settlings from reactions between the copper tube and an aluminum screw. By the use of a pipette, a sample was taken from layer a and b, and two samples taken from layer c and d. The samples were tested for salinity and pH value by SevenCompact™ S230 Conductivity meter and SevenEasy™ pH Meter S20, respectively, both delivered by Mettler Toledo. The results are provided in the table below.

Number	Depth [cm]	Salinity [$\mu\text{S}/\text{cm}$]	pH
1	5	1390	9,07
2	16	1764	9,13
3	23	2040	8,47
4	23	2010	8,25
5	32	2170	7,95
6	52	2180	7,75



According to the color of the solutions, it is reasonable to assume the acidity of solution number 1 to be highest, and the pH value of number 3 and 4 to be equal. The reason for this hypothesis to be false, is perhaps the instability of the system and lack of accuracy when collecting the samples. Due to the poor viscosity in the fluid, the molecules quickly begin to move about when the pipette is immersed.

However, the main overview is obtained by both the mean decrease of pH in the table and the colors in the figure (containers with the samples)

The salinity increases towards the bottom, although it appears constant throughout the yellow zone. To achieve finer results, samples from the cylinder should be more carefully gathered, perhaps with a time difference for the system to regain its stability. Several samples can also be collected from each layer to verify the samples.

The separation in the cylinder works as a terrific scene to visualize the effect of the internal flow on the external reservoir. As the internal flow was started, a set up camera shot frames along the cycle at different time intervals. With an interval of three seconds, the image below illustrates the movement of the basic layer as it is cooled down.

Appendix 3 Enthalpy Table and Data from IWMAC

Table of enthalpy

904

PROPERTY TABLES AND CHARTS

TABLE A-4
Saturated water—Temperature table

Temp., T °C	Sat. press., P_{sat} kPa	Specific volume, m^3/kg		Internal energy, kJ/kg			Enthalpy, kJ/kg			Entropy, kJ/kg·K		
		Sat. liquid, v_f	Sat. vapor, v_g	Sat. liquid, u_f	Evap., u_{fg}	Sat. vapor, u_g	Sat. liquid, h_f	Evap., h_{fg}	Sat. vapor, h_g	Sat. liquid, s_f	Evap., s_{fg}	Sat. vapor, s_g
0.01	0.6117	0.001000	206.00	0.000	2374.9	2374.9	0.001	2500.9	2500.9	0.0000	9.1556	9.1556
5	0.8725	0.001000	147.03	21.019	2360.8	2381.8	21.020	2489.1	2510.1	0.0763	8.9487	9.0249
10	1.2281	0.001000	106.32	42.020	2346.6	2388.7	42.022	2477.2	2519.2	0.1511	8.7488	8.8999
15	1.7057	0.001001	77.885	62.980	2332.5	2395.5	62.982	2465.4	2528.3	0.2245	8.5559	8.7803
20	2.3392	0.001002	57.762	83.913	2318.4	2402.3	83.915	2453.5	2537.4	0.2965	8.3696	8.6661
25	3.1698	0.001003	43.340	104.83	2304.3	2409.1	104.83	2441.7	2546.5	0.3672	8.1895	8.5567
30	4.2469	0.001004	32.879	125.73	2290.2	2415.9	125.74	2429.8	2555.6	0.4368	8.0152	8.4520
35	5.6291	0.001006	25.205	146.63	2276.0	2422.7	146.64	2417.9	2564.6	0.5051	7.8466	8.3517
40	7.3851	0.001008	19.515	167.53	2261.9	2429.4	167.53	2406.0	2573.5	0.5724	7.6832	8.2556
45	9.5953	0.001010	15.251	188.43	2247.7	2436.1	188.44	2394.0	2582.4	0.6386	7.5247	8.1633
50	12.352	0.001012	12.026	209.33	2233.4	2442.7	209.34	2382.0	2591.3	0.7038	7.3710	8.0748
55	15.763	0.001015	9.5639	230.24	2219.1	2449.3	230.26	2369.8	2600.1	0.7680	7.2218	7.9898
60	19.947	0.001017	7.6670	251.16	2204.7	2455.9	251.18	2357.7	2608.8	0.8313	7.0769	7.9082
65	25.043	0.001020	6.1935	272.09	2190.3	2462.4	272.12	2345.4	2617.5	0.8937	6.9360	7.8296
70	31.202	0.001023	5.0396	293.04	2175.8	2468.9	293.07	2333.0	2626.1	0.9551	6.7989	7.7540
75	38.597	0.001026	4.1291	313.99	2161.3	2475.3	314.03	2320.6	2634.6	1.0158	6.6655	7.6812
80	47.416	0.001029	3.4053	334.97	2146.6	2481.6	335.02	2308.0	2643.0	1.0756	6.5355	7.6111
85	57.868	0.001032	2.8261	355.96	2131.9	2487.8	356.02	2295.3	2651.4	1.1346	6.4089	7.5435
90	70.183	0.001036	2.3593	376.97	2117.0	2494.0	377.04	2282.5	2659.6	1.1929	6.2853	7.4782
95	84.609	0.001040	1.9808	398.00	2102.0	2500.1	398.09	2269.6	2667.6	1.2504	6.1647	7.4151
100	101.42	0.001043	1.6720	419.06	2087.0	2506.0	419.17	2256.4	2675.6	1.3072	6.0470	7.3542
105	120.90	0.001047	1.4186	440.15	2071.8	2511.9	440.28	2243.1	2683.4	1.3634	5.9319	7.2952
110	143.38	0.001052	1.2094	461.27	2056.4	2517.7	461.42	2229.7	2691.1	1.4188	5.8193	7.2382
115	169.18	0.001056	1.0360	482.42	2040.9	2523.3	482.59	2216.0	2698.6	1.4737	5.7092	7.1829
120	198.67	0.001060	0.89133	503.60	2025.3	2528.9	503.81	2202.1	2706.0	1.5279	5.6013	7.1292
125	232.23	0.001065	0.77012	524.83	2009.5	2534.3	525.07	2188.1	2713.1	1.5816	5.4956	7.0771
130	270.28	0.001070	0.66808	546.10	1993.4	2539.5	546.38	2173.7	2720.1	1.6346	5.3919	7.0265
135	313.22	0.001075	0.58179	567.41	1977.3	2544.7	567.75	2159.1	2726.9	1.6872	5.2901	6.9773
140	361.53	0.001080	0.50850	588.77	1960.9	2549.6	589.16	2144.3	2733.5	1.7392	5.1901	6.9294
145	415.68	0.001085	0.44600	610.19	1944.2	2554.4	610.64	2129.2	2739.8	1.7908	5.0919	6.8827
150	476.16	0.001091	0.39248	631.66	1927.4	2559.1	632.18	2113.8	2745.9	1.8418	4.9953	6.8371
155	543.49	0.001096	0.34648	653.19	1910.3	2563.5	653.79	2098.0	2751.8	1.8924	4.9002	6.7927
160	618.23	0.001102	0.30680	674.79	1893.0	2567.8	675.47	2082.0	2757.5	1.9426	4.8066	6.7492
165	700.93	0.001108	0.27244	696.46	1875.4	2571.9	697.24	2065.6	2762.8	1.9923	4.7143	6.7067
170	792.18	0.001114	0.24260	718.20	1857.5	2575.7	719.08	2048.8	2767.9	2.0417	4.6233	6.6650
175	892.60	0.001121	0.21659	740.02	1839.4	2579.4	741.02	2031.7	2772.7	2.0906	4.5335	6.6242
180	1002.8	0.001127	0.19384	761.92	1820.9	2582.8	763.05	2014.2	2777.2	2.1392	4.4448	6.5841
185	1123.5	0.001134	0.17390	783.91	1802.1	2586.0	785.19	1996.2	2781.4	2.1875	4.3572	6.5447
190	1255.2	0.001141	0.15636	806.00	1783.0	2589.0	807.43	1977.9	2785.3	2.2355	4.2705	6.5059
195	1398.8	0.001149	0.14089	828.18	1763.6	2591.7	829.78	1959.0	2788.8	2.2831	4.1847	6.4678
200	1554.9	0.001157	0.12721	850.46	1743.7	2594.2	852.26	1939.8	2792.0	2.3305	4.0997	6.4302

Çengel, Y. A. (2017). *Fundamentals of thermal-fluid sciences*. New York, N. Y., McGraw-Hill Education.

IWMAC

Date of data visualization is displayed in the top left corner of each clipping. All data delivered by IWMAC.

For the thesis, the IWMAC presentation of the heat pumps, geothermal wells and an overview of energy production and utilization is used. To display the appearance, a clipping of each of them is presented below. All clipping represents data from the 18th of March, at 12:00.

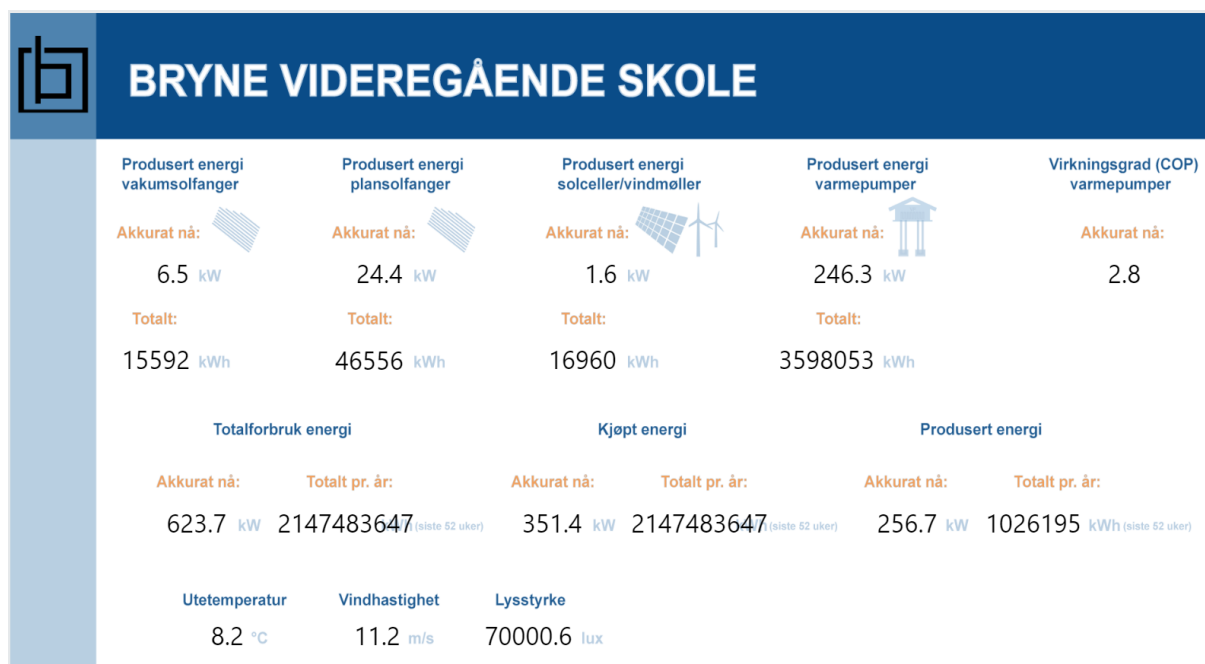


Figure 3 Energy production and utilization at BVGS (18.03.19)

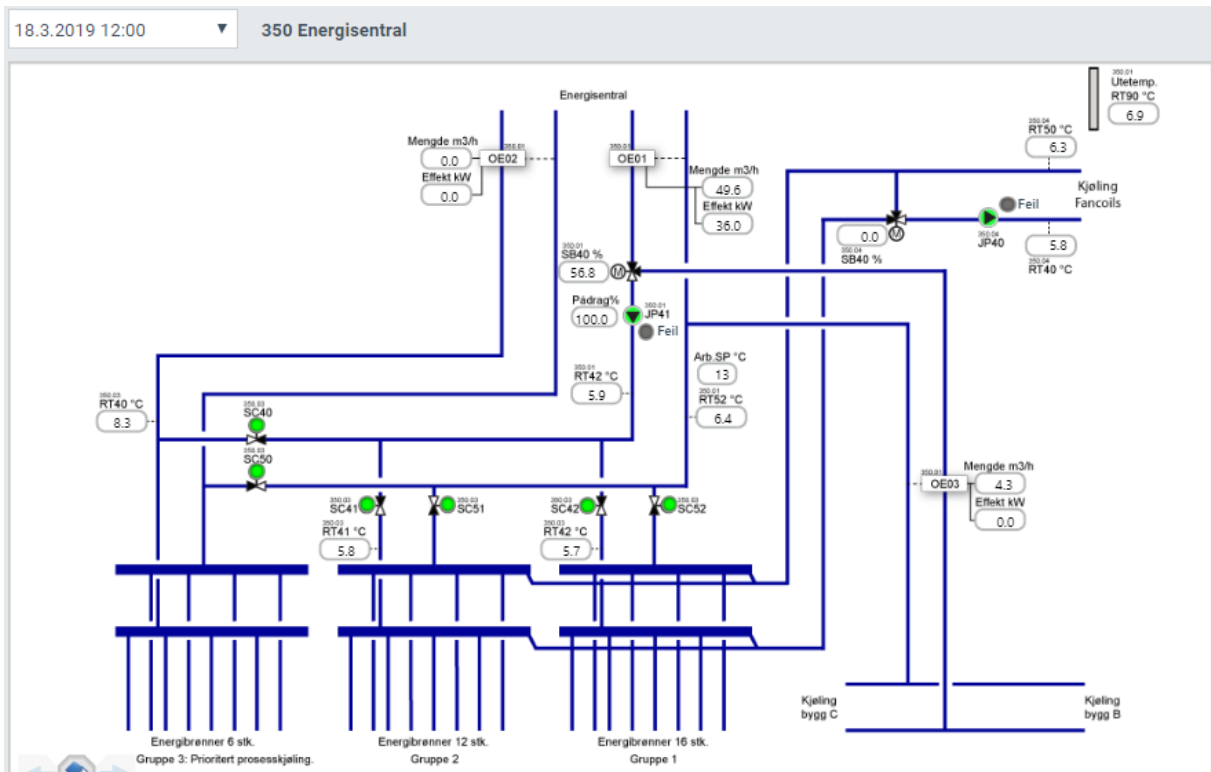


Figure 2 The geothermal well system

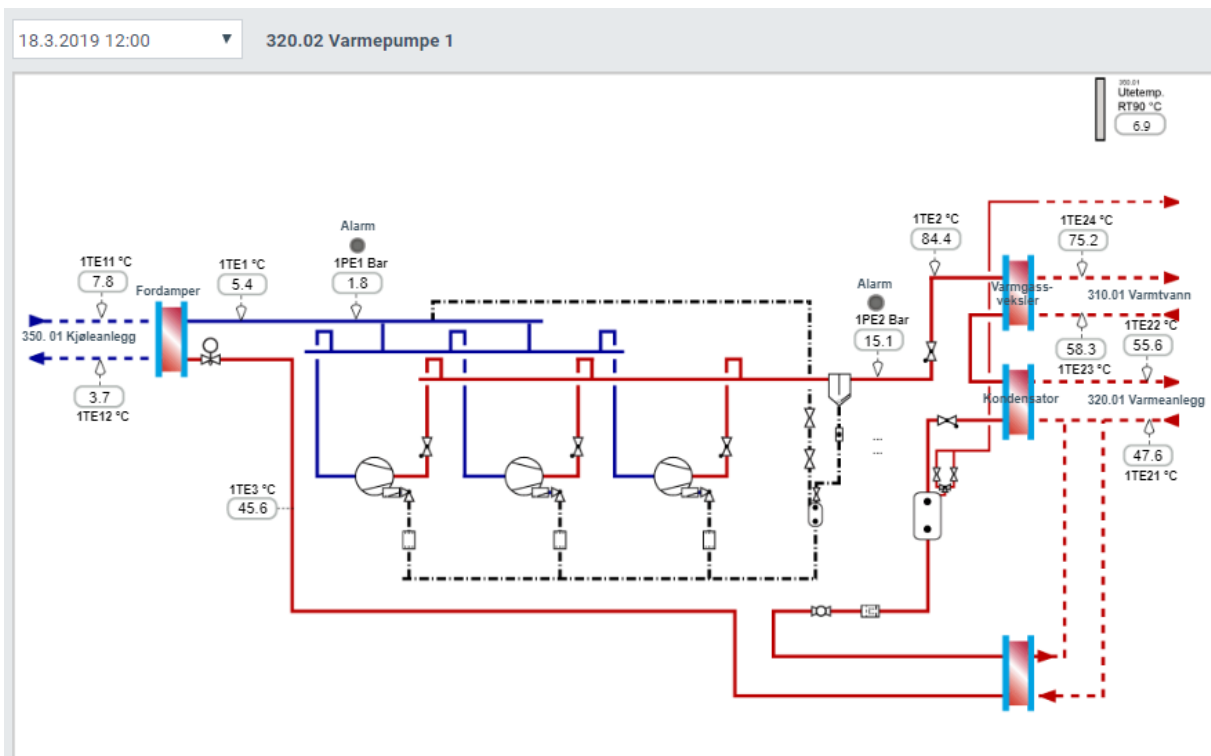


Figure 3 Heat pump 1 (18.03.19)

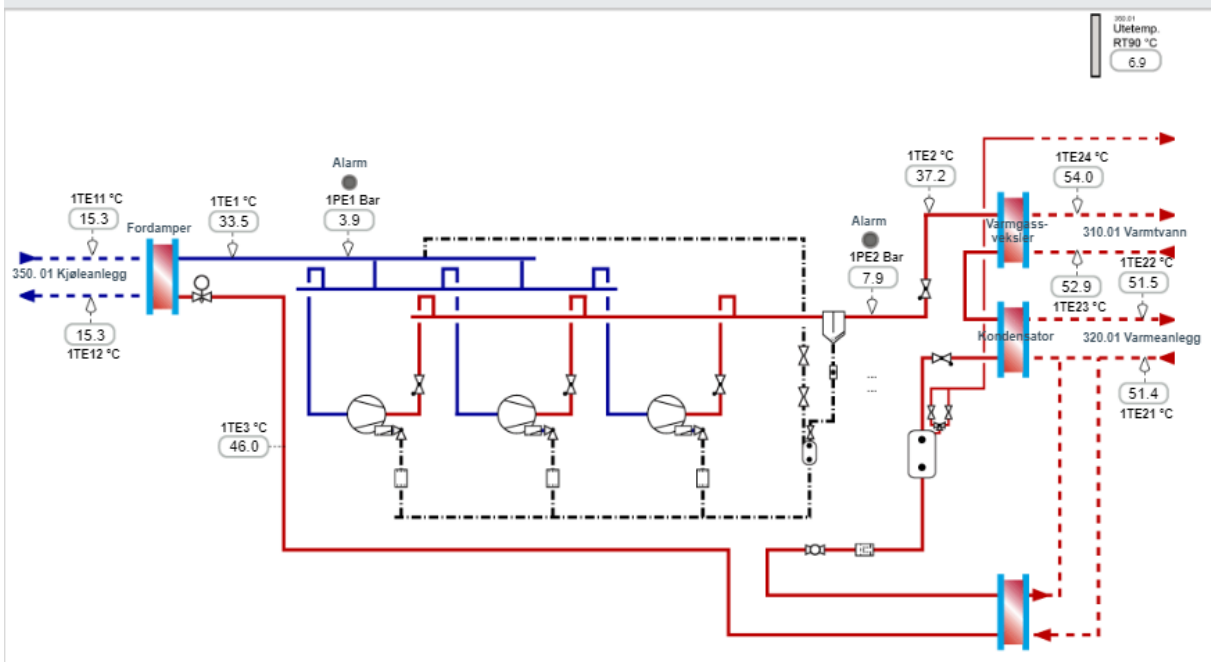
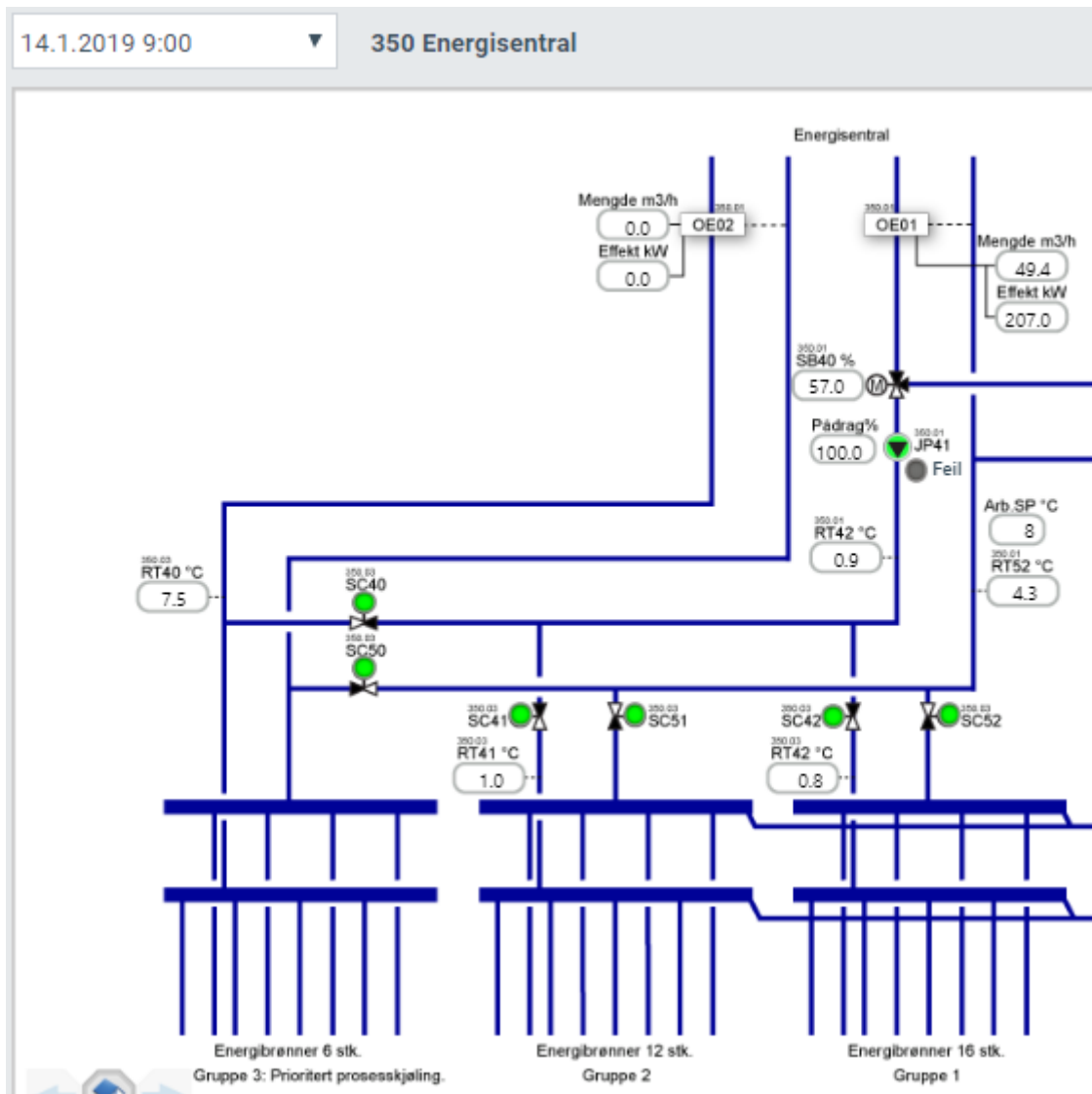
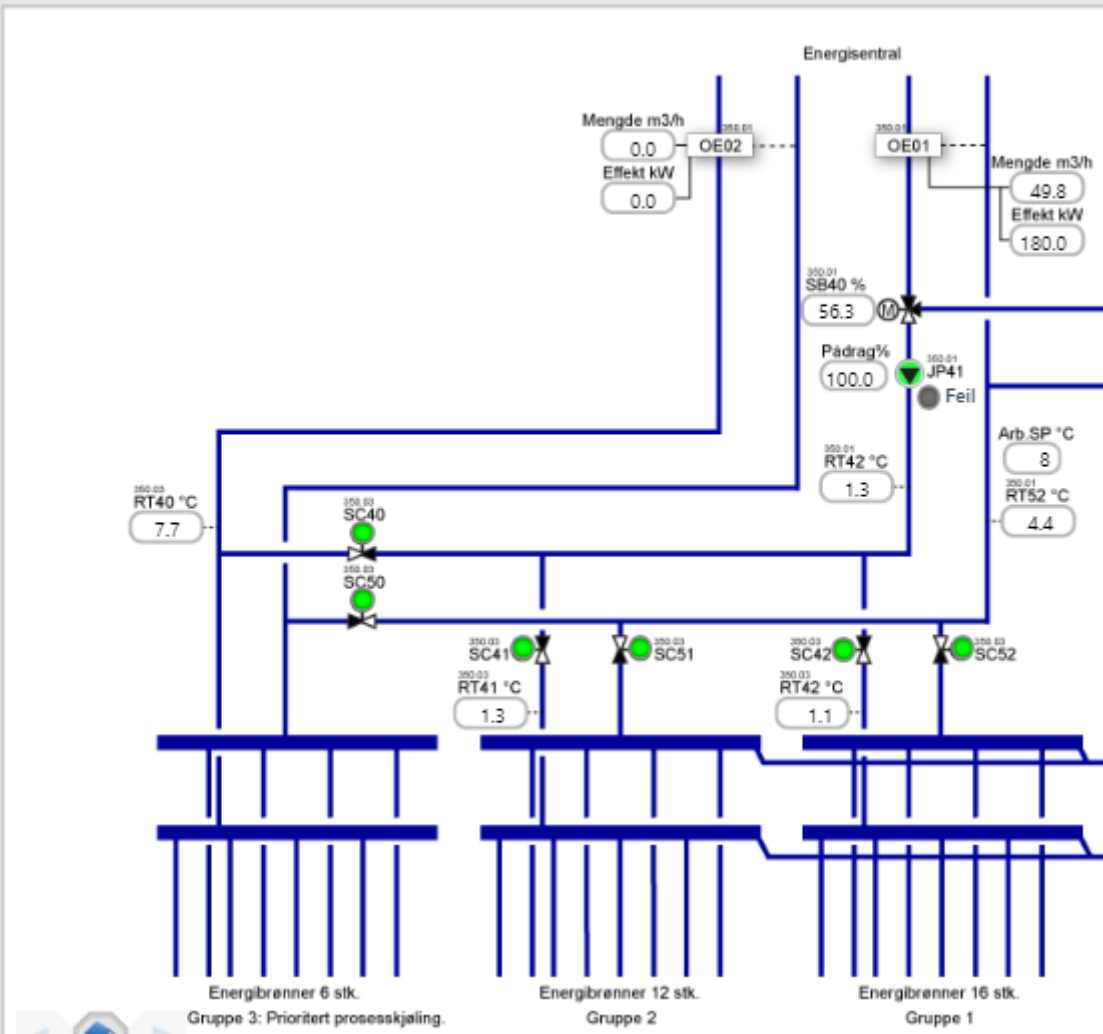


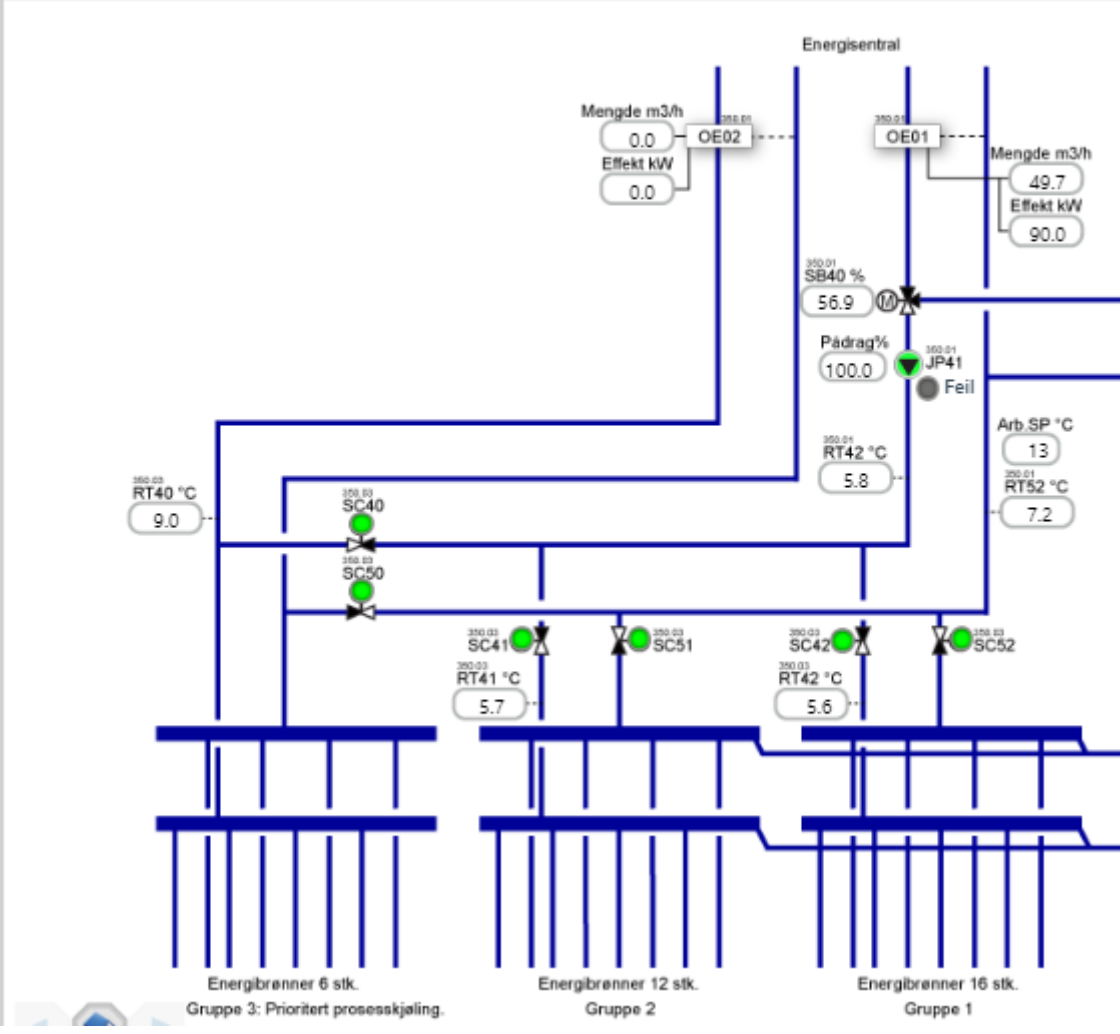
Figure 4 Heat Pump 2

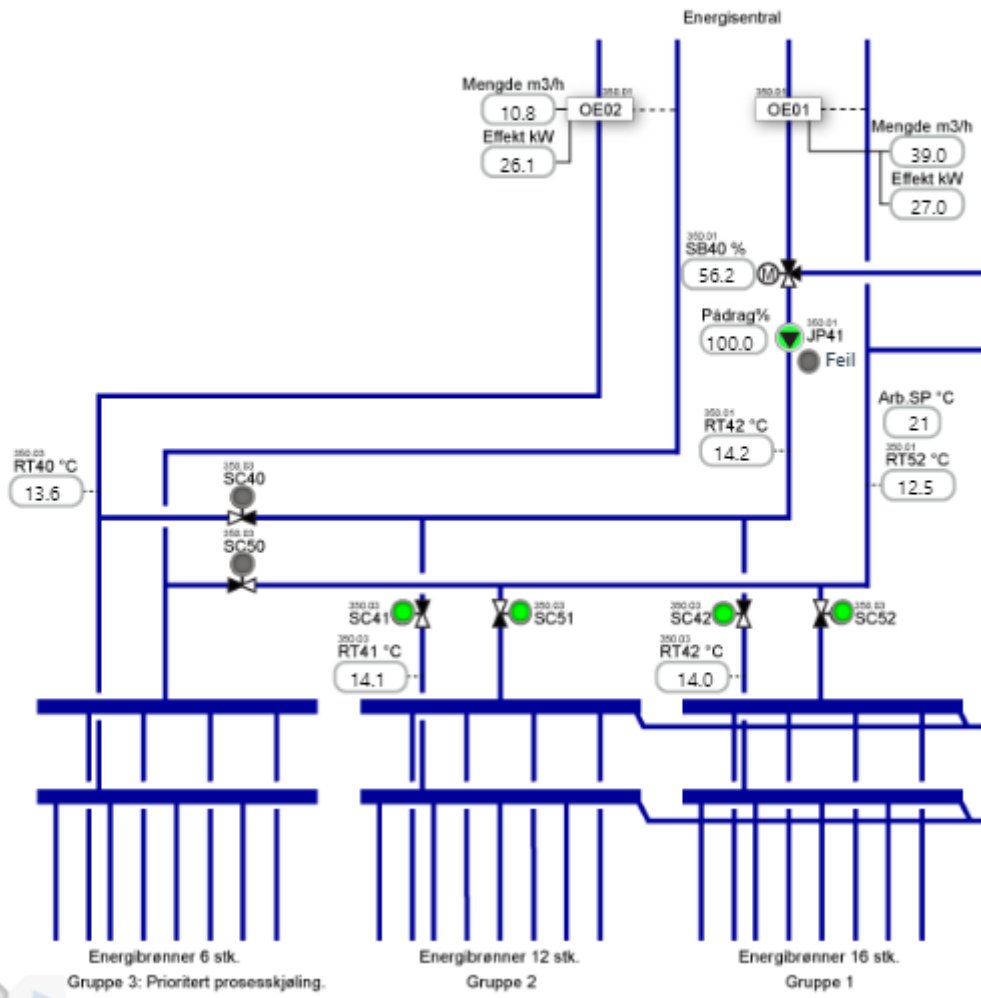
Data for table 3.3.1

Geothermal Wells

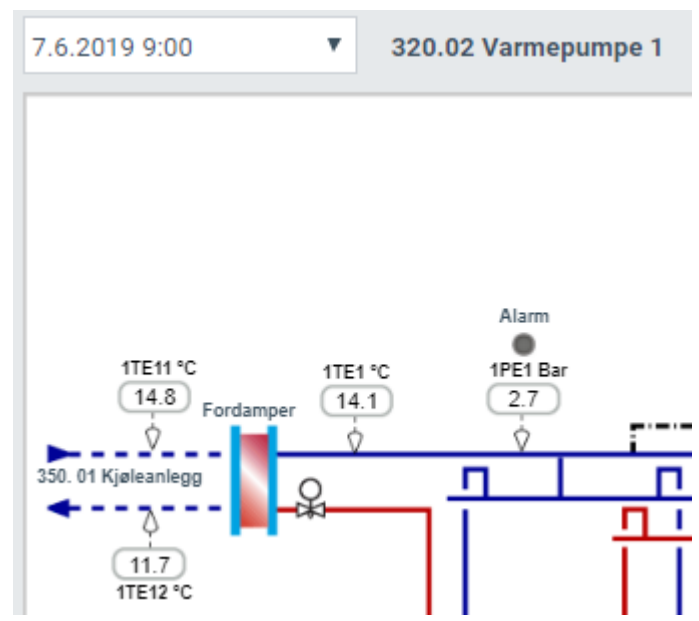
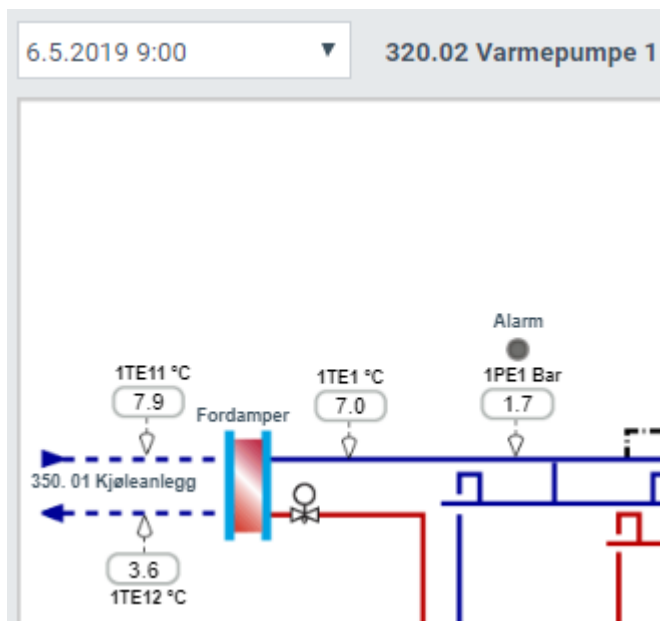
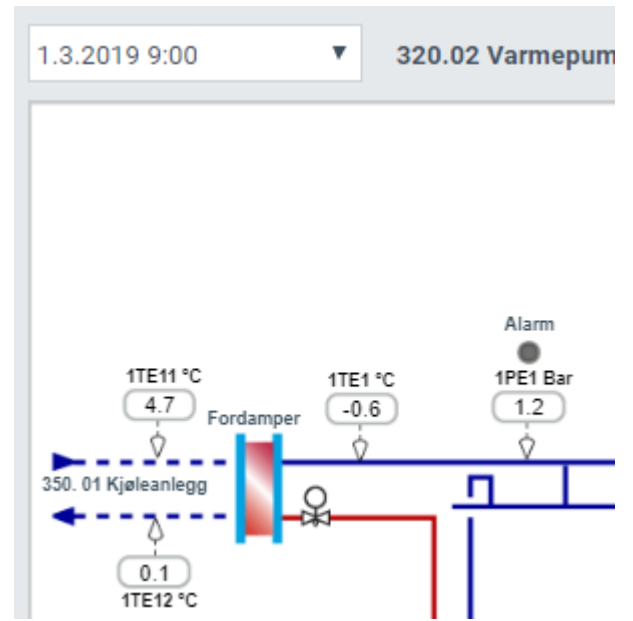
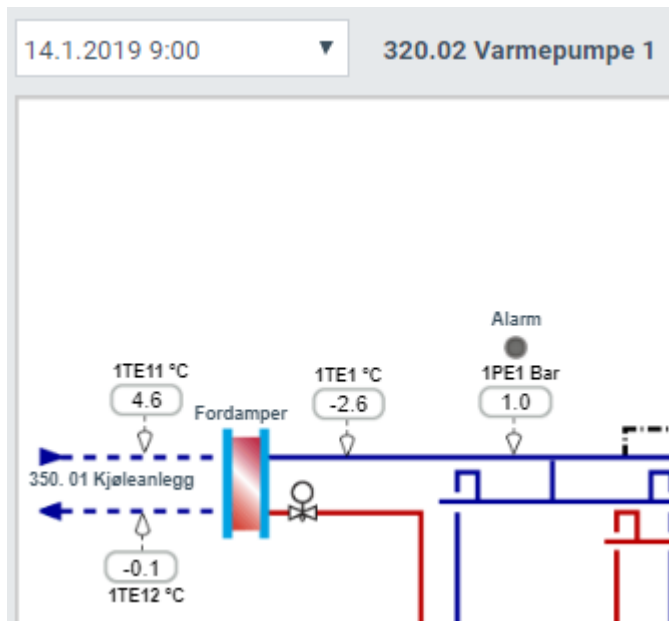




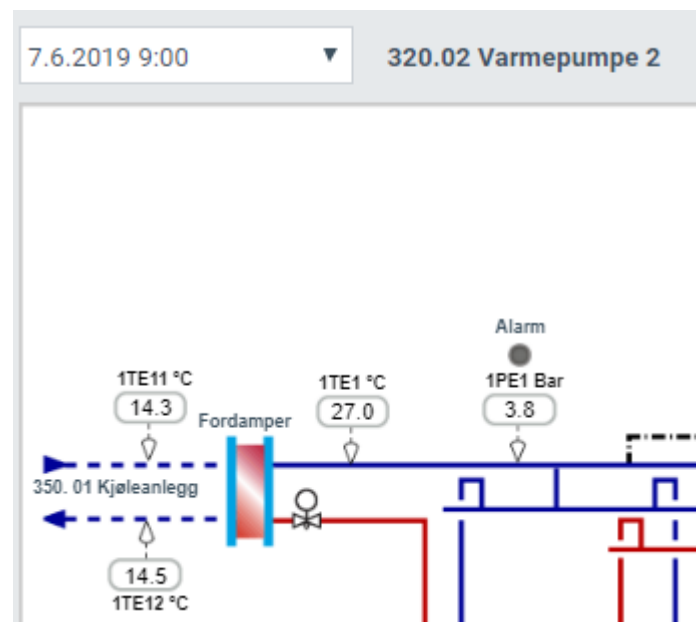
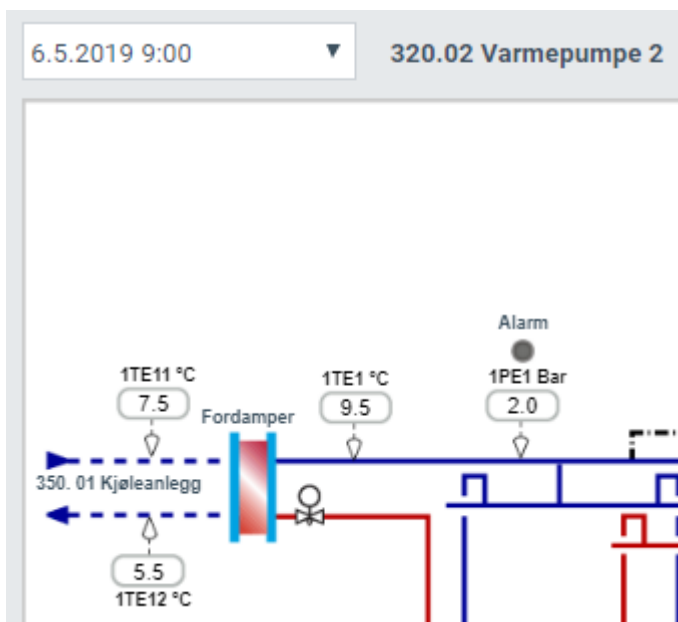
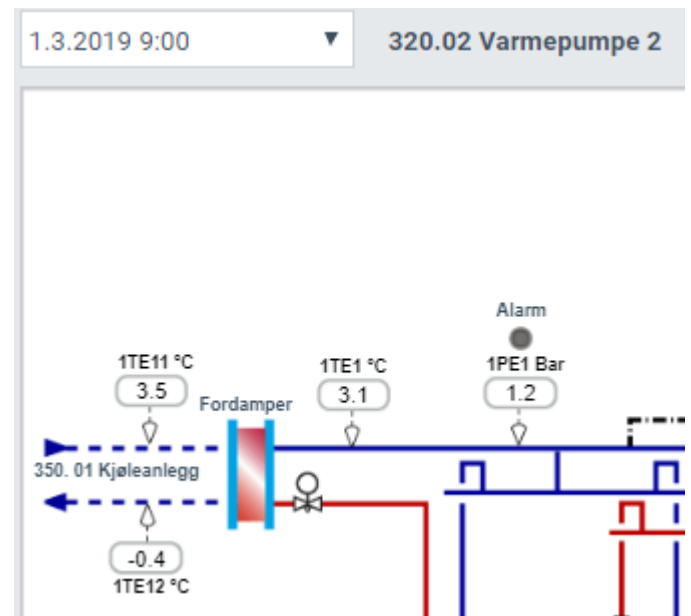
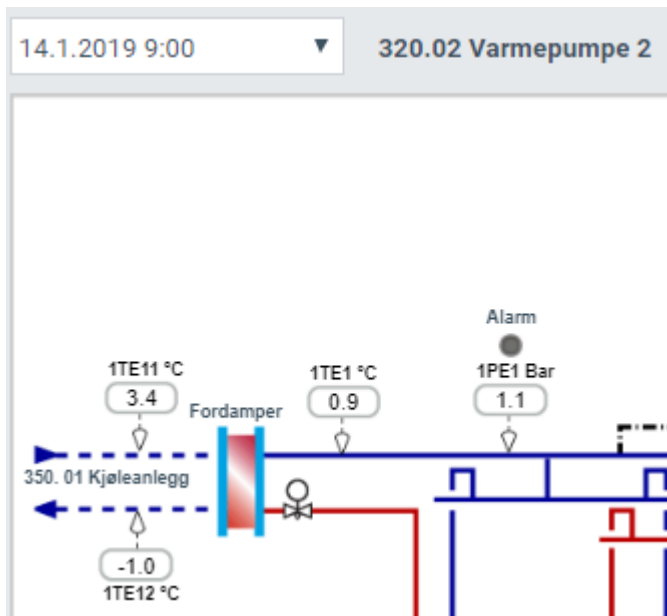




Heat Pump 1



Heat Pump 2



Appendix 4 – other calculations of optimal rate

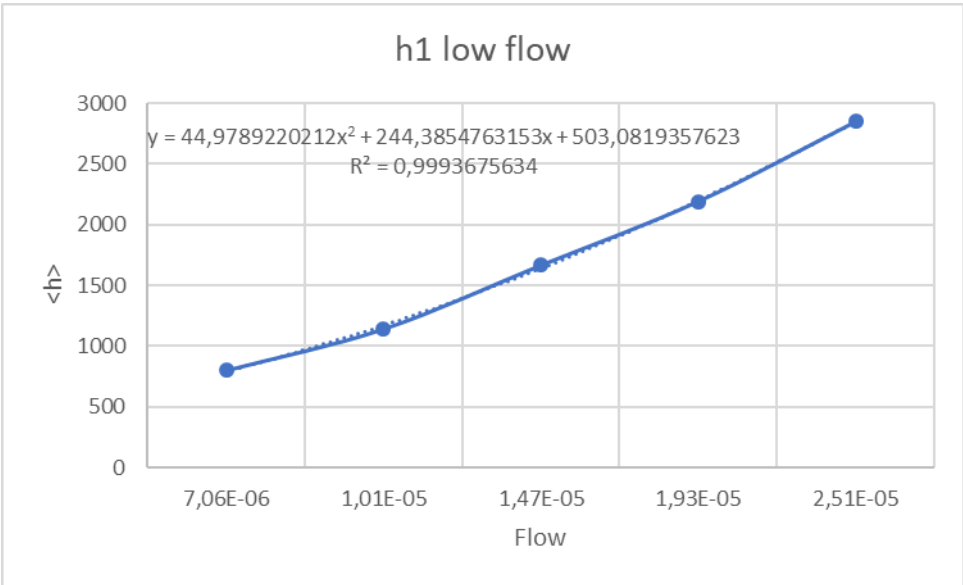
Equation 2.3

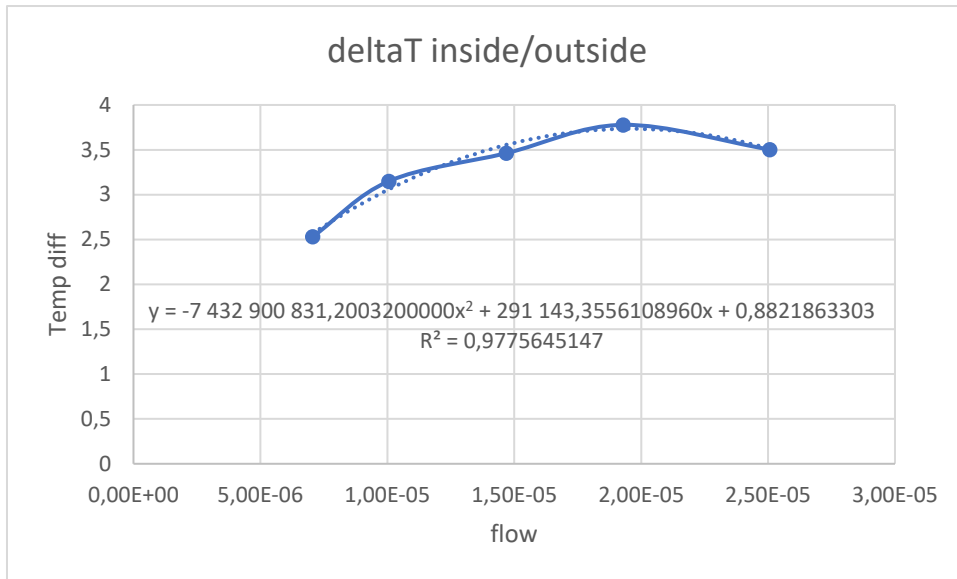
$$Q = UA_0\Delta T$$

$$U = \frac{1}{\frac{A_0}{h_1A_1} + \frac{A_0\Delta r}{kA_{lm}} + \frac{A_0}{h_2A_2}}$$

A0	A1	Alm	A2	delta r	h2	k
7,85E-05	0,0377	0,04224	0,04712	0,001	400	400

Flow	Tinside	Toutside	deltaT inside/outside	h1	U	Q
7,06E-06	8,79	11,32	2,53	802,191767	1,48E+05	29,36
1,01E-05	7,7	10,85	3,15	1143,28193	1,67E+05	41,28
1,47E-05	7,985	11,44667	3,46167	1668,03602	184480,873	50,16
1,93E-05	7,235	11,0133	3,7783	2192,79011	195246,452	57,94
2,51E-05	7,58	11,0833	3,5033	2848,73272	203957,9	56,12





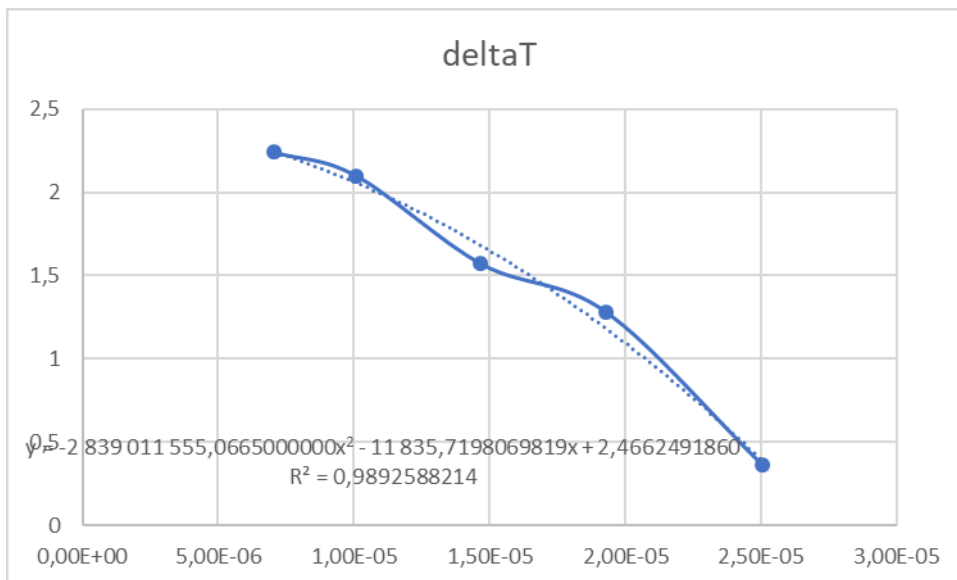
By use of the equations for the trendlines, $\langle h \rangle$ and Temp difference is calculated based on the flowrate from the earlier tests. The highest value of Q is found by change of the flowrate by Solver in Excel.

Flow	$\langle h \rangle$	U	Temp diff ins/outsi	Q
x	y		y	
2,15E-05	2448,96	1,99E+05	3,70	57,93

Equation 2.6

$$Q = \dot{m}c_p\Delta T$$

Flow	m	deltaT	Q
7,06E-06	0,00680529	2,24	63,5668842
1,01E-05	0,00980366	2,1	85,8506176
1,47E-05	0,01441652	1,57	94,3835292
1,93E-05	0,01902939	1,28	101,571262
2,51E-05	0,02479547	0,36	37,2229605

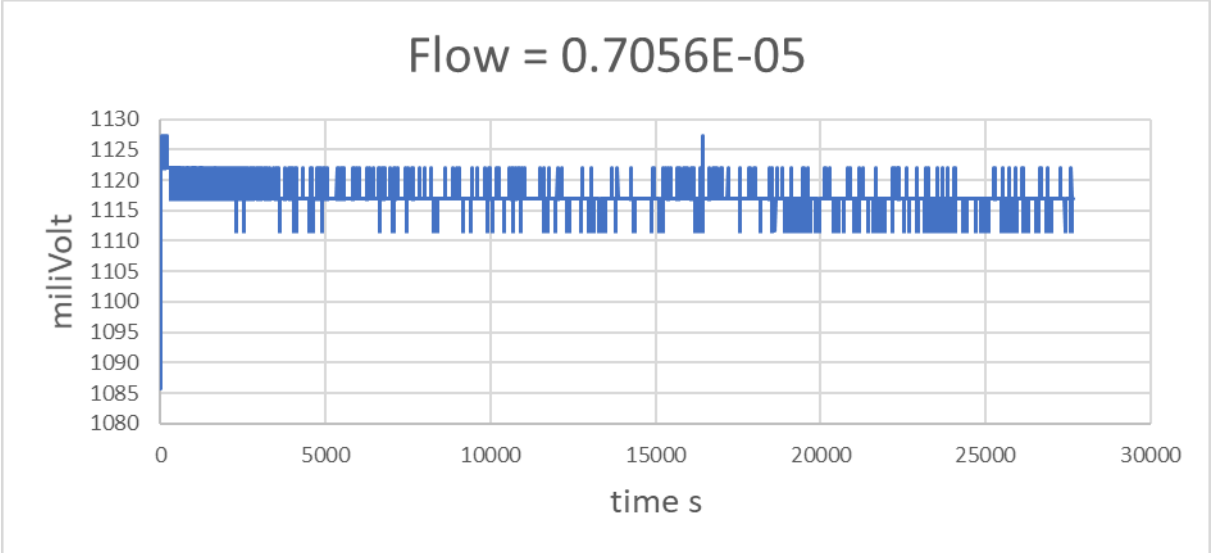
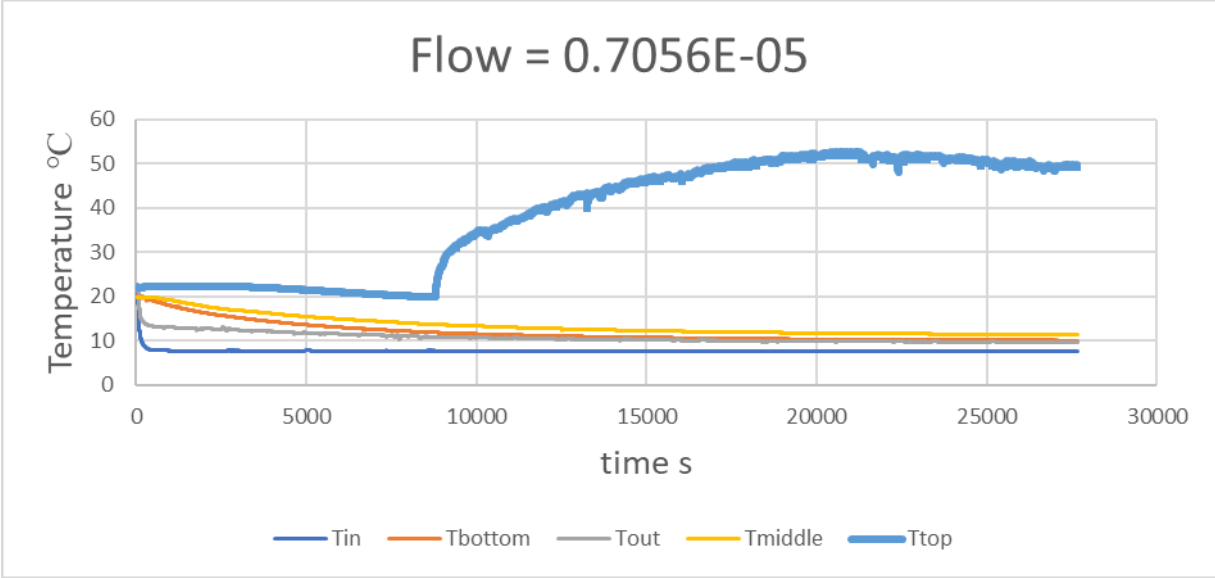


The mass (kg/s) is directly calculated from the flowrate ($q \cdot \rho$), and delta T is found by the trendline equation. The highest value of Q is obtained by use of Solver adjusting the flow.

Flow	Mass	deltaT	Q
1,57E-05	0,0156813	1,58	103,467588

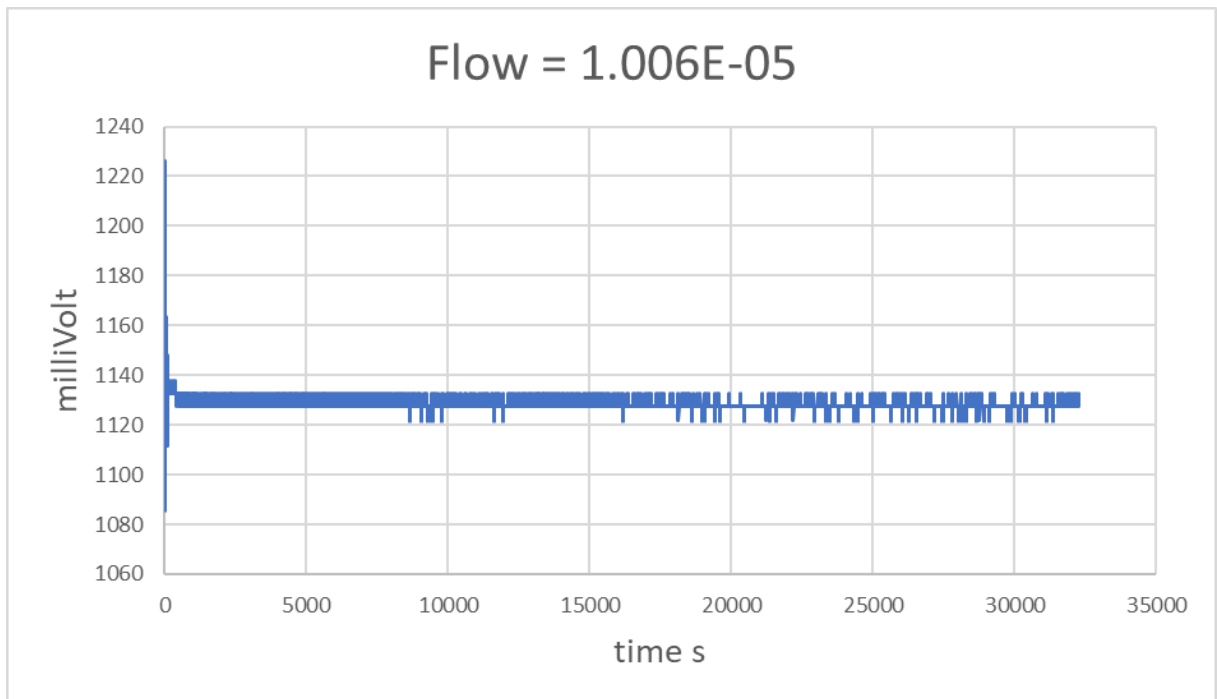
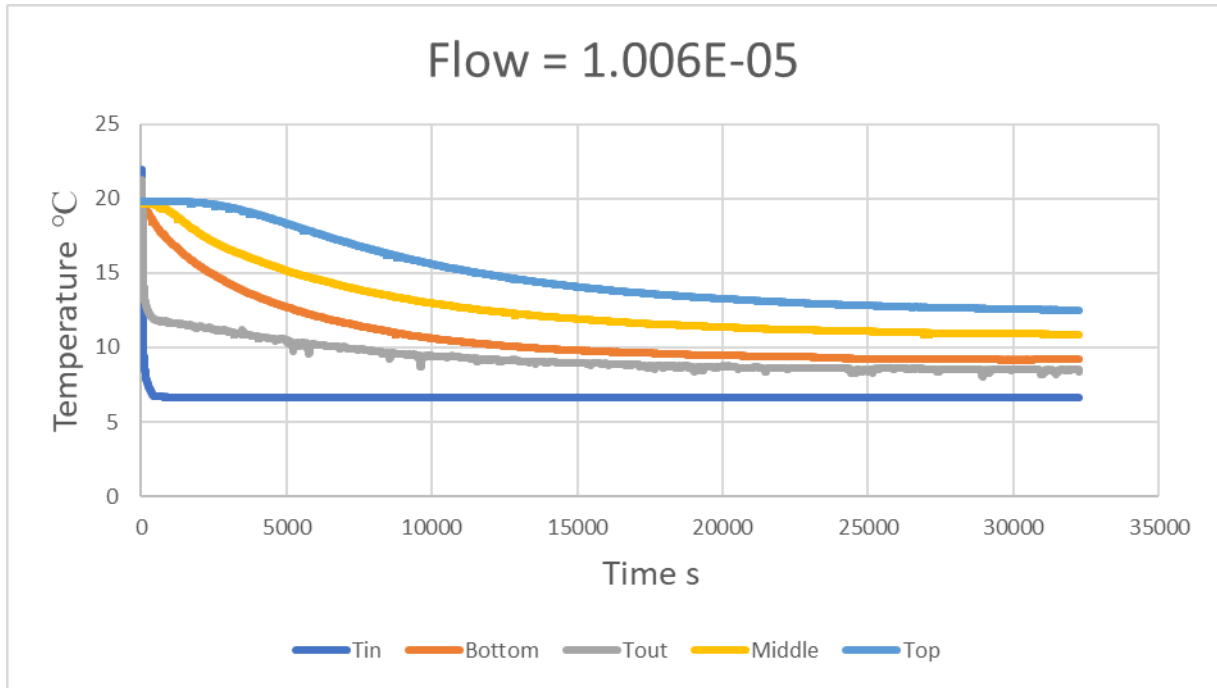
Appendix 5 Experimental Graphs

Flow = 0.7056E-05

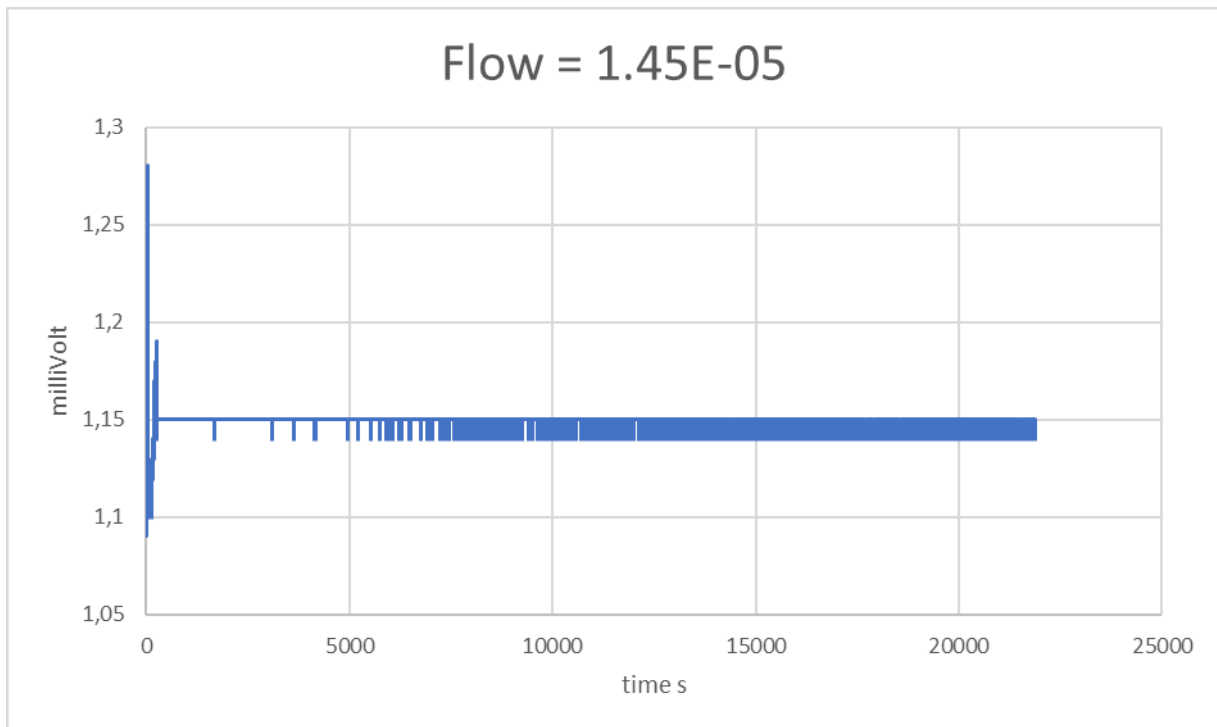
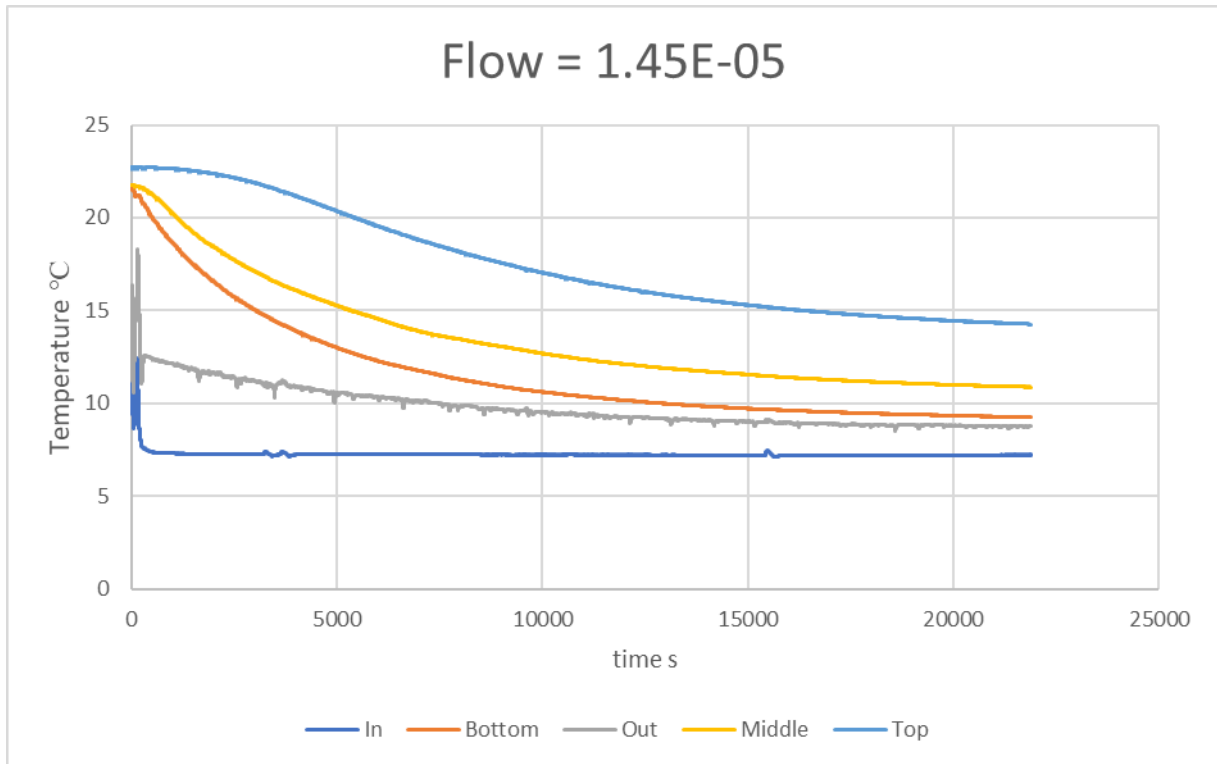


Comment: The temperature sensor displaying the top temperature in the cylinder stopped working correctly at time = 800 s, and should not be used in any analyzing after this point.

Flow = 1.006E-05

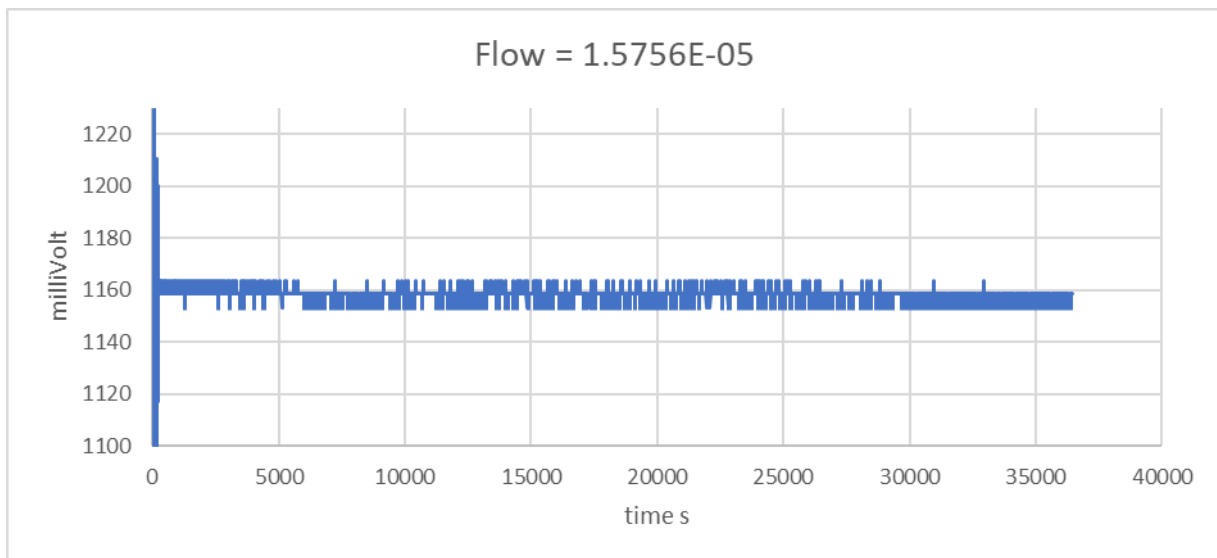
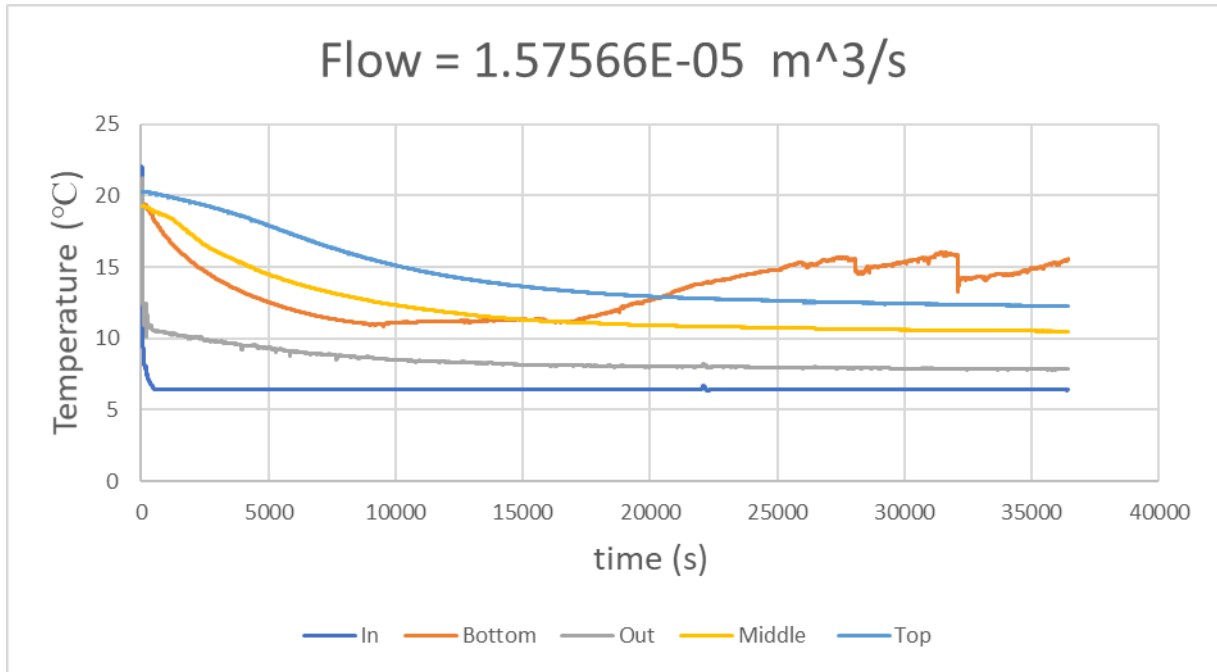


Flow = 1.45E-05



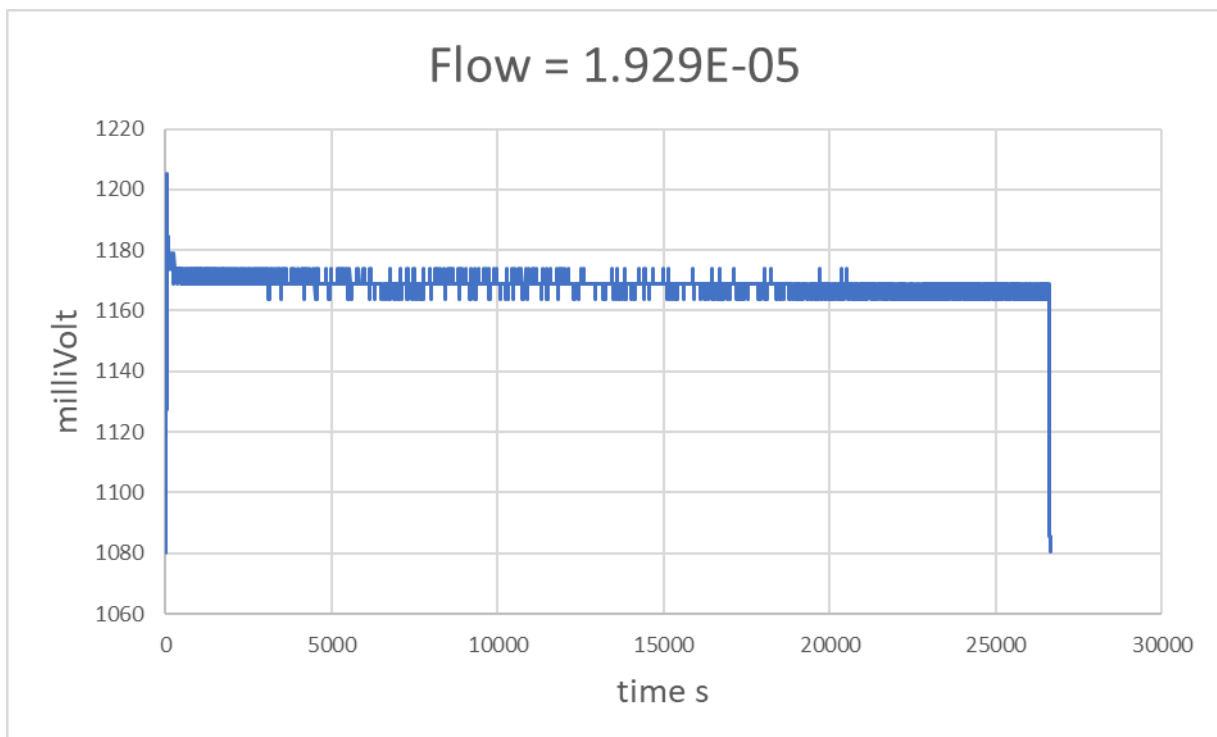
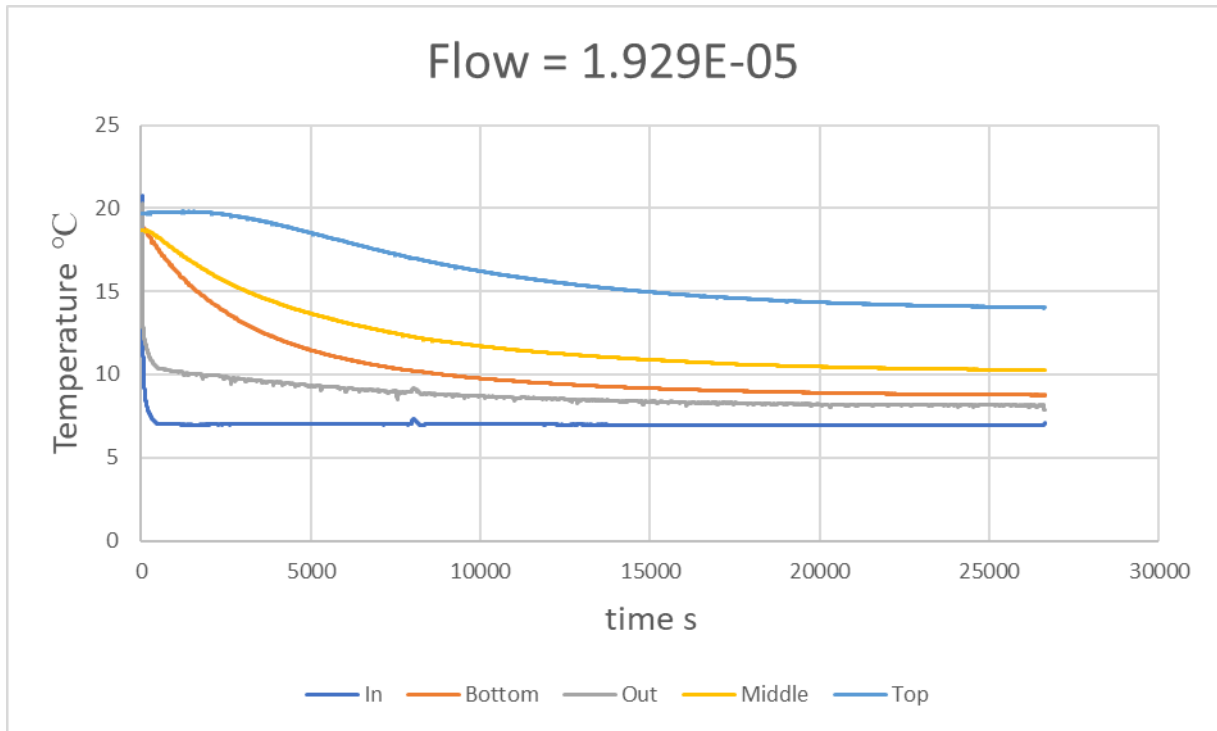
Flow = 1.576E-05

This was the Optimal flowrate



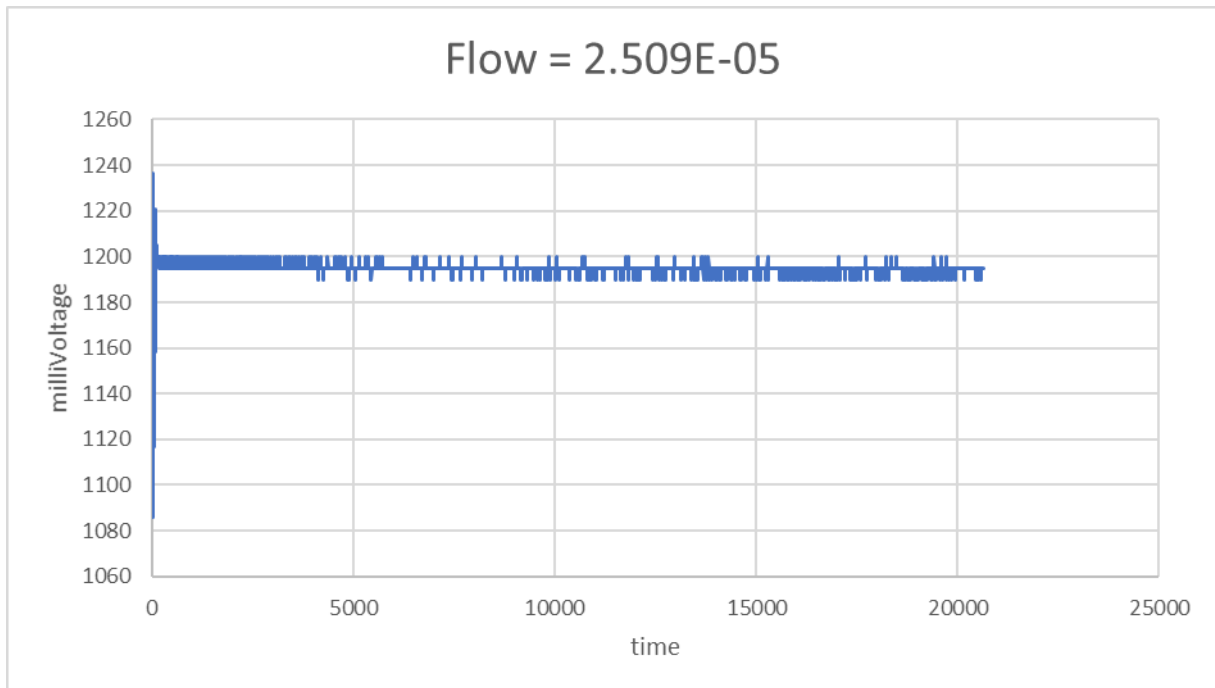
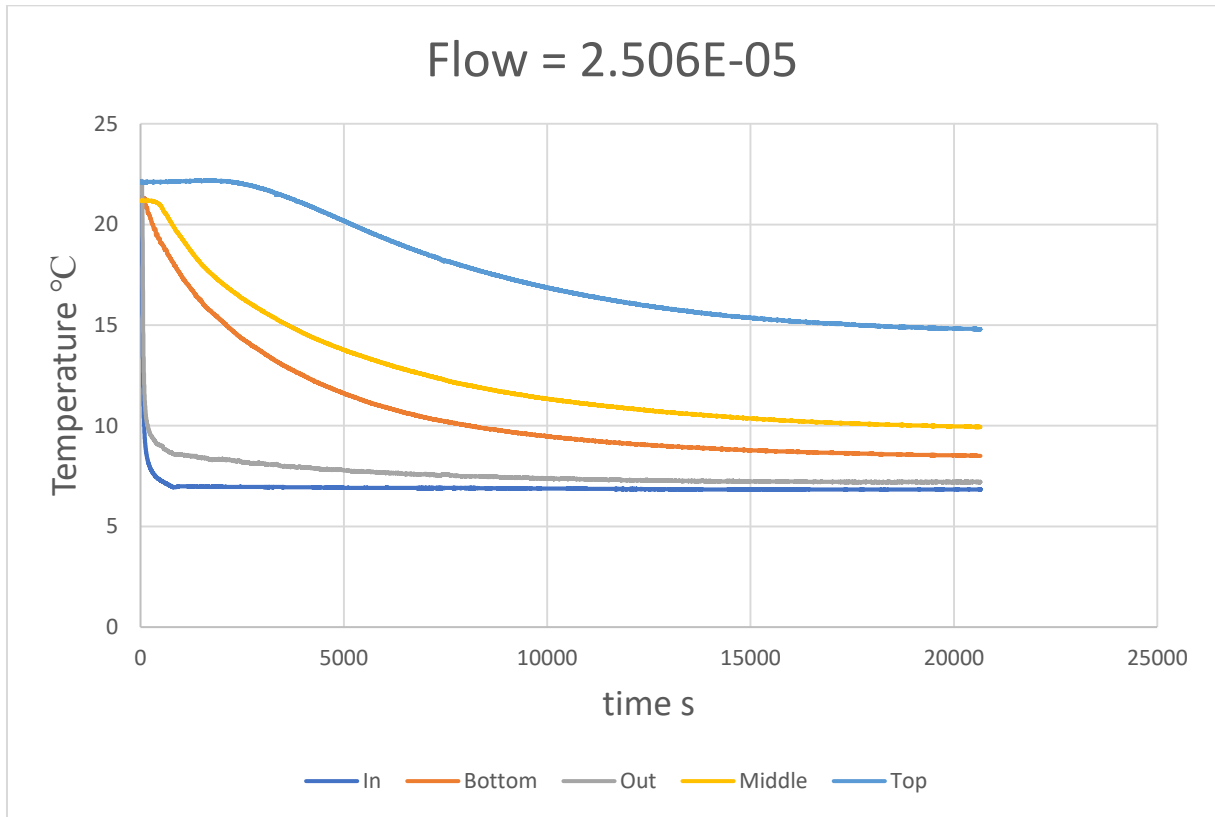
Comment: The sensor measuring the bottom temperature of the cylinder stopped working after 9000 seconds. Hence, the measured temperature for this sensor after this point should not be used for analyzes.

Flow = 1.929×10^{-5}

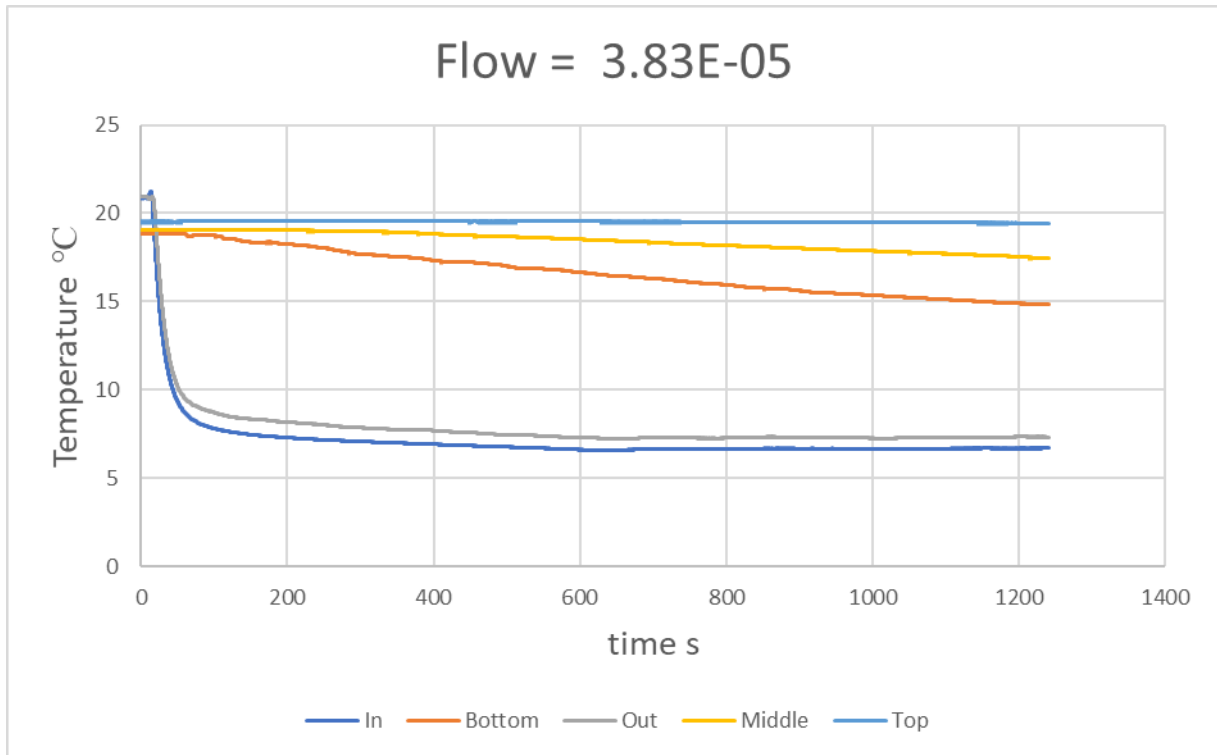


Comment: As the flow was stopped, the measured voltage quickly returns to the initial amount.

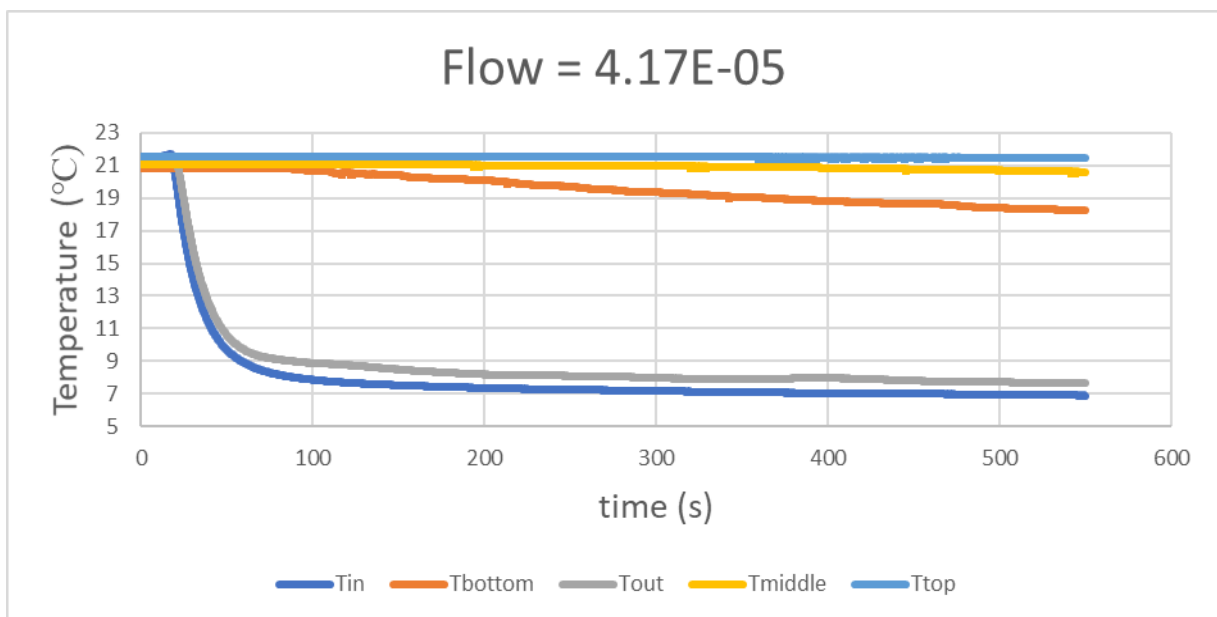
Flow = 2.506 E-05



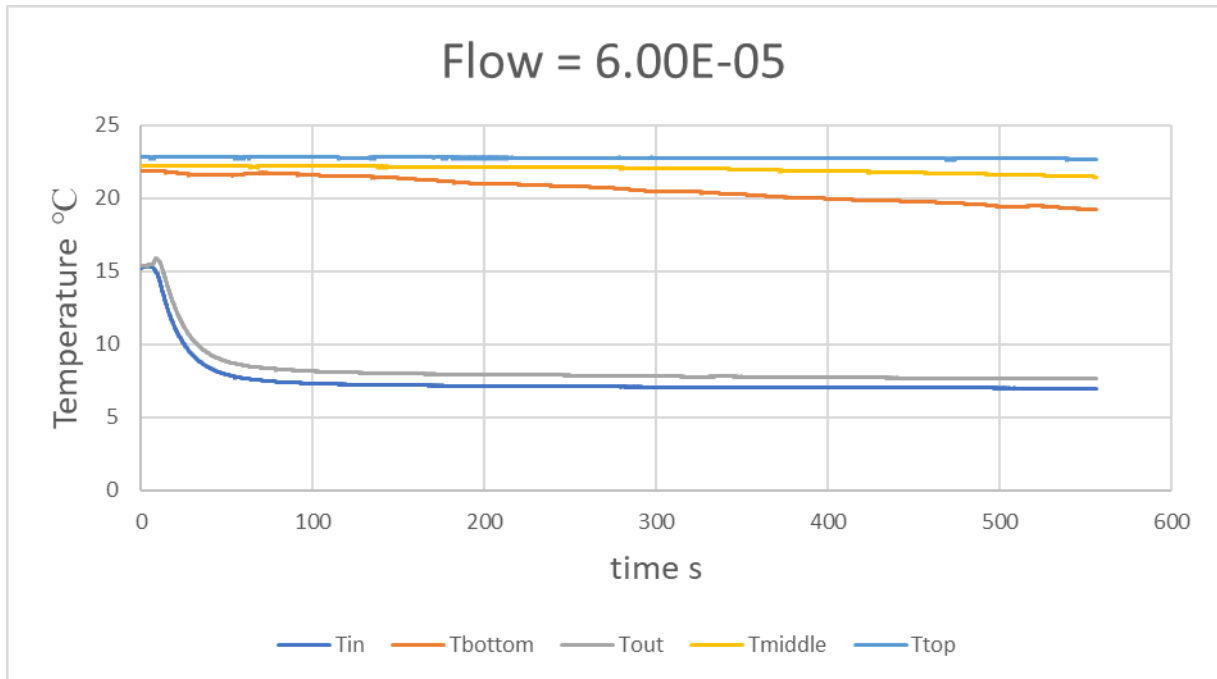
Flow = 3.83E-057



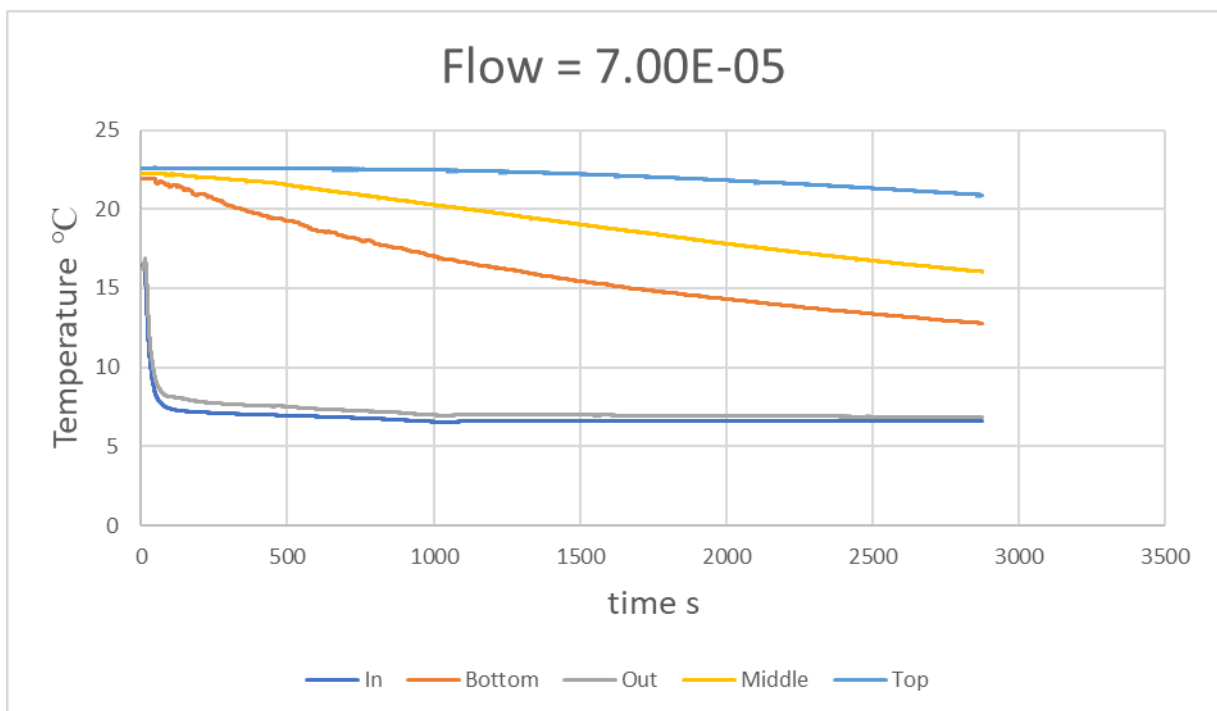
Flow = 4.17E-05



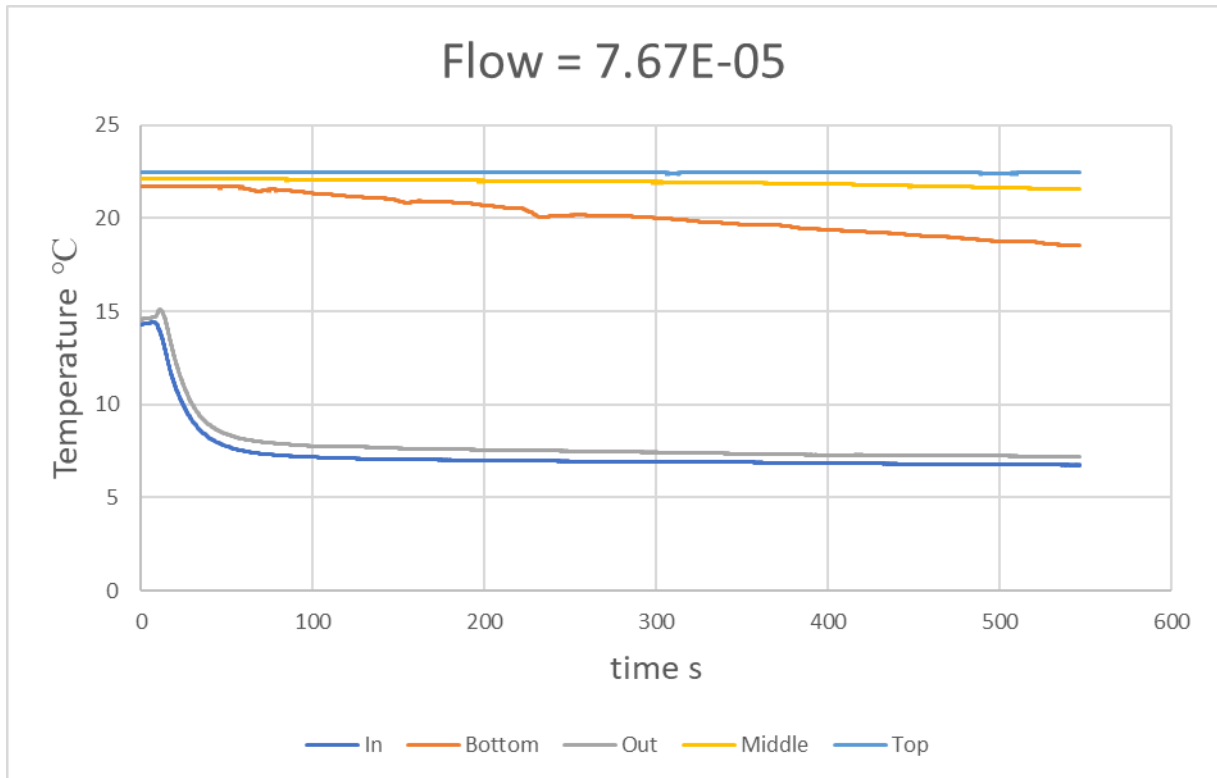
Flow = 6.00E-05



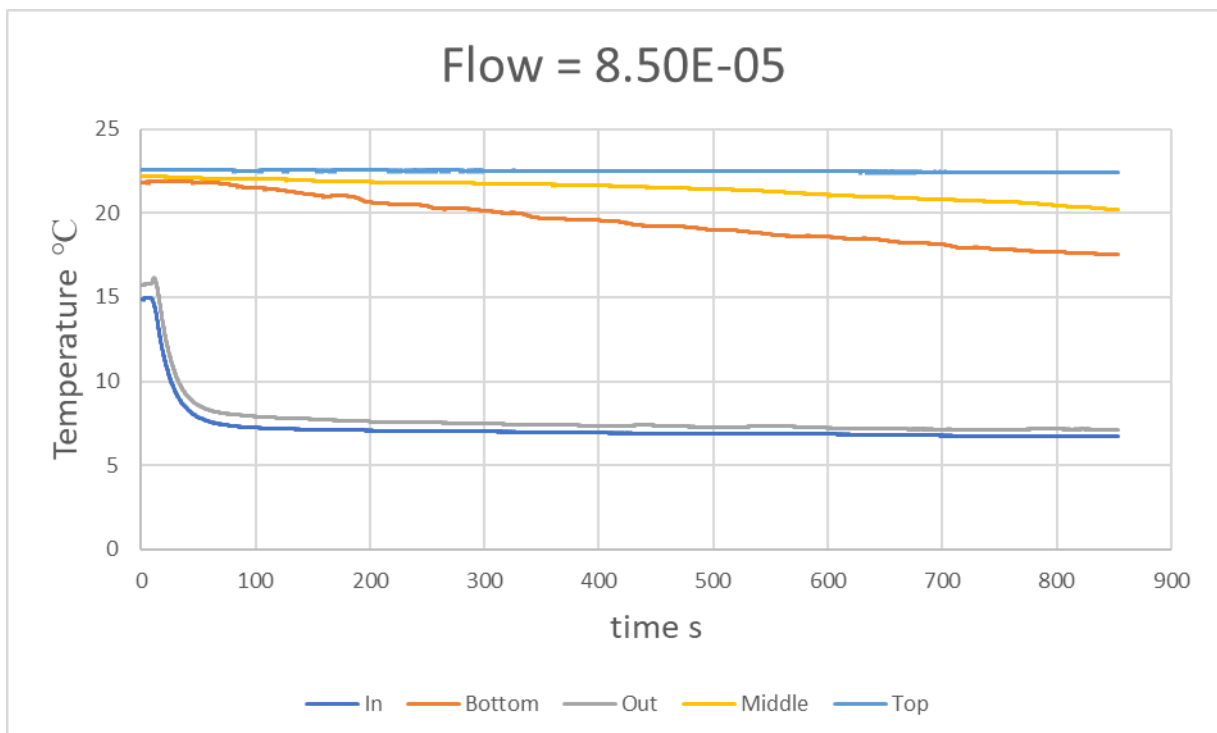
Flow = 7.00E-05



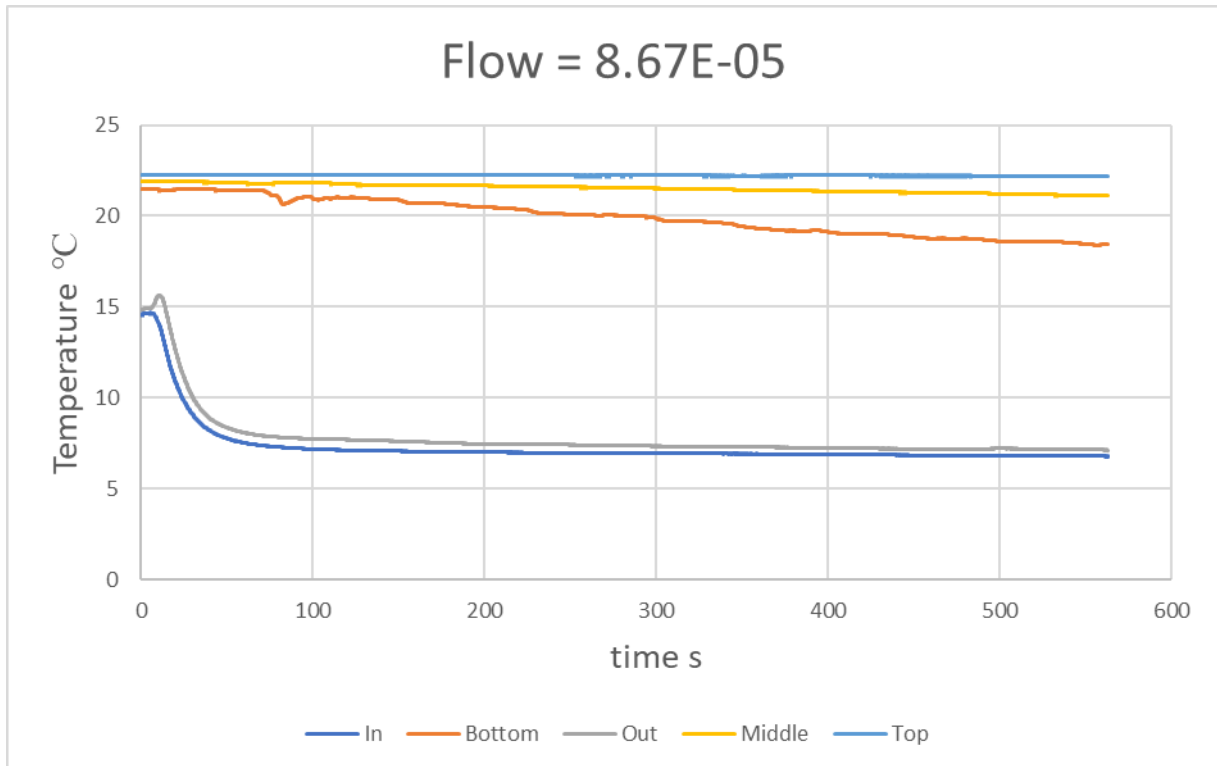
Flow = $7.67E-05$



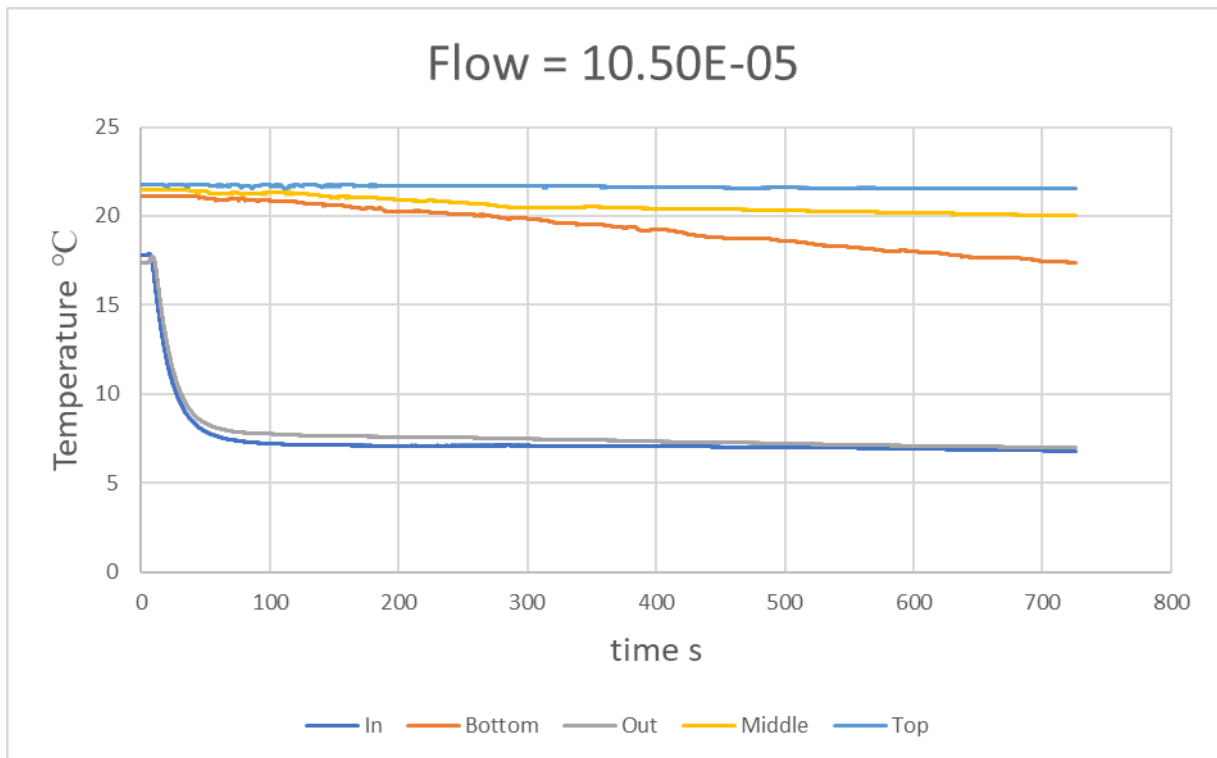
Flow = $8.50E-05$



Flow = $8.67E-05$

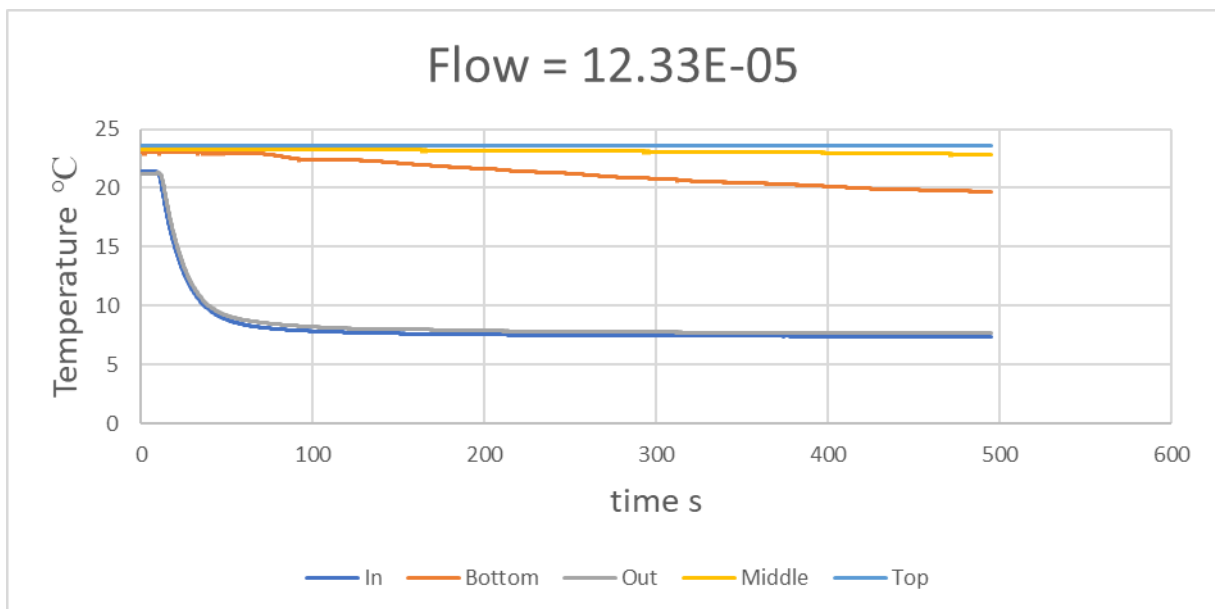
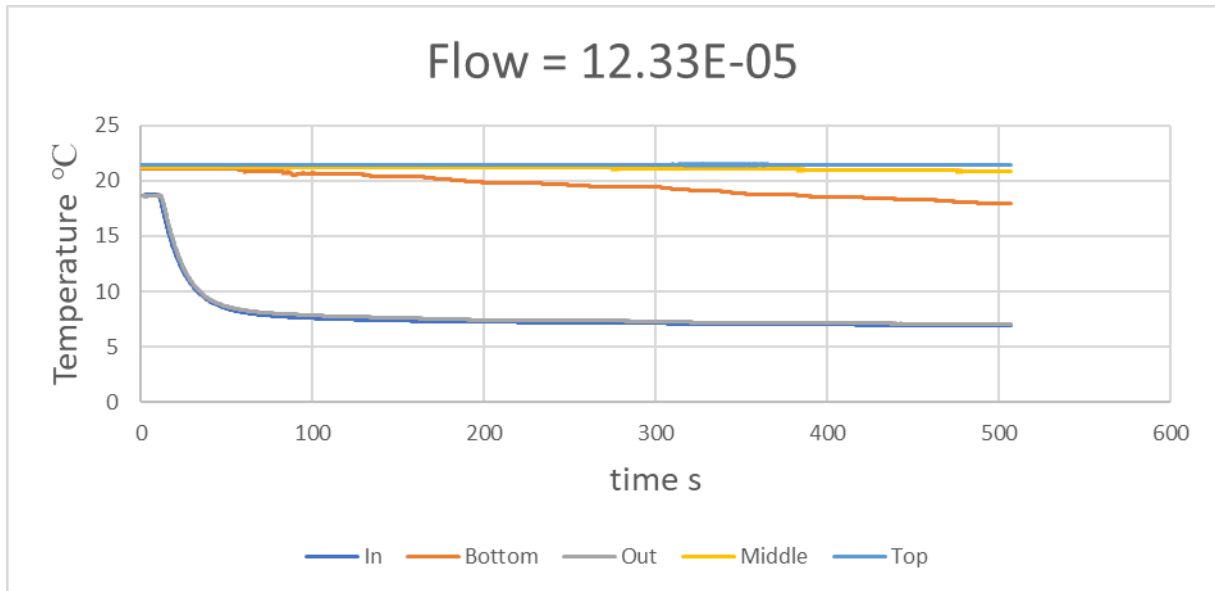


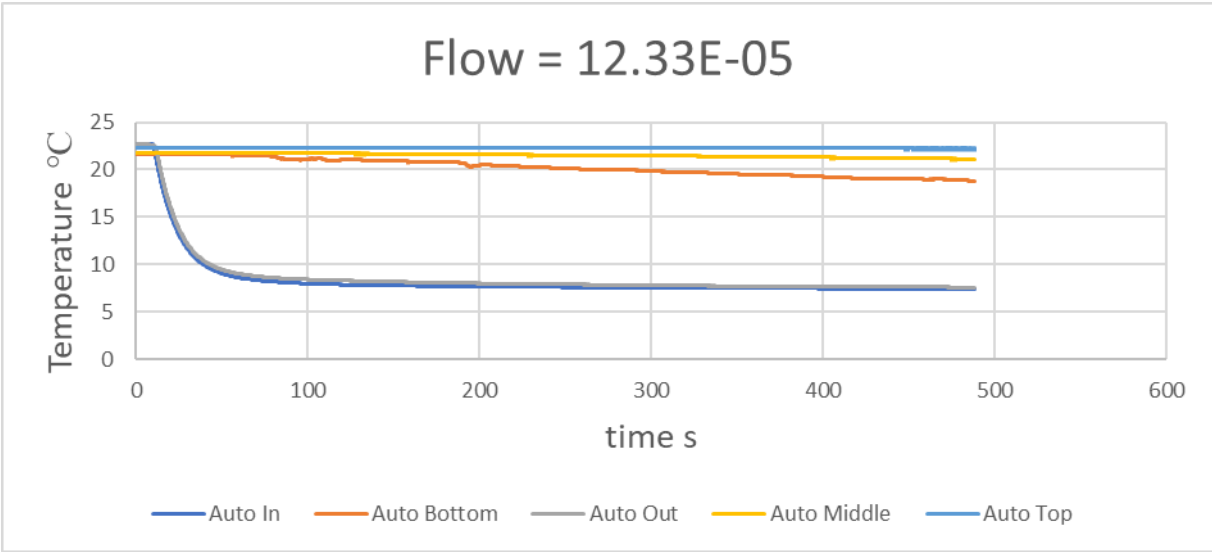
Flow = $10.50E-05$



Flow = 12.33E-05

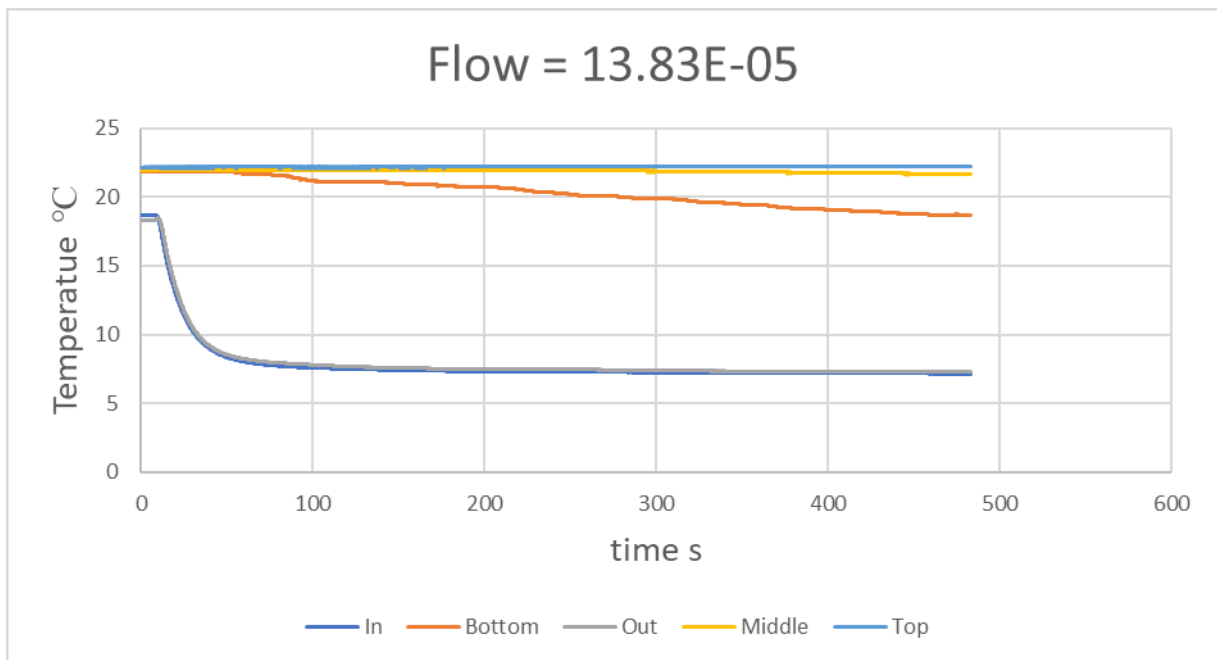
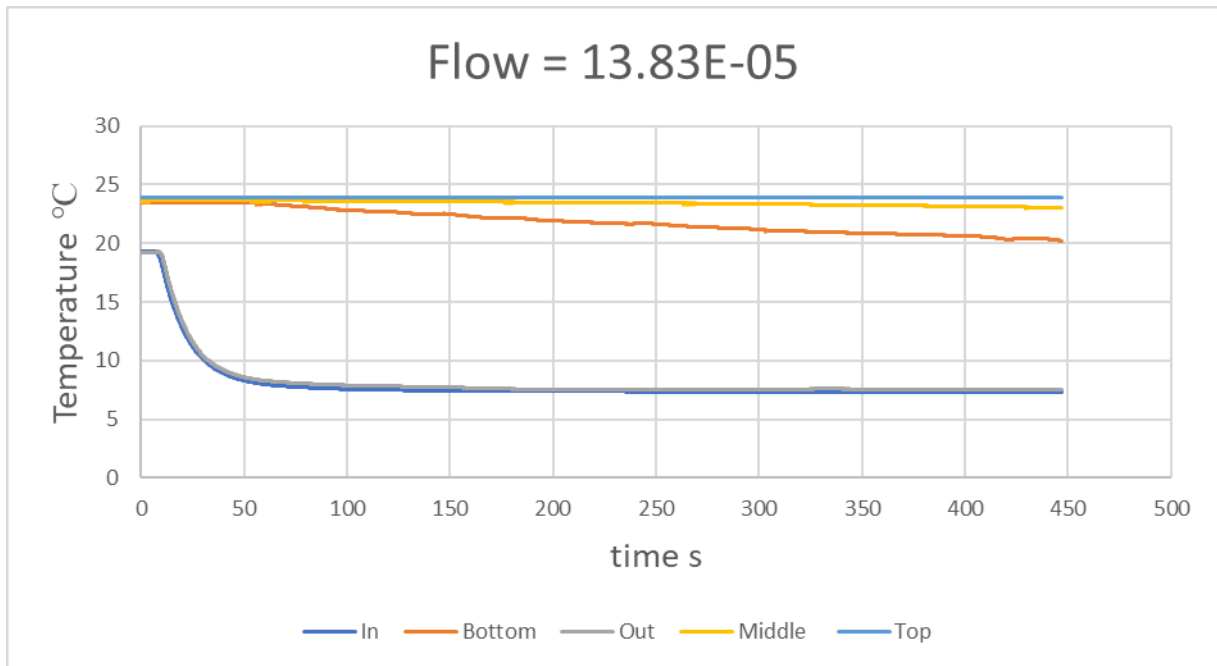
Pump = 1





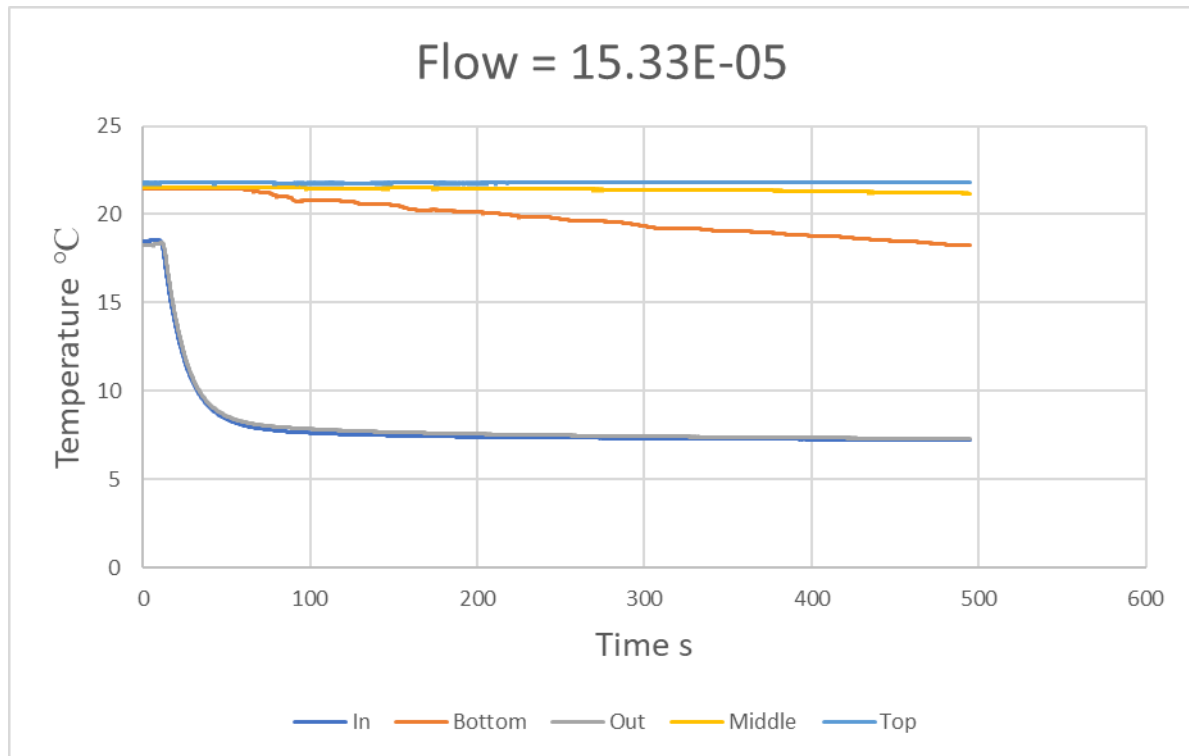
Flow = $13.83E-057$

Pump = 2



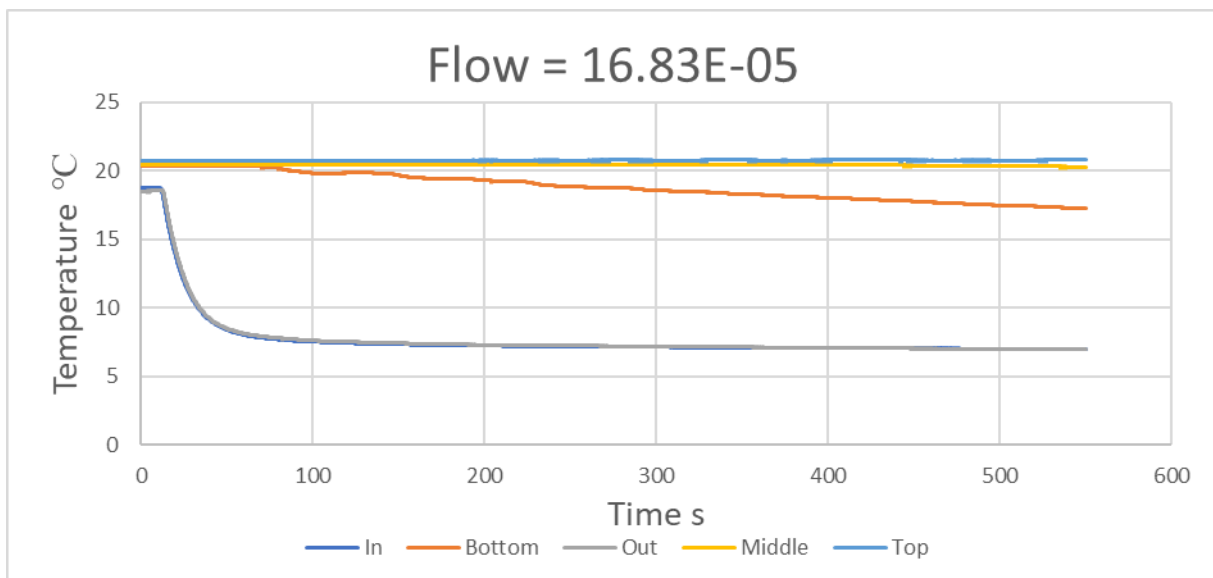
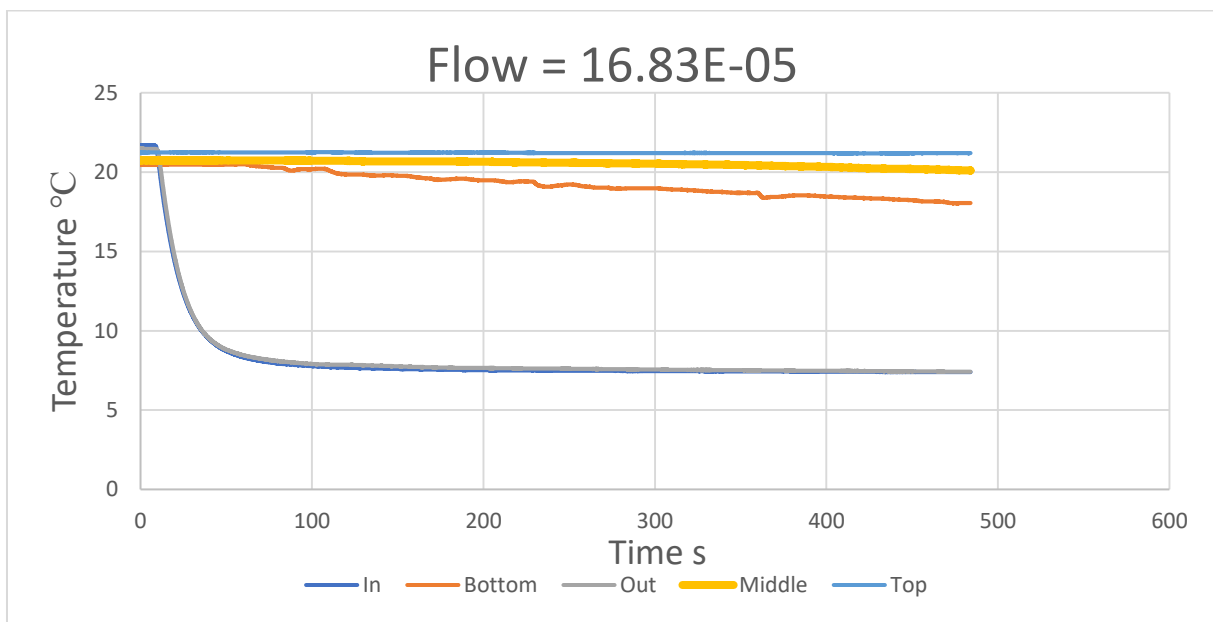
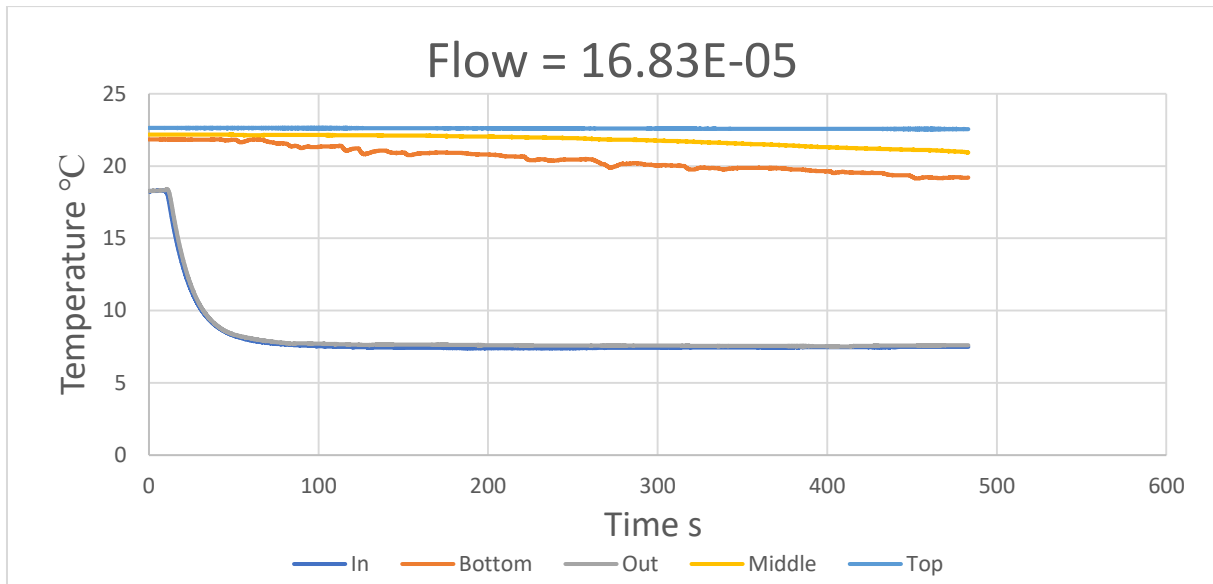
Flow = $15.33E-05$

Pump = 3

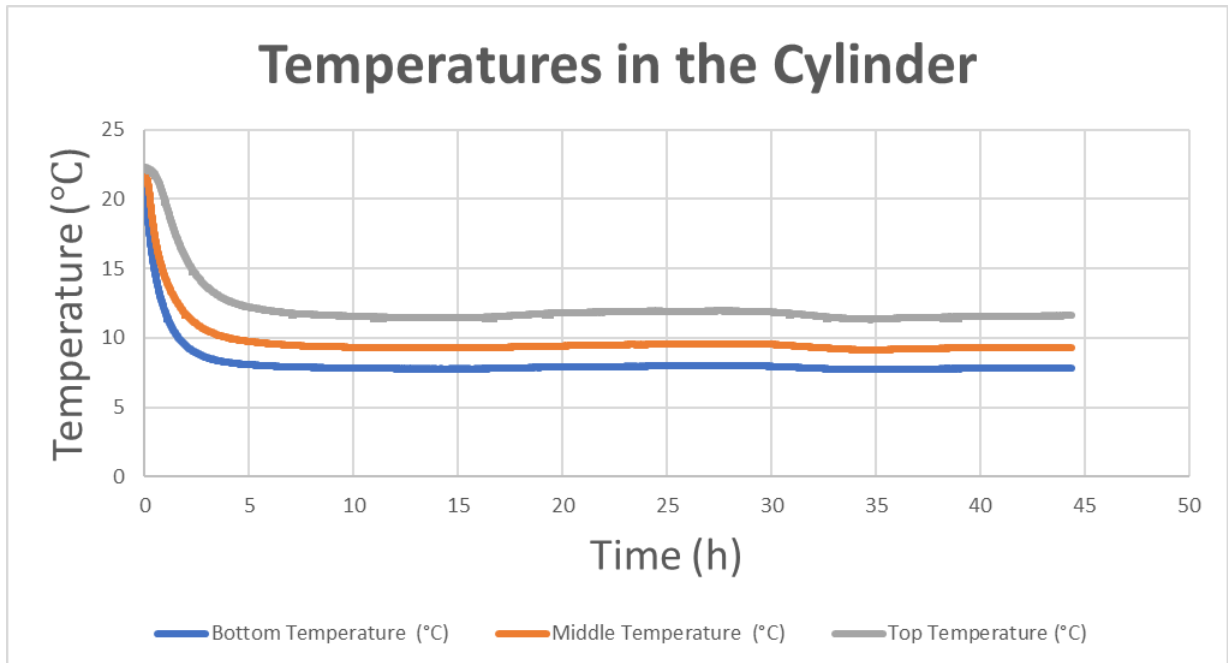


Flow = $16.83E-05$

Pump = 4



44 Hour Test, Flow = $8.33\text{E-}05 \text{ m}^3/\text{s}$



Room Temperature, 27 Hours

